THERMAL NON-EQUILIBRIUM IN DISPERSED FLOW FILM BOILING IN A VERTICAL TUBE

Robert P. Forslund
Warren M. Rohsenow

Report No. 75312-44
Contract No. NSF GK 39

Department of Mechanical Engineering
Massachusetts Institute of Technology

November 1966

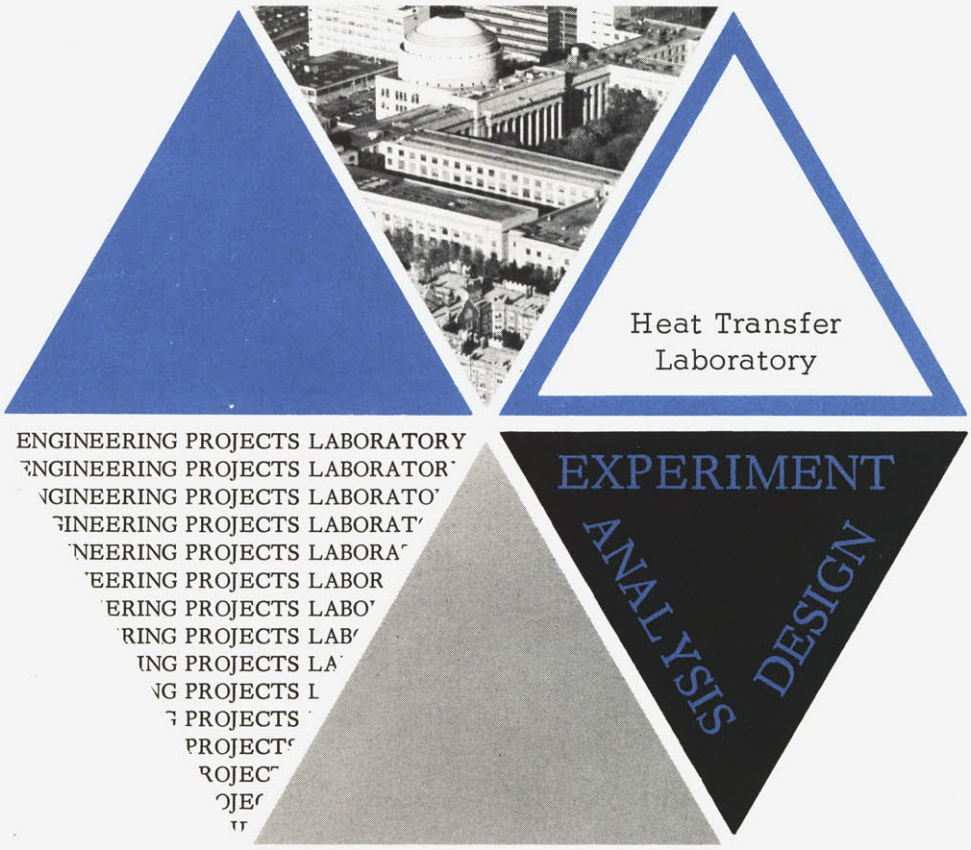

TECHNICAL REPORT NO. 75312-44

THERMAL NON-EQUILIBRIUM IN DISPERSED FLOW FILM BOILING IN A VERTICAL TUBE

by

Robert P. Forslund

Warren M. Rohsenow

Sponsored by the

National Science Foundation

Contract No. NSF GK 39

D.S.R. Project No. 75312

November, 1966

Department of Mechanical Engineering

Massachusetts Institute of Technology

Cambridge 39, Massachusetts

ABSTRACT

The departure from thermal equilibrium between a dispersed liquid phase and its vapor at high quality during film boiling is investigated. The departure from equilibruim is manifested by the high resistance to heat transfer between the dispersed and continuous phases, which result in much higher vapor temperatures and a defect in the amount of vapor generated. The effect on the overall heat transfer is to raise the tube wall temperature, and incomplete evaporation occurs within the tubes.

Film boiling tests with liquid nitrogen ($70{,}000 \leq G \leq 190{,}000$ lbm/hr/ft^2 and $5000 \leq q/A \leq 25{,}000$ Btu/hr/ft^2) were made with 0.228, 0.323, and 0.462 inch ID tubes, 4 and 8 foot long. Visual observations showed that complete evaporation occurs at heat inputs much greater than the required heat of evaporation based on thermal equilibruim ($\Delta H_{input} > H_{fg}$); in terms of quality, the heat input was as large as 300% quality for G = 70,000 lbm/hr/ft^2. The departure from equilibruim is principally a function of the total mass velocity, being less at higher mass velocities.

The non-equilibruim quality was measured experimentally by a helium tracer gas technique; reliable quality data at G = 70,000 lbm/hr/ft^2 was found to be in agreement with the departure from equilibruim calculated by applying a modified single phase heat transfer coefficient to the film boiling data.

A kinematic-heat transfer analysis of the core flow, which takes into account the acceleration, evaporation and breakup of a droplet, confirmed the trends in the departure from equilibrium. A Weber number criterion ($We_c = 7.5$) was found to adequately describe the breakup of droplets over a partial range of test conditions.

Film boiling pressure drop is also reported.

ACKNOWLEDGMENTS

This study was supported by a grant from the National Science Foundation. Electronic machine computations were done on the IBM 7094 Computer located at the MIT Computation Center.

The authors are indebted to Professor Peter Griffith for his suggestions which led to the use of the tracer gas technique for determining the departure from equilibrium, and to Professors Arthur Bergles and Philip Hill for their help in this work.

TABLE OF CONTENTS

LIST OF FIGURES

NOMENCLATURE

A	Inside surface area of tube
B.D.L.	Barely detectable liquid
C	Constant
C_A	Helium concentration at test section exit
C_B	Helium concentration at system exhaust
C_D	Drag coefficient
Cp	Specific Heat
D	Tube diameter
G	Mass velocity ρV
g	Gravitational acceleration
h	Heat transfer coefficient
h_D	Mass transfer coefficient
H	Enthalpy
H_{fg}	Heat of vaporization
I	Electric current
k	Conductivity
K_D	Mass diffusivity
ℓ	Tube length
m	Constant in exponent 1/m or molecular weight
M	Momentum flux ρV^2
n	Constant in exponent 1/n
N	Numerical concentration of droplets
Nu	Nusselt number hD/k or $h\delta/k$
N.L.	No liquid
P	Pressure
Pr	Prandtl number $\mu C_p/k$
Q	Heat rate, Btu/hr

Q_1	Heat input at inlet flange
q/A	Heat flux from tube wall
$\mathcal{R}$	Tube resistance
R	Gas constant
r	Radius
Re	Reynolds number $\rho VD/\mu$ or $\rho V \delta /\mu$
Sc	Schmidt number $\mu/\rho K_D$
Sh	Sherwood number $h_D \delta /K_D$
T	Temperature
t	Time
V	Velocity or Voltage
W	Mass flow rate, lbm/hr
X	Flowing quality of vapor
X_A	Actual quality
X_E	Equilibrium quality $0 \leq X_E \leq 1.0$
X_E'	Equilibrium quality (can be negative and greater than 1.0)
X_{tt}	Martinelli parameter
α	Void fraction or exponent
$\mathcal{B}$	$(T_c - T_w)/T_w$
δ	Droplet diameter
μ	Viscosity
σ	Surface tension
ρ	Density
ϕ^2	Martinelli two phase factor

Subscripts

amb	ambient
A	actual
b	bulk
℄	centerline
e	evaporation
E	equilibrium
f	film $T_f = (T_w + T_b)/2$
He	helium
i	inside, or, index of location
l	liquid
m	mean or throughput
max	maximum or centerline
meas	measured
N_2	nitrogen
o	outer
sat	saturation
ss	stainless steel
SP	single phase
T	total
v	vapor
vi	vapor interface
w	wall

CHAPTER 1

INTRODUCTION

1.1 Background

Heat transfer by forced flow film boiling has come to importance in recent years due to advancements in various technologies; such as in cryogenics, materials, and rocketry. Film boiling was usually avoided as a means for heat transfer in the past since the large temperature differences between the heated surface and the liquid, which are characteristic of film boiling, often result in destructively high surface temperatures. With developments in high temperature strength of materials, film boiling of fluids like water and fuels becomes attractive. Applications for such are nuclear steam power generation and the regenerative cooling of rocket motors. Cryogens are finding more applications as cooling fluids, and are particularly applicable where ordinary materials are used since they have the advantage of being at much lower temperatures.

Although the presence of film boiling has been known for quite some time, little work has been done on this subject until recent years. Most of the work with film boiling in forced flow occurs in the literature after 1960. Prior to this, investigations had primarily been confined to pool boiling.

In most investigations of film boiling in forced convection, a rather sharp tube wall temperature rise along the tube is observed after the dry wall condition occurs (burn-

out, CHF). The temperature reaches a maximum at some location a short distance downstream and then decreases. The dry wall conditions can also occur immediately on entering the boiler. It is in this region of low vapor quality or subcooled liquid conditions that true film boiling exists; a situation in which a vapor film separates a liquid core from the wall. At higher qualities the flow is a dispersed type in which liquid droplets are carried along by the vapor. These flow regimes have been observed in visual tests at MIT (1, 2). The change between the two regimes is a gradual one that roughly occurs around 10 to 20% quality for the test conditions of the referenced studies. The term film boiling is also applied to the high quality region since it is assumed that a film of vapor covers the heating surface. Droplets are prevented from touching the surface by the Leidenfrost effect (spheroidal state of the liquid droplets). A more appropriate terminology for this region would be post burnout dispersed flow heat transfer. It is this high quality dispersed flow region that is the subject of this current investigation. Consequently, the following discussion will be limited to it.

An exact analysis of heat transfer to a dispersed flow would require that the fundamental equations of momentum, mass and energy be applied to both phases along with the appropriate phenomenological equations of heat and mass transfer. However, distributions of droplet sizes and velocities

obviously occur in dispersed flow, and distributions can vary along the length of the heated tube. In addition to describing the kinematics and heat transfer within the flow, the effect of liquid on the heat transfer at the heated surface must be accounted for. Since an exact analysis is much too complex, quantitative descriptions of film boiling in dispersed flow are generally in the form of operational correlations.

Operational correlations for film boiling heat transfer in the literature are generally formed around heat transfer correlations for the vapor phase where the appropriate single phase correlation (such as the Dittus-Boelter or Colburn equation) for the fluid question is used. Alterations are made to the correlations by either adding additional terms or multipliers to the correlation and by modifying the original terms of the expression. Generally an analytical model governs the choice of modification.

Since the flow regime in film boiling is usually a dispersed type of flow over a large range of quality, and only pure vapor is thought to be in contact with the walls, one of the obvious ways for describing the heat transfer in the two phase flow is to compare it with the heat transfer that would result if only the existing vapor flowed alone in the tube. Heat transfer coefficients should increase along the length of the tube due to the increasing vapor mass velocity that occurs in boiling, and should do so in the same propor-

tion as is expected for single phase flow. This trend is observed in most film boiling studies in which the tube wall temperature decreases with length. For this reason, the velocity in the Reynolds number of the single phase correlation is usually taken to be a vapor velocity or some average velocity.

Figure 1 shows a very simple example of what typical tube wall temperature profiles might look like for the boiling and superheated regions in a straight through boiler at constant heat flux. A constant heat transfer coefficient, $h_o = KG^{0.8}$, is assumed to apply in the superheating region so that the tube wall temperature (curve A) increases according to the equilibrium superheating gradient. In the film boiling region several temperature profiles might be possible. If the heat transfer process from the tube wall is dependent only on the vapor velocity (or on vapor flow rate $h = KG^{0.8} X^{0.8} = h_o X^{0.8}$, as shown in the figure), curve B results. However, if the presence of liquid contributes to or inhibits the heat transfer process at the wall, a modifying term, such as the ψ_1 or ψ_2 in the figure, is applied to the correlation and curves C or D result. The ψ_1 and ψ_2 might be functions of the fluid properties and flow conditions. Superposition is sometimes considered in the case of liquid contribution; an additive term is used instead of the multiplier. Under certain conditions, a fourth type of profile, curve E, may exist. This type of profile is

indicative of a non-equilibrium situation in which highly superheated vapor along with liquid droplets at saturation temperature exist in the core flow. The tube wall temperature profiles are higher due to; 1) the elevation in the non-equilibrium vapor temperature T_{VNE} and 2) the reduction of the heat transfer coefficient caused by the decreased flow rate. Once this phenomenon occurs it continues into the superheating region. This non-equilibrium phenomenon is the particular subject of this present work.

Film boiling can arrive either immediately at the tube entrance or further downstream after a certain length of annular flow depending on the preheat conditions of the tube. Curves G show burnout and film boiling development after a length of annular flow. Actual temperature profiles can be a combination of the simple forms presented in figure 1. A few of the various means for correlating film boiling heat transfer are cited in the following literature review. Attention is also drawn to the case where the condition of non-equilibrium appears.

1.2 Literature review

An example of the additive term approach is the work of Parker and Grosh (4) with water. They suggested

$$q/A = h_{SP} (T_w - T_{sat}) + (q/A)_e = h_{meas} (T_w - T_{sat}) , \qquad (1)$$

where the single phase vapor heat transfer coefficient, h_{SP}, can be represented by the Colburn correlation for the exist-

ing vapor and $(q/A)_e$ is the droplet evaporation at the wall which is a product of the droplet diffusion coefficient, the local droplet concentration and the heat of vaporization. They found that this description of the heat transfer might be adequate in the region after burnout up to a point where a "spheroidal" state of the liquid droplets exists. The diffusion coefficient however had no predictable basis in this region of applicability, consequently no correlation was offered. It was found that after the spheroidal state, the measured heat transfer coefficient was lower than that predicted by the Colburn equation. When it was assumed that no further evaporation of the liquid droplets occur either at the wall or in the core and that the heat input went to superheating the existing vapor, the measured heat transfer coefficient ($h = (q/A)/(T_w - T_v)$) could be correlated by the Colburn equation. Thus a situation typical of curve E of figure 1 resulted. This assumption was supported by the detection of droplets past the location of 100% equilibrium quality with the aid of a capacitance probe spray analyzer located at the tube exit. This observation however, was limited to a very small superheating region since the maximum exit quality was limited to 102%. Some liquid will always be present just after the 100% equilibrium quality location since some degree of non-equilibrium is associated with the thermal boundary layer.

A comparative-type correlation for film boiling of water applicable to curve D of figure 1 was presented by

Miropolski. (5)

$$Nu_b = 0.023\ Pr_w^{0.8}\ (G_T D/\mu_b)^{0.8}\left[X + (1 - X)\ (\rho_v/\rho_\ell)\right]^{0.3} y\ , \quad (2)$$

where

$$y = 1 - 0.1\ (\rho_\ell/\rho_v - 1)^{0.4}\ (1 - X)^{0.4}\ .$$

The term in the brackets modifies the Reynolds number to reflect the average mixture velocity with zero slip (sometimes called throughput velocity). The factor y is supposed to correct for variation in slip. The first portion of the correlation is similar to the Dittus-Boelter correlation except for the evaluation of the Prandtl number and was found to adequately describe heat transfer to pure steam. Note that y is less than unity for film boiling.

Close examination of his measured axial tube wall temperature profiles shows that, when projected, the intersection of the film boiling profiles with the superheating profiles occurs somewhat past the location of 100% quality and not at 100% quality as the correlation predicts. The difference is small but does indicate that some non-equilibrium may exist. A similar phenomenon is observed in the smoothed temperature data of Schmidt (6).

Polomik, et al. (7) have investigated post burnout film boiling with water in annuli and have correlated their data by

$$Nu_f\ Pr_f^{1/3} = 0.00136\ \ (G_T D/\mu_f)^{0.852}\left(\frac{1 - X}{X}\right)^{0.853}\left(\frac{\alpha}{1 - \alpha}\right)\ , \quad (3$$

where α is the void fraction, correlated by

$$(1/\alpha) = 1 + \left(\frac{1 - X}{X}\right) \quad (\rho_v/\rho_\ell)^{2/3} .$$

Swenson, et al. (8) suggest

$$Nu_w = 0.076 \quad (\rho_w \, V_m \, D/\mu_w)^{0.8} \, Pr_w^{0.4} , \qquad (4)$$

for their data for film of water in tubes.

Bishop, et al. (9) have investigated film boiling of water after burnout in a "once thru" type boiler. Their data for $G \geq 10^6$ and the data of (5) correlate well by

$$Nu_w = 0.098 \, (\rho_w \, V_m \, D/\mu_w)^{0.8} \, Pr_w^{0.83} \quad (\rho_v/\rho_\ell)^{0.5} . \qquad (5)$$

At mass velocities below 10^6 the measured heat transfer coefficients were lower than predicted. It was postulated that these lower values might be due to an isolating condition in which the vapor at the wall is prevented from mixing with the core flow by a thin layer of liquid. It is also suggested that non-equilibrium probably occurs, as evidenced by the axial tube wall temperature profiles. The minimum temperature occurs in the superheating region for the lower mass velocities whereas the minimum location is very close to 100% quality for the higher mass velocities.

A condition of non-equilibrium after burnout was inferred by Bennett, et al. (10) in the tests with water in an annulus. The experimental heat fluxes required to produce a particular surface temperature were lower than those pre-

dicted based on equilibrium by as much as 40%.

Laverty and Rohsenow (2) investigated film boiling of nitrogen in the high quality region. They found also that the measured heat transfer coefficients were much lower (as much as 50%) than those predicted by a Dittus-Boelter type equation which uses the throughput velocity in the Reynolds number. The theory developed to explain these results assumed that a two step heat transfer process occurs in which heat is first transferred from the wall to a superheated vapor only, no evaporation of the liquid occurs at the walls; secondly the heat is transferred from the superheated vapor to the liquid droplets. In the first step it was assumed that the modified Dittus-Boelter equation could adequately describe the heat transfer in the first step and was used to evaluate the temperature of the superheated vapor. Part of the heat thus transferred goes to superheating the existing vapor, the rest goes into evaporation and raising the temperature of the resulting vapor up to the local vapor temperature. A heat balance yielded droplet heat absorption coefficients for the second step. These absorption coefficients were assumed to be represented by the heat transfer equation for a solid sphere. Simultaneous solution of this equation along with a kinematic equation for a droplet resulted in local droplet sizes that were less than 1 mm in diameter as observed in a preliminary visual flow regime test with an electrically heated glass

tube. The calculated drop sizes however could not be used in working back through the theory to predict wall temperatures since the heat balance involved was sensitive to the rate of superheating.

Heat transfer and pressure drop characteristics for film boiling of hydrogen was investigated by Hendricks, et al. (11). They found that the tube wall axial temperature profiles decreased with length in most of their runs except for a few cases in which a slight rise occurs towards the end of the tube. This occurance was attributed to a vapor binding effect similar to that experienced by Dengler (12) with water. This behavior may be represented in figure 1 as a transition between curves C and B or D. Heat transfer was correlated by Hendricks, et al. (11) as follows

$$Nu_f = 0.023\ Re_{f,m}^{0.8}\ Pr_f^{0.4} / (0.611 + 1.93 X_{tt}) \quad , \tag{6}$$

where $Re_{f,m} = (\rho_{f,m}\ V_m\ D/\mu_f)$,

and $X_{tt} = \left(\frac{1 - X}{X}\right)^{0.9} \left(\frac{\mu_\ell}{\mu_v}\right)^{0.1} \left(\frac{\rho_f}{\rho_\ell}\right)^{0.5}$,

and $(1/\rho_{f,m}) = X\ (1/\rho_f) + (1 - X)\ (1/\rho_\ell)$.

Examination of this correlation shows that at high qualities ($X \rightarrow 1.0$ or $X_{tt} \rightarrow 0$), the heat transfer coefficient is larger than that predicted for pure vapor. It was suggested that in this region heat transfer might be augmented by the presence of non-equilibrium quantities of colloidal particles (liquid H_2). It is however possible that the

numerator in the correlation is not an accurate description of heat transfer in the superheating region in the neighborhood of 100% quality (curve A).

An analytical and experimental pressure drop study was included in their work. Pressure drop appears to be chiefly due to momentum changes and can be accurately predicted by neglecting the friction and hydrostatic head and by assuming equilibrium flow conditions with no slip between the phases. These pressure drop measurements are further discussed in section 2.3.3 in this report.

Further work with cryogenics was made at NASA by Lewis, et al. (13). They were concerned primarily with burnout, consequently no correlation of film boiling past burnout was offered.

Burke and Rawdon (14) experimentally investigated film boiling of nitrogen in a horizontal 0.25 inch ID tube. They utilized a thermal capacitor cool down technique to supply heat to the test section. The tests show that the heat transfer coefficient decreases strongly with quality; a completely opposite effect than one might expect. Flow rate dependence was surprisingly small. The heat transfer coefficients near 100% quality were much lower than equivalent single phase coefficients which led them to suggest that non-equilibrium occurs between the phases. They state also that their temperature measurements with a shielded thermocouple in the exit flow suggests that vapor superheat

may exist in film boiling.

Chi, et al, (15) also noted a non-equilibrium condition in the slug flow chill down process in cryogenic lines. Thermocouple measurements of the vapor slugs showed them to be much hotter than the liquid.

Quinn, Kunsemiller, Sorlie and Hench of General Electric have investigated heat transfer after the critical heat flux in annuli and multirod systems. In correlating their data Quinn (16) has stated that non-equilibrium superheating plays a large roll in developed film boiling. He has broken down the heat transfer process after the critical heat flux into three regions. A transitional boiling region occurs in which nucleate and film boiling alternately take place. It is marked by a fluctuation in the terminus of the annular film upstream of film boiling. The second region is characterized by a thermal vapor boundary layer growth and non-equilibrium superheating of the core flow. The third region, fully developed film boiling, is characterized by further superheating of the vapor and evaporation of dispersed droplets. Little or no evaporation of the droplets occurs at the tube wall in the last two regions. Their treatment of the fully developed region was similar to that of Laverty and Rohsenow (2). A modified form of the Sieder-Tate equation was assumed to be valid for the heat transfer between the wall and the superheated steam. Heat absorption coefficients for the droplets were determined from their

test data, and an average of these values were used in determining the overall heat transfer coefficient.

1.3 Discussion of Laverty's Investigation

Before discussing the purpose and scope of the current study, a more detailed discussion of the Laverty investigation is made here since the results of his work have stimulated this present study. His range of test conditions and his analysis and results provide a starting point for further investigation.

In Laverty's analysis of non-equilibrium film boiling a one dimensional two step heat transfer model is assumed, as shown in figure 2 a. Droplets of local uniform size are assumed to be distributed uniformly across the diameter of the core. Their local axial velocity distribution and the velocity and temperature distributions of the vapor across the core are also assumed uniform. A negligibly thin boundary layer of vapor occurs at the tube wall and is not penetrated by the droplets. The description for the vapor is a fairly accurate one for single phase heat transfer since at very high Reynolds numbers the temperature and velocity profiles are fairly flat except for small region next to the wall where steep gradients occur. Temperature spikes shown in the figure indicate the temperature drop between the vapor and the liquid droplets.

The superheated vapor temperature is determined by a modified form the the Dittus-Boelter equation applied in

the first step of his two step heat transfer model.

$$(q/A)_{meas} = 0.023\ (k_v/D)\ Re_m^{0.8}\ Pr_v^{0.4}\ (T_{w\ meas} - T_v)\ . \qquad (7)$$

The modified Reynolds number contains a throughput velocity, which is in effect the average fluid velocity assuming no slip between the phases.

$$Re_m = (G_T D/\mu_v)\ \left[X_A + (1 - X_A)\ \ (\rho_v/\rho_\ell)\right]\ , \qquad (8)$$

where vapor properties are taken at the superheated vapor temperature and X_A is the actual quality defined by

$$X_A = (Q/W)\ /\ (H_v - H_{\ell\ sat})\ , \qquad (9)$$

where $$H_v = f(T_v,\ P)\ .$$

The last term in the brackets can be neglected in the high quality region for nitrogen since the density ratio is always smaller than 0.01 near atmospheric pressure. The heat transfer coefficient here can be arranged in the more concise form

$$h = 0.023\ (G_T^{0.8}/D^{0.2})\ \ (k\ Pr^{0.4}/\mu^{0.8})_v\ X_A^{0.8}\ . \qquad (10)$$

Since T_v is not explicit in the heat transfer equation, iteration for it is required. Superheated vapor temperature profiles such as the one shown in figure 1 result.

In the second step, the heat going to evaporation of the droplets and superheating of the resulting vapor is obtained by the heat balance

$$Q_e = (q/A)(4/D) - GXC_p\,(dT_v/d\ell) = G(H_v - H_{\ell\text{-sat}})\,(dX/d\ell)\ . \qquad (1$$

Since a sizable slip velocity exists between the droplets and the vapor, the superheating portion of the heat transfer in the second step is considered to occur instantaneously upon mixing with the existing vapor downstream of the droplet. The heat required for evaporation is described by the heat transfer correlation for forced convection about a solid sphere.

$$h\,\delta/k_{vi} = 0.37\ (\rho_{vi}\,\Delta V\,\delta/\mu_{vi})^{0.6}\ . \qquad (1$$

Although a distribution of droplets sizes exists, it is assumed that an average droplet size can represent the distribution. The number of droplets per unit volume is then

$$N = G_T\ (1 - X)/(\pi\,\delta^3/6)\,\rho_\ell\,V_\ell \qquad (1$$

where $$V_\ell = V_v - \Delta V\ .$$

Upon introducing equations 11, 12, and 13, and the surface area per droplet, the heat transfer equation (for evaporation only) becomes

$$Q_e\ (H_{fg}/(H_v - H_{\text{-sat}})) = 2.22\ k_{vi}\ (\rho_{vi}\,\Delta V\,\delta/\mu_{vi})^{0.6}\cdot \qquad (1$$
$$G_T\ (1 - X)\ (T_v - T_{sat})\ /\rho_\ell\,\delta^2\ (V_v - \Delta V)\ .$$

Since equation 14 contains two unknowns, ΔV and δ, the kinematic equation for the droplet is introduced to supply the second equation

$$V_\ell (dV_\ell / d\ell) = 0.75\ C_D \rho_v \Delta V^2 / \delta \rho_\ell \quad - g \ . \tag{15}$$

The third unknown $(d\psi/dx)$ which appears here was estimated from a kinematic analysis of a few typical droplet sizes. It varied between 60% and 100% of $(dV_\ell/d\ell)$ as drop sizes varied between 1 mm and 0.1 mm. Droplet sizes were obtained by simultaneous solutions of equations 14 and 15.

Laverty's experimental test conditions were:

Tube diameter	0.319 inch
Tube length	4 ft
Pressure	$\sim$20 psia
Mass Velocity	70,000 to 210,000 lbm/hr/ft^2
Heat flux	3,000 to 29,000 Btu/hr/ft^2
Maximum exit quality	170%

The two step analysis in the region of applicability (heat transfer coefficients lower than that predicted by the Dittus-Boelter equation) resulted in:

1. Values of actual vapor quality significantly lower than the equilibrium values. At the maximum equilibrium exit quality of 170%, the calculated exit quality was only 80%. Actual quality appears to be asymptotic to 100% at values of equilibrium qualities much greater than 170%.
2. This departure from equilibrium decreases principally with increase in mass velocity and to a small degree with increase in heat flux.
3. Calculated droplet sizes were less than 1 mm in accordance with the size droplets observed in the limited visual

tests.

4. At the same quality, higher heat fluxes produce smaller calculated drop sizes, while higher flow rates, which require longer lengths to produce the same quality, also produce smaller droplets.

In view of the results of Laverty's investigation the following questions arise:

1. Does the Dittus-Boelter correlation best describe heat transfer to single phase nitrogen vapor under these test conditions?

2. What is the extent of non-equilibrium?

3. Can a single phase heat transfer correlation be used to calculate the degree of non-equilibrium in film boiling? In other words, can a single phase correlation in conjunction with a knowledge of the degree of non-equilibrium be used to predict tube wall temperatures?

4. Is tube diameter a weak parameter ($D^{0.2}$) as suggested by the two step theory?

5. How closely do the calculated drop sizes represent the actual average drop sizes?

6. Why is mass velocity an important parameter in regards to the degree of non-equilibrium?

7. Can drop sizes be determined by means independent of the two step theory?

1.4 Objectives and Scope of this Investigation

The objectives of the present investigation are the answers to the questions asked in section 1.3 and form the basis for the following seven part experimental and analytical program.

Experimental

1. Obtain single phase nitrogen vapor heat transfer data to determine the proper single phase heat transfer correlation to be used in film boiling analysis.
2. Extend the range of the film boiling studies well out into the superheating region to determine the extent of the non-equilibrium.
3. Determine the degree of non-equilibrium experimentally, by independent means so that it can be compared with that obtained by heat transfer analysis.
4. Extend the range of tube sizes to determine if there is a significant diameter effect.
5. Determine the actual droplet sizes more accurately.

The range of test conditions for the experimental program is:

Inlet pressure	25 psia
Tube lengths	4 to 8 feet
Tube diameters	0.228 to 0.462 inches
Mass velocity	70,000 to 190,000 lbm/hr/ft^2
Heat flux	5,000 to 25,000 Btu/hr/ft^2

Analytical

6. Further analyze the kinematics and heat transfer to a droplet to determine the effect that both heat and mass flux have on the degree of non-equilibrium.

7. Determine means for predicting the actual droplet sizes.

CHAPTER 2

DISCUSSION OF PRESENT INVESTIGATION

2.1 Single Phase Heat Transfer Correlations

Even when it is assumed that no liquid penetrates to the wall in the first step of the heat transfer process, there is the question as to whether or not a single phase correlation can be used to predict the vapor temperature and the quality. Investigators (17, 18) in two phase flow have shown that in isothermal two-phase annular-dispersed flow, the presence of liquid radically alters the vapor velocity profile. Laminar type profiles result even when Reynolds numbers indicate a turbulent flow. This may have an effect on the heat transfer coefficient.

In addition, many single phase correlations other than the Dittus-Boelter correlation appear in the literature and might be equally applicable for determining the departure from equilibrium. Sizable differences between the various correlations would lead to uncertainty in the estimates of the vapor temperature. In view of this second question, five other correlations in general usage were chosen for comparison. They are listed below in a form comparable to equation

Dittus-Boelter (film properties)

$$h = 0.023 \left(G_T^{0.8}/D^{0.2}\right) \left(kPr^{0.4}/\mu^{0.8}\right)_f X_A^{0.8} \left(\rho_f/\rho_b\right)^{0.8} . \quad (16)$$

Desmon-Sams (for large $(T_w - T_b)$ with air), (19)

$$h = 0.20 \, (G_T^{0.8}/D^{0.2}) \, (kPr^{0.4}/\mu^{0.8})_b X_A^{0.8} \, (\rho_f/\rho_b)^{0.8} \, (\mu_b/\mu_f)^{0.8}, \quad (17)$$

Colburn (19)

$$h = 0.023 \, (G_T^{0.8}/D^{0.2}) \, (kPr^{0.33}/\mu^{0.8})_b X_A^{0.8} \, (\mu_b/\mu_f)^{0.467}, \quad (18)$$

Sieder-Tate (19)

$$h = 0.027 \, (G_T^{0.8}/D^{0.2}) \, (kPr^{0.33}/\mu^{0.8})_b X_A^{0.8} \, (\mu_b/\mu_w)^{0.14}, \quad (19)$$

Simoneau-Hendricks (for air), (20)

$$h = 0.0042 \, (G_T^{0.8}/D^{0.2}) \, X_A^{0.8} \, (T_b/T_w)^{0.5}. \quad (20)$$

As an example of the variation between the correlations in evaluating the departure from equilibrium, the six are compared in figure 3 in a plot of predicted heat flux versus vapor temperature for the operating conditions of station 13 of the film boiling run 260 of the present study. This low mass velocity run was chosen so that a larger non-equilibrium effect could be seen. In addition the station chosen represents the point where approximately 100% equilibrium quality exists, thus serves well as a point from which the departure from equilibrium quality can be compared. The actual quality in figure 3 is related to the vapor temperature by the heat balance

$$X_A = X_E / \left[C_p \, (T_v - T_{sat})/H_{fg} + 1.0 \right]. \quad (21)$$

All the correlations except the Desmon-Sams correlation predict heat fluxes much higher than the measured heat flux of

10150 But/hr/ft^2 when equilibrium conditions (T_v = 148^{o}R) are assumed. Only at higher vapor temperatures (lower actual qualities) does the predicted heat flux match the measured, but there is a considerable spread in vapor temperature (100 R^o) for the various correlations at the intercepts. Note that the Desmon-Sams and the Dittus-Boelter correlations are double-valued due to the large variation in the viscosity and density ratios. Since the purpose of using property ratios evaluated at various temperatures is to shift the predicted temperature profiles (or heat flux curves in figure 3), but not distort them, it appears that if property ratios are to be used, they must be used with care. The Dittus-Boelter (film) correlation was abandoned for this reason by Laverty in favor of the standard Dittus-Boelter correlation. The differences in actual quality predicted by the first five correlations is rather small in this case although a sizable calculated vapor temperature variation exists.

As a further test of the applicability of a single phase correlation to predict the actual quality and vapor temperature, the hydrogen film boiling data of reference 11 was tested. The results of using the Dittus-Boelter and Simoneau-Hendricks correlations along the entire length of the test section for their high quality run 22-3 are shown in figure 4 . At the end of the tube a difference of over 100 degrees results, but more significant is the large

difference in actual quality. Also, the variation in quality along the tube doesn't appear reasonable since it decreases along the tube instead of increasing. The third actual quality line paralleling the equilibrium quality line was obtained from a kinematic-heat transfer analysis of the droplets in the core flow, which is discussed in more detail in section 2.4.

These two studies point out the fact that an arbitrary choice of one of the conventional single phase correlations for use in predicting the departure from equilibrium should not be made, unless the correlation has been confirmed with single phase vapor heat transfer data for the fluid in question in the same range of test conditions.

Tests In order to select an adequate correlation for use in this study, heat transfer tests were run on test section #1 with pure nitrogen vapor supplied from a pressurized bottle at room temperature. A description of the experimental apparatus is given in Appendix A. Ideally, the bulk temperature of the vapor should be as close to the saturation temperature as possible so that large wall to bulk temperature ratios may be obtained. However, the length required for the development of the thermal boundary layer precludes obtaining fully developed thermal data at such low temperatures. Since nitrogen vapor is a well behaved gas, the heat transfer property ratio ($k\ Pr^{0.4}/\mu^{0.8}$) varying little over a wide range of temperatures (figure 28),

the use of higher temperature nitrogen in these tests was considered a valid procedure.

Results The results of six tests for flow rates between 40,000 and 120,000 lbm/hr/ft^2 and heat fluxes between 3000 and 10,000 Btu/hr/ft^2 are shown in figure 5 in the standard form $Nu/Pr^{.4}$ vs Re and are also tabulated in Table I. The method for reducing the data is described in Appendix B . It was found that the fully developed data for the downstream half of the tube correlated best when bulk properties were used. The resulting correlations are given by

$$Nu_b = 0.035\ Re_b^{0.743}\ Pr_b^{0.4} \quad , \tag{22}$$

or

$$Nu_b = 0.019\ Re_b^{0.8}\ Pr_b^{0.4} \quad , \tag{23}$$

when the exponent 0.8 is retained, which is about 18% lower than that predicted by the Dittus-Boelter equation. Equation 22 is considered to be the proper one to use in the analysis of film boiling data of this study.

2.2 Film Boiling Tests

The film boiling tests can be subdivided into the following several series of tests.

1. q/A vs ΔT data and visual observation of flow issuing from the exit of the 4 foot long, 0.323 inch ID test section. The test conditions for these runs were limited to mass velocities of 70,000; 130,000; and 190,000 lbm/hr/ft^2 and average heat fluxes ranging in steps of 5000 Btu/hr/ft^2 up to 25,000. The purpose of these runs is to obtain visual observations of the droplets in the same basic range of test conditions of Laverty's investigation, as well as to check the apparatus and experimental technique against his.

2. q/A vs ΔT data and visual observations with an 8 foot long, 0.323 inch ID test section. Tests were run at the same mass velocities and electrical current settings as in the first series so that this series of runs would constitute an exact extension of the runs in the first series, well out into the superheating region. The purpose of these experiments was to, 1) obtain q/A vs ΔT data further out in the superheating region, 2) obtain visual observation of the droplets issuing from the test section, and 3) to find out the point at which the droplets are completely evaporated.

3. q/A vs ΔT data and visual observations with 8 foot tubes of 0.228 and 0.462 inch ID. The purpose of this series is to test the two step theory as regards the influence of tube diameter. Since it is the heat transfer mechanism in

the core flow which governs the degree of non-equilibrium, the degree of non-equilibrium calculated via a single phase type heat transfer correlation should be the same.

4. Experimental measurement of the actual quality. A helium injector-probe system is used in this series of repeated runs to determine the actual quality existing at the tube exit. This data is to be compared with the actual quality predicted by a single phase correlation.

Results of Film Boiling Tests

2.2.1 Heat transfer data The tube wall temperature profiles obtained for all the tests with the four test sections are shown in figures 6 through 12 . These are outside wall temperatures, but differ very little from the inside wall temperatures ($\Delta T < 4^{\circ}R$). The data of both the long and short 0.323 inch ID tube is shown in the same figures since the data for the long tube is an extension of the data for the short tube. The heat fluxes indicated in these figures are only approximate since a variation in heat flux occurs along the tubes as discussed in Appendix B. The actual local values of heat flux, inside wall temperature and equilibrium bulk temperature are given in Table II. Shown also in the figures are the asymptotic values of tube wall temperature that would result if equilibrium conditions existed from the point where 100% equilibrium quality occurs. These asymptotes were calculated by the use of equation 22 which was found to best describe the single phase heat trans-

fer tests in this study. It can be seen that the film boiling temperature profiles are asymptotic to these values. The location of 100% equilibrium quality is indicated by arrows above each profile.

2.2.2 Comparison with Laverty's data The tube wall temperature profiles for the short test section are in agreement with those of Laverty, except near the entrance of the test section and at the higher mass velocities. At a mass velocity of 210,000 lbm/hr/ft^2, Laverty observed the strange temperature profile behavior depicted in figure 13 This phenomena was not observed in this study; the temperature profiles were always monotonic in the quality region, except very near the test section entrance. This discrepancy is probably due to a difference in inlet flow conditions, since different inlet control valve assemblies were used. Since this abnormal condition did not appear in any of the tests with the various tube diameters in this study, with and without the helium injector in place (see Appendix A), it is thought that it might be due to a swirl flow generated in his valve assembly.

A second phenomenon not observed in the present study was the persistant slug like flow of groups of dispersed droplets that were experienced by Laverty. It was found that when pressure fluctuations in the test section were minimized, the distribution of the droplets issuing from the test section exit was fairly uniform with time. Pressure

fluctuations could be minimized by providing sufficient inlet subcooling in order to prevent vapor locking in the inlet control valve, and by maintaining film boiling in the exit lines so that flooding could not occur downstream of the test section.

2.2.3 Visual studies The results of the visual study with a short electrically heated glass section at the test section exit are reported at the bottom of Table II . These observations were made by eye with the aid of a high intensity strobe light and by microflash photography. In all but three runs, droplets were seen to issue from the test section exit. The runs in which the liquid was barely detectable or where no liquid was seen are indicated in the temperature plots by the symbols B.D.L. and N.L respectively. It is seen that in these cases the exit end of the tube wall temperature profile agrees very well with the asympote except in the case of run 292. These points for near or complete evaporation are plotted in figure 14 in terms of the equilibrium exit quality as a function of mass velocity. The exact location for complete evaporation is rather difficult to observe since it is sensitive to the small fluctuations in flow and would require a more closely spaced series of runs; therefore both points are plotted in the figure. It is seen that complete evaporation, hence the departure from equilibrium is a strong function of mass velocity. If an extrapolation can be made in the figure, it indicates that

near-equilibrium can only be obtained at mass velocities above 500,000 for nitrogen. Power requirements precluded obtaining complete evaporation data for the large diameter tube. A slight diameter effect appears here; smaller diameter tubes are closer to equilibrium.

Some of the better photographs of the droplets issuing from the 0.323 inch ID tube are shown in figures 15, 16 and 17. The photos in figure 17 were taken during the tests with the long tube. Those in figures 15 and 16 were taken during duplicate tests with a helium concentration probe in place. This particular probe had an additional five inches of heated tube length, consequently differences in heat and mass flux and exit quality occur. However the size and quantity of the droplets are very similar to those noted in the tables. There are no equivalent runs reported in the tables for figures 15C and 17C since film boiling is unstable at these conditions and can be maintained only for a short while. The droplets were illuminated by reflecting the microflash light off a white background behind the glass section. In figures 16a,d and 17d,e a black background was used which provided more contrast to the light reflecting from the small droplets; but in these cases the boundary of the droplets cannot be determined.

The photos are arranged in groups of three, with each group at approximately the same heat flux, so that the striking dependence of drop size on vapor acceleration (or heat

flux for a particular tube diameter) can be shown. At a given heat flux, the droplet sizes are approximately the same for all mass velocities. Heat fluxes from 5,000 to 20,000 are shown for the short test section. Only the lower two heat fluxes are shown for the long test section since the higher heat fluxes over the longer length produce droplets too small to be photographed.

If the departure from equilibrium and minor effect that the two phase void fraction has on vapor velocity are neglected for the moment, one can see that the same vapor velocities and accelerations exist for the same heat flux though total mass fluxes may differ. Under these conditions, the existing liquid should experience the same degree of spray formation and similar drop sizes should result for any amount of liquid present. At higher mass fluxes, the droplet size should be about the same but there will be more of them. When non-equilibrium is present in boiling of cryogenics, vapor velocities are higher than those based on equilibrium although the amount of vapor generated is less. This is due to the large gas density variation with temperature at cryogenic temperature levels. The vapor momentum flux however, varies very little with departure from equilibrium (see curves for $V_\ell / V_v = 0$ in figure 22). Since it is the vapor momentum initially which is reflected in the Weber number which governs the droplet sizes, little difference in droplet size should occur with the variation in the departure

from equilibrium from one mass flux to the next. The foregoing argument has been substantiated in the results of a kinematic heat transfer analysis of the core flow, which is presented in section 2.4.

A plot of the drop sizes taken from figures 15 and 16 is shown in figure 18 along with the mean effective drop sizes calculated by Laverty (3) . The most prominent drop size and the spread are indicated by open symbols and vertical lines respectively. The agreement between the two is extremely good considering the assumptions that were required in Laverty's kinematic and heat transfer analysis of droplets. The larger droplet sizes could be determined fairly well from the enlarged photos with the use of a plastic scale scribed in approximately 1/3 mm. The smaller droplets sizes had to be estimated.

2.2.4 Calculated quality Since equation 22 predicted the asymptotic values very well and the location of these values were in agreement with the visual observations, this equation was used to predict what the degree of non-equilibrium might be. To take into account the variation in actual vapor flow rate, the equation was modified to include the actual quality in the Reynolds number. The resulting equation,

$$(hD/k_{vb}) = 0.035\ (G_T\ X_A\ D/\mu_{vb})^{0.743}\ Pr_b^{0.4}\ , \qquad (24)$$

was used in the heat transfer equation,

$$q/A_{meas} = h(T_w - T_{vb}) \quad , \tag{25}$$

along with the heat balance,

$$T_{vb} = (h_{fg}/C_p) \cdot (X'_E - X_A)/X_A - T_{sat} \quad , \tag{26}$$

to iterate for the actual quality. These values for actual quality are shown in figure 19 as a function of the equilibrium quality. The highest and lowest heat fluxes for each mass velocity and tube diameter are shown in the figure.

The departure from equilibrium appears to be chiefly dependent on the mass velocity. The influence of heat flux and tube diameter is small; higher heat flux data are closer to equilibrium, while smaller diameter data are farther from equilibrium. The latter trend is contradictory to the visual observations, however the differences are small. The single phase correlation developed in this study was not tested for variation in tube diameter and may be the reason for this discrepancy.

Shown also in figure 19 is the approximate location of complete evaporation taken from figure 14.

2.3 Measurement of non-equilibrium Techniques

In the experimental program to determine the degree of non-equilibrium existing in the dispersed flow film boiling the following methods were considered:

1. Direct measurement of vapor temperature

2. Measurement of momentum flux

3. Measurement of pressure drop

4. Measurement of liquid fraction and velocity

5. Separation and measurement of flow rate of each phase

6. Tracer gas technique to determine vapor flow rate

Of the six, the tracer gas technique was found to be the most reliable or the most expedient.

Before discussing the tracer gas technique in more detail, the difficulties involved in making the measurement of non-equilibrium with the other techniques are reviewed here.

2.3.1 Direct measurement of vapor temperature In the direct measurement of the average superheat in the vapor, either a single temperature measurement should be made on a liquid free, well mixed flow of vapor, or temperature profile measurements should be made in the two phase flow providing the measuring device is shielded from the liquid. In the first case there is the difficulty of separating the liquid in a manner such that the non-equilibrium nature of the flow is preserved. The separator must produce a sufficient amount of separation with as little mixing of the two phases as possible in as short a time as possible. However, there doesn't appear to be a device that meets these requirements. A simple U tube separator in which the liquid is supposed to be centrifuged to the outer walls was considered and tested. It was found however that this

device suffers from secondary flow effects which drive a larger part of the liquid to the inside walls of the tubes. A sketch of this observation is shown in figure 20. The thickness of the liquid film clinging to the tube wall is indicated by the diagonal terminus of the burnout location in the heated portion of the U tube. A similar liquid concentration was observed with droplets during startup when a dry wall condition still existed in the unheated portion of the U tube. A twisted tape swirl separator and cyclone separators were also considered but they too would suffer from secondary flow effects and would generate a large amount of mixing. Since rapid separation appeared unreliable, no further consideration was given to measuring the temperature or flow rate of the vapor phase.

In the second case, a thermocouple suspended in a two plase flow must be shielded from the liquid droplets, otherwise it will become coated with liquid, thus producing a saturation temperature reading. At higher qualities and/or high non-equilibrium vapor superheats, a film boiling condition may exist at the thermocouple, in which case heat is exchanged from the superheated vapor to the liquid droplets via the thermocouple surface. Under these conditions, the thermocouple will read a temperature somewhere between the saturation and superheated vapor temperature. Both these conditions were noted with a bare stationery thermocouple located in the visual section downstream of the long test

sections used in this study. This thermocouple was intended to be used only when little or no liquid was present to indicate the accuracy of the heat balances. Readings for all the runs however were taken and are reported in table II.

Early in the experimental program, an attempt was made to get a measurement of the vapor temperature with the aid of a suction thermocouple. This temperature probe (figure 21) contained a constantan wire stretched axially within a 0.090 inch stainless tube to support a Cu-Cn junction located between two entrance ports for the vapor. A cone shaped teflon baffle was provided upstream of the ports to deflect the liquid away from the probe. The length of tubing upstream of the junction was necessary to prevent conduction effects in the constantan support wire. The vapor flow rate into the probe was controlled by a valve downstream of the probe. The probe was supported in the exit tube by a teflon spider further downstream. Since the structural and thermal requirements dictate such a relatively large probe, it could not be used to traverse the diameter.

The results of this preliminary work for mass velocities between 70,000 and 130,000 and equilibrium exit qualities between 80% and 140% are also shown in the figure. The open symbols represent the highest temperatures measured during rather large temperature fluctuations that occurred at low or zero suction probe flow rates. The results indi-

cate that non-equilibrium does exist in the tube, but the vapor temperatures are not as high as those predicted by heat transfer analysis using the modified Dittus-Boelter equation. The results do show however that higher mass velocities tend towards equilibrium. The darkened symbols represent the fairly steady temperature readings taken at higher or maximum probe flow rates.

The reason for the large discrepancy between the predicted and measured temperature is probably due to the probe sampling the colder vapor boundary layer spilling over the baffle. At higher probe flow rates some of the liquid spilling off the baffle enters the probe, thus lowering the temperature even more. The fluctuations at the lower flow rates are probably due to purging of the probe caused by test section pressure fluctuations. The baffle used here is probably too large and presents too much "capture" area for the droplets. Since this method appeared to be unreliable, no further work was done with it.

2.3.2 Measurement of momentum flux When there is a departure from equilibrium there will be a difference in the momentum flux of both the liquid and vapor. The momentum fluxes for one dimensional flow are,

$$M_{vapor} = G_v V_v = G_T X_A V_v = G_T^2 X_A^2 / \rho_v \qquad (27)$$

where $V_v = G_T X_A / \rho_v$, neglecting the effect of holdup on velocity, and

$$M_{liquid} = G_\ell V_\ell = G_T (1 - X_A) V_v (V_\ell / V_v) = (G_T^2 X_A / \rho_v) \cdot (1 - X_A) (V_\ell / V_v) . \quad (28)$$

When the perfect gas law, $\rho_v = RT_v/P$, is applied along with the heat balance equation for the vapor temperature

$$T_v - T_{sat} = H_{fg} (X'_E - X_A)/C_p X_A , \quad (29)$$

the total momentum flux becomes

$$M_A = G^2 RT_{sat}/P \left[(H_{fg}/C_p T_{sat}) (X'_E - X_A) + X_A \right] \cdot \left[X_A + (1 - X_A) (V_\ell / V_v) \right] . \quad (30)$$

This equation can be normalized by dividing it by the total momentum flux that would occur for equilibrium conditions ($X_A = X_E$). The variation in this ratio, $(M_A/M_E)_{total}$, with departure from equilibrium is shown in figure 22 for various equilibrium qualities , X'_E, and liquid to vapor velocity ratios. The curves in the figure terminate at the maximum departure from equilibrium predicted for the tests in this study so that the maximum variations can be readily seen.

The vapor momentum alone (represented by the solid lines where $V_\ell / V_v = 0$) varies very little (15% maximum) and also is ambiguous at smaller amounts of non-equilibrium; consequently measurement for it with a Dussord type probe (21) would be dubious. A sufficient variation in total momentum flux exists for velocity ratios greater than 0.5, so that total

thrust measurements might be made on the flow. The difficulty here is that the average liquid velocity must be known and this would involve a second experiment such as high speed photography to determine it. This technique would require examining distributions of droplet sizes and velocities to arrive at a proper average velocity; a very tedious operation. The dual measurement of liquid fraction and velocity was abandoned also for this reason.

2.3.3 Pressure drop measurements

The use of static pressure drop to indicate the degree of non-equilibrium also suffers the same difficulty as does the momentum flux thrust measurement; a knowledge of the average liquid velocity is necessary for the momentum flux terms in the expression for pressure drop. In addition, an accurate method for determining the friction portion of the pressure drop is needed. Since this must be integrated along the tube, a functional form for the departure from equilibrium would also be required. The estimated values for frictional pressure drop are relatively large for the conditions of this study, thus further compromising the use of pressure drop to indicate the degree of non-equilibrium. An example of the values of the calculated equilibrium and non-equilibrium pressure drops and measured pressure drops experienced in this study is listed below. In this example (Run 261), the friction factor and the two phase factor ϕ^2 were determined by the methods sug-

gested by reference 22 (as reported in 19) and reference 23 respectively. A velocity ratio of 0.5 was assumed. The predicted pressure drops for the non-equilibrium case are shown in parentheses.

Tube length (inches)		48		96	
ΔP measured - psi		1.54		5.52	
ΔP calculated - psi		1.129	(1.426)	5.079	(5.961)
ΔP momentum	% of calculated value	72%	(61%)	57%	(48%)
ΔP hydrostatic	% of calculated value	7%	(6%)	2%	(2%)
ΔP friction	% of calculated value	21%	(33%)	41%	(50%)
Average ϕ^2		1.5	(2.0)	1.1	(1.4)

That an accurate knowledge of the liquid velocity is mandatory, even in the case where frictional contributions are negligible, is pointed out in figure 23 which is based on an analysis of the pressure drop data of reference 11 In this analysis both the equilibrium and the non-equilibrium (predicted by Dittus-Boelter equation) cases depicted in figure 4 were considered for two velocity ratios. If the velocity ratio V_ℓ/V_v is 0.5, little difference in pressure drop results while a large difference exists for homogeneous flow. The discrepancy in the equilibrium homogeneous flow pressure profiles calculated in this analysis and in the analysis of reference 11 is due to neglecting the variation in the saturated liquid enthalpy with pressure. It was taken into account in the present study to arrive at the data in figures 4 and 23.

A kinematic heat transfer analysis (described in section 2.4) on the core flow for this run indicates that the velocity ratio is greater than 90% over most of the tube length, so it would appear that a near-equilibrium, homogeneous process occurs in the tube. This being the case, it can be inferred that the variation in saturated liquid enthalpy with pressure along the tube should not be considered since the dashed line (no variation in $H_{\ell\text{-sat}}$) represents the measured data better. This is reasonable since the time required for a droplet to lose the required amount of saturation enthalpy is much greater than the transit time of the droplets ($\sim$0.003 sec.). To lose approximately 80% of the required amount of enthalpy the transit time must be greater than approximately 0.2 second, assuming a solid sphere model for the droplets.

It is obvious from the foregoing that pressure drop techniques are not reliable for determining the departure from equilibrium.

2.3.4 Helium gas tracer techniques

The helium gas tracer technique for determining the vapor quality has the advantage that it will give a better average measurement than a temperature measurement. Since the flow is turbulent and helium is a very mobile gas, and since evaporation is assumed to occur uniformly in the core flow only, a fairly uniform concentration of helium gas should appear across the flow area. As in the measurement of vapor

temperature, the liquid must be separated before entering the concentration probe. This is not quite as difficult in this case since the concentration probe and baffle can be made much smaller so that less liquid is captured by it, and the probe itself can operate at any temperature, providing it meets the requirements of separation.

In this study the two concentration probes employed are discussed in Appendix A , and shown in figures 40 and 41. The stationary probe (probe #1) was used in some preliminary work with the 4 foot test section to evaluate the merits of this technique. In this earlier work it was assumed that the helium concentration was uniform across the tube so that the exit quality could be obtained simply by the ratio of the concentration of helium based on the entire flow to the concentration measured at the test section exit.

$$X_A = \frac{C_B}{C_A} \tag{31}$$

The results of these tests for a variety of nitrogen mass velocities and equilibrium exit qualities is shown in figure 24 along with data of probe 2. As in the tests with the thermocouple probe it was found that a variation in the measurement of concentration occurs with probe suction flow rate. The effect however is in the opposite direction; a higher concentration of helium or greater departure from equilibrium is indicated at higher probe flow rates.

It is suspected that this is due to sampling the helium-poor boundary layer about the probe at low probe flow rates. At higher probe flow rates the vapor outside the boundary layer is probably sampled. This effect is however extremely small for the lower nitrogen mass flux of 70,000 lbm/hr/ft^2. Because of this, the concentration measurements at the lower mass flux are considered more reliable. Although less reliable, the higher mass flux data in general does exhibit the trend toward equilibrium.

As a check on the uniformity of the concentration across the tube, concentration measurements were made with a traversing probe (probe #2). Similar difficulties were also experienced with the traversing probe at the higher flow rates; occasionally no helium was detected, which indicated that a wet probe condition existed. The lower flow rate concentration data however was reproducible and it was consistant with the center line data of the stationary probe. Typical concentration ratio profiles, $C_A\ (r)/C_B$, are shown in figures 25 and 26 for the lower mass velocity of 70,000. These profiles are not as uniform as was originally desired, however they do not differ too radically from uniformity and can generally be described by

$$C/C_{\text{℄}} = (1 - r/ro)^n \quad \text{where } n = 1/7 \text{ or } 1/9 \ . \tag{32}$$

The reasons for the non-uniformity are two-fold. Firstly, the evaporation rate is not uniform across the diameter;

greater amounts of evaporation occur near the tube wall where a higher concentration of droplets and a higher vapor temperature exists. The helium is diluted in this region more rapidly than it can be replaced by diffusion and mixing. Secondly, it is more difficult to prevent the higher concentrations of liquid from entering the probe in this region. The occurance of larger amounts of liquid near the walls can be inferred from the data of figures 25 and 27 where the probe port was facing the oncoming liquid. It was first thought that the location of the helium injector might influence the shape of the profile, but it was found that the location of the injector port made little difference in a preliminary test with low probe flow rates (figure 27).

If the appropriate integrations (Appendix C) are made with the 1/9 power-law-concentration-profiles along with assumed velocity and temperature profiles represented by 1/3 to 1/7 power laws, the actual quality will be between 10 to 15% larger than the quality calculated by using the maximum measured concentration in equation 31. The use of the 1/3 power law for velocity is prompted by the fact that turbulent two phase flows can have laminar type velocity profiles. Since this increase is small and probably compensates for the inefficiency of separation, the maximum value of measured concentration is taken to be a reasonably good measurement of the vapor quality.

Concentration data was also taken with the traversing probe on both the 0.323 and 0.462 inch ID, 3 foot test sections for an equilibrium exit quality of 100% and a mass flux of 70,000 lbm/hr. The results of these runs agree favorably with the concentration data taken with the short test section, thus confirming the results of figure 19, that the departure from equilibrium is principally a function of the mass flux.

Shown also in figure 24 is the curve for exit qualities predicted by the heat transfer analysis for the mass velocities tested. The measured values for G = 70,000 are in good agreement with the predicted values.

2.4 Core flow analysis

Since the droplet sizes predicted by Laverty (figure 18) are in agreement with those from the visual observations, it is evident that his kinematic-heat transfer analysis of the core flow has merit. The difficulty with Laverty's analysis is that it cannot be used in working backwards to get the wall temperature, since the vapor temperature gradient is difficult to predict at a particular point in the tube. The obvious reason for this difficulty is that the kinematic-heat transfer equations should be integrated along the tube, not just evaluated at each location along the tube. Some successful results of integrating the kinematic-heat transfer equations is reported by Kearsey (24) in his analysis of post burnout heat transfer with water. As in Laverty's analysis Kearsey worked back through a two step process from the tube wall temperature to get an initial droplet size that would occur just after burnout. The variation in this drop size along the length of the tube was governed by the rate of evaporation only. His calculations involved the optimization of the initial drop size so that the calculated axial tube wall temperature matched the measured temperatures. The difficulty of knowing before hand what effective mean drop size to use still remains. Since the droplet sizes observed in this study are dependent on the vapor acceleration rate (heat flux), a critical Weber number criterion for droplet size might be a valid addition

to a kinematic heat transfer analysis.

In the following analysis, kinematic and heat transfer equations similar to those used by Laverty along with a heat balance equation for the entire flow and continuity equations for the liquid and vapor are integrated along the tube. The significant modification in the calculation is the assumption that the droplets continually breakup to a size determined by a critical or maximum magnitude of a Weber number.

Heat transfer Laverty assumed a solid sphere model in his analysis and obtained from McAdams (25) the heat transfer correlation

$$(h\,\delta/k_f) = 0.37\ (G\,\delta/\mu_f)^{0.6}\ , \tag{33}$$

which he modified to

$$(h\,\delta/k_{vi}) = 0.37\ (\rho_{vi}\,\Delta v\,\delta/\mu_{vi})^{0.6}\ , \tag{34}$$

since it was thought that the properties should be evaluated at the colder evaporating interface. The error involved in using the interface temperature instead of the film or bulk temperature is not too great (20%) if the density in the term for mass velocity is to be evaluated at the same temperature at which k and μ are evaluated (see figure 28)

Many other correlations for heat transfer to spherical particles are reported in the literature. Tsubouchi and Sato (26) have reviewed a considerable number of these

correlations in regard to correlating their data on convective heat transfer from very small near-spherical (δ =.6 mm) thermistors in air. They found that their data was best correlated over a wide range of Reynolds numbers ($0.3 < Re < 3000$) by modifying Froessling's correlation for mass transfer from evaporating droplets (27)

$$Sh = 2.0 + 0.55\ Re^{0.5}\ Sc^{1/3}\ , \tag{35}$$

to

$$(h\delta/k_f) = 2.0 + 0.55\ (V\delta/\nu_f)^{0.5}\ Pr_f^{1/3} \tag{36}$$

by invoking the analogy between heat and mass transfer. Most other correlations are in form of equation 36 with various coefficients ranging from 0.19 to 1.18. Elzinger and Banchero (28) have found that heat transfer between dispersed liquid droplets in liquid can be correlated by Kramer's correlation (29)

$$Nu = 2.0 + 1.3\ Pr^{0.5} + 0.66\ Pr^{0.31}\ Re^{0.5}\ , \tag{37}$$

when the droplet viscosity is larger than the viscosity of the continuous phase. This correlation agrees closely with equation 36 and with that of Ranz and Marshal(30)

$$Nu = 0.60\ Re^{0.5}\ Pr^{1/3}\ , \tag{38}$$

for heat and mass transfer to evaporating droplets. Although equation 34 agrees moderately well with these other equations in the range of Reynolds numbers (50 to 4000) encountered in this study, Tsubouchi and Sato have found however that the exponent 0.6 is too steep and does not follow

the trends of their data.

The selection of the proper temperature at which the vapor properties are to be evaluated is less serious when the exponent 0.5 is used for the Reynolds number. If film or bulk temperature are to be used for all the properties, the property term differs negligibly from that evaluated at the saturation temperature (figure 28). If the bulk density is to be used in the term for G when film properties are used, a maximum variation of approximately 20% in the property term can occur.

In this study, these heat transfer correlations are used in the heat transfer equation for the droplet

$$Q = h \Uparrow \delta^2 \, (T_v - T_{sat}) \, , \tag{39}$$

where T_{sat} is evaluated at the local pressure in the tube.

Kearsey has used the method of Ryley (31) in arriving at the heat transfer rate to the droplets.

$$q = h \Uparrow \delta^2 \, (T_v - T_s) \, , \tag{40}$$

where the T_s is the elevated temperature of the liquid droplet caused by the "total" pressure rise required in the neighborhood of the droplet to produce diffusion of the resulting vapor away from the droplet. This is evaluated by relating the total heat flux to the droplet to the energy flux carried by the diffusing vapor away from the drop

$$2 \, K_d \, \frac{(P_s - P_v)}{RT} \, h_{fg} = 2K \, (T_v - T_s) \, , \tag{41}$$

where P_s is obtained from the saturation temperature-pressure relationship.

This diffusion resistance however is found to be negligible for nitrogen; $(T_s - T_{sat})/T_v - T_s)$ is in the range of 1 to 5% for the superheated vapor temperature experienced in this study, consequently this resistance is neglected. The heat transfer coefficient used by Kearsey was obtained from the equation

$$Nu = 2F \ ,$$

where F is Froessling's ventilation factor ($1.0 + 0.276 \ Re^{1/2} \ S_c^{1/3}$) for mass transfer from spheres subjected to forced convection (equation 35).

Droplet evaporation rate By relating the heat transfer rate to the evaporation rate of the droplet, the change in droplet size with time or distance can be obtained by

$$d\delta/dt = V_\ell \ (d\delta/d\ell) = (2/h_{fg} \rho_\ell \ \delta \ ). \\ k \left[2.0 + C \ k \ (\rho \Delta V \delta/\mu)^{\alpha}\right](T_v - T_{sat}) \ . \qquad (42)$$

Kinematics Equation 15 is used here

$$dV_\ell/dt = V_\ell \ (dV_\ell/d\ell) = (3C_D \rho_v/4\rho_\ell \ \delta \ ) \ \Delta V^2 - g \ . \qquad (43)$$

Laverty used a value of 0.5 for the drag coefficient. This is a reasonable average value for a solid sphere for the

droplet Reynolds number range in his experiments. Kearsey has used the drag coefficient suggested by Ingebo (32)

$$C_D = 27/(\rho_v \Delta V \delta/\mu)^{0.84} \quad (4 < Re < 500) \ . \tag{44}$$

In the Reynolds number range of interest (50 to 5,000) this equation predicts drag coefficients that are much lower than the standard values of C_D for a solid sphere (figure 29). This drag coefficient was developed from measured acceleration rates ($\frac{dV}{dt} \geq 6000$ ft/sec^2) for small evaporating and non-evaporating particles ($\delta \leq 100$ microns) entrained in a constant velocity air stream ($V \leq 180$ ft/sec). The standard coefficient of drag for a solid sphere in steady flow shown in figure 29 might also be used.

Variation in quality The variation in quality along the tube can be taken from

$$\frac{dX}{d\ell} = - \frac{(1-Xo)}{\delta o^3} \ 3\delta^2 \ \frac{d\delta}{d\ell} \ , \tag{45}$$

when it is assumed that the number of droplets flowing along the tube remains constant. Xo and δo are known values of quality and drop size at particular location in the tube. When the drops are allowed to break up into smaller droplets, Xo and δo take on the local values of the known quality and droplet size immediately after breakup.

Vapor temperature gradient The vapor temperature gradient is taken from the heat balance

$$(q/A)\pi D = (G\pi D^2/4)\ (h_v - h_{\ell\text{-sat}})\ dX/d\ell + X(G\pi D^2/4)\ Cp_v dT/d\ell \ . \tag{46}$$

In terms of the equilibrium quality gradient $dX'_E/d\ell$

$$dT/d\ell = \frac{dX'_E/d\ell - \left[1-(C_pT_{sat}/h_{fg}) + (C_p/hfg)T\right] dX/d\ell}{X(C_p/h_{fg})} \ . \tag{47}$$

Vapor velocity The vapor velocity is obtained by

$$V_v = (GX/\rho_v)\ \left[1 - G(1 - X)/\rho_\ell V_\ell\right]^{-1} \tag{48}$$

where the term in the brackets is the vapor void fraction.

Droplet breakup process A critical Weber number criterion is used to define the points at which the droplets are split in two. When the droplet Weber number, $We = (\rho_v \Delta V^2 \delta/\sigma)$, exceeds a critical value, the droplets are split in two. This can occur anywhere in the tube.

Integration The three differential equations 43, 45, and 47 are integrated by a single step finite difference method. The length of the interval over which the three gradients are projected is set by a variety of limitations so that a well behaved integration occurs. Typical interval lengths are in the range of one inch or less.

Starting point for integration The calculations are started at an arbitrary value for the equilibrium quality X_{E_o} that occurs at a particular point along the tube. Equilibrium conditions are assumed at this point and upstream of it.

The typical values of X_{E_o} used in this analysis are between 5 and 15%, which is reasonable, considering that dispersed flow film boiling begins around these values. The initial droplet size and velocity occuring at this point is determined by iterating for a slip velocity that will produce a net droplet acceleration of zero, for a droplet size that is consistant with the critical Weber number. In other words, the integration starts with a droplet which has a particular positive velocity but no net acceleration and which is on the verge of breaking in two. The technique for arriving at this condition is to start with a liquid-to-vapor velocity ratio close to unity. The continuity equations are solved to get the vapor and liquid velocities and their difference. The slip velocity is applied to the critical Weber number to get a critical droplet size which is then applied to the drag equation. If the net acceleration is less than zero, the velocity ratio is reduced to a point where the net acceleration is sufficiently close to zero. It may also be necessary to increase the initial arbitrary value of X_{E_o} when the velocity ratio is too close to the unrealistic value of zero.

Results of core flow analysis The objective of this analysis is to see if the calculated and measured qualities depicted in figures 19 and 24 can be predicted by analysis of the core flow. Since many parameters, G, q/A, the choice of We_c, the heat transfer coefficient, and the drag coefficient, are

involved in this analysis, each parameter is varied separately in order to evaluate the trends in the departure from equilibrium.

The first phase of this investigation was to obtain a value for the critical Weber number, one that would produce drop sizes approximately the same size as the measured ones. For this phase, the heat transfer coefficient described by equation 34 but with the properties evaluated at the bulk vapor temperature was arbitrarily chosen, along with the standard curve for the drag coefficient. The design conditions for these calculations were G = 70,000; 130,000; and 190,000 lbm/hr/ft^2; q/A = 5000; 10,000; 15,000; and 20,000 Btu/hr/ft^2 for the 0.323 inch ID tube, and a constant pressure of 25 psia. Critical Weber numbers from 15 down to 5 were tested. The choice of value 15 was prompted by the results of reference 34 in which the maximum droplet sizes generated by the entrainment in a spray annular flow of water were described by critical Weber numbers between 13 and 22. It was found that the value of 15 was a little too large, the optimum value being about 7.5. A plot of the droplet breakup process is shown in figure 30 for the various heat and mass flux conditions. Note that the calculated drop sizes are principally a function of the heat flux (vapor acceleration) and fairly independent of mass velocity as discussed in section 2.2.3. The calculated drop sizes are in very good agreement with the measured

values of the "most prominent" drop sizes at the lower heat fluxes. At higher heat fluxes the calculated drop sizes are larger than the measured. This value of 7.5 for the critical Weber number was found to be in excellent agreement with the value of 6.5 measured by Isshiki (35) in his work on the breakup of single droplets in an accelerating airstream. Since the breakup process in this analysis of film boiling is confirmed by Isshiki's work, it appears that a critical Weber number criterion is a valid addition to an analysis of the core flow.

The effect that the choice for the value of the critical Weber number has on the departure from equilibrium is shown in figure 31b , for values of 5 and 15. Higher values of We_c are further from equilibrium since larger droplets, which constitute less total area for evaporation, are produced.

The effect of not allowing the droplet to break up is shown in figure 31e for various initial drop sizes. The necessity for knowing the drop size is evident in this figure.

The technique for obtaining an initial drop size in the initiation of the integration is tested in figure 31a by starting the integration at various qualities or distances along the tube. It is seen that the departure from equilibrium quickly converges to the same values further downstream. The droplet sizes also converge quickly to the same

values. At higher initial qualities the breakup process is very rapid, taking, in a short distance, approximately the same number of breakup steps that would occur up to that point if a lower initial quality had been used.

The most important phase of this analysis is the effect of heat and mass flux on the departure from equilibrium, as shown in figures 31c and 31d. Contrary to the results of the heat transfer analysis of section 2.2.4, the departure from equilibrium is greater at higher heat fluxes. The reason for the greater departure from equilibrium is due to the fact that although the droplets are beneficially smaller at higher heat fluxes, their transit time is smaller due to the higher vapor velocities. One reason for this discrepancy is probably the choice of the vapor temperature that should be used in the heat transfer equation in this analysis. As indicated from the results of the helium concentration work, some evaporation occurs near the tube walls where the vapor temperature is higher. At higher heat fluxes the film temperature will be larger, and greater evaporation will occur and the trend will be toward equilibrium. Another reason for this discrepancy is the inability of the drop breakup calculations to produce droplets as small as those measured at the higher heat fluxes.

The departure from equilibrium with variation in mass flux is in the direction expected; higher mass velocities tend toward equilibrium. The reason for the smaller amount of departure at higher mass fluxes can be seen if one con-

siders that, for a given heat flux the droplet sizes are the same from one mass flux to the next. At higher mass fluxes there are more droplets; consequently more surface is available to transfer heat in order to cool the superheated vapor. The variation however is not as strong as predicted from the test data as shown in figure 19. One might expect from the trends of the visual observations shown in figure 14 that a near-equilibrium process should occur for mass fluxes above 500,000. But analysis of this sort for larger G still result in a sizable departure from equilibrium. The results for G = 700,000 are shown in figure 31d. This type of analysis was also run for hydrogen data of reference 11 Although near equilibrium conditions are inferred from their data, a sizable departure still occurs (long-short dashed line in figure 4)

The third phase of this analysis is the evaluation of the choice of the drag coefficient. A constant value of $C_D = 0.5$, the steady state solid sphere C_D and Ingebo's C_D were investigated. Little difference in the departure from equilibrium exists between the cases in which the constant C_D and the steady state solid sphere C_D are used, as shown in figure 32c. It was found that Ingebo's drag coefficient is much too low at low quality or low heat flux conditions. The large droplet sizes that occur at these conditions cannot be supported by the vapor stream against gravity if this coefficient is used. Higher quality

conditions are needed before the integrations can be started, as shown in figure 32c. At higher qualities the droplet velocity calculated by using this coefficient is much lower than that calculated by using the conventional steady state drag coefficient. This produces greater convective heat transfer and longer residence time for the droplet, hence less departure from equilibrium as indicated in figure 32c.

Some high speed motion pictures of the droplets issuing from the test section were taken to see if their velocities could be measured. Although the films are somewhat limited in quality, they do indicate that for the condition of run 208 the velocity of the larger droplets (approximately 25 ft/sec) is a little larger than that predicted by use of the standard C_D (18 ft/sec) and much larger than that predicted by the use of Ingebo's C_D (8 ft/sec). The calculated non-equilibrium vapor velocity is approximately 35 ft/sec for these conditions. At low heat fluxes and qualities, the droplet acceleration rates are small ($dV_\ell/dt < 500$ ft/sec^2). It is apparent then that at lower droplet acceleration rates, C_D is better represented by the steady state drag coefficient. At higher acceleration ratios ($dV_\ell/dt > 5000$) the Ingebo drag coefficient should be used. Between these values a weighted average of the two drag coefficients should perhaps be used. There is the benefit that at the higher heat fluxes where high acceleration rates occur at higher qualities, the Ingebo C_D will give larger slip veloc-

ities, which in turn produce smaller droplets when the same critical Weber number is used. It appears reasonable that the drag coefficient should also be a function of the droplet acceleration. The following weighted average of the two drag coefficients is assumed.

$$C_D = C_{D\ \text{solid sphere}} - (C_{D\ \text{solid sphere}} - C_{D\ \text{Ingebo}}) \frac{(a_1 + a_2)}{2} \qquad (49)$$

where a_1 and a_2 are the weighting factors for the solid sphere and Ingebo accelerations.

$a = 0$ $\qquad (dV_\ell/dt) < 500$

$a = (dV_\ell/dt - 500)/5000$ $\qquad 500 < (dV_\ell/dt) < 5500$

$a = 1.0$ $\qquad 5500 < (dV_\ell/dt)$

This weighted drag coefficient is considered to be the proper one to be used in analysis of core flow for the actual test conditions.

The effect of using equation 34, 36, and 37 for the heat transfer coefficients is shown in figure 32b. These equations are considered the most reliable since they are supported by a considerable amount of both heat and mass transfer data. Although the difference between them is small, equation 36 yields qualities that are more in line with the calculated and measured qualities for G = 70,000 (ie a greater departure from equilibrium).

In the final phase of this analysis, the actual test conditions for selected runs with 0.323 inch ID tube, inclu-

ding the measured pressure drop, are analyzed. Equations 49 and 36 are used for the drag and heat transfer coefficients, along with a critical Weber number of 7.5. The results for these tests are shown in figure 32a for the nominal heat flux of 15,000 Btu/hr/ft^2. The departure from equilibrium is approximately the same as shown in figure 31d but the spread is a little greater between the various mass fluxes. The discrepancy in the effect of heat flux on the departure from equilibrium still remains, but it is less severe than that shown in figure 31c. The case for the lower heat flux for G = 70,000 is shown as a dashed line in figure 32a. This is the worst discrepancy noted for the experimental data.

The predicted departure from equilibrium is also compared in figure 19 with the values calculated by the heat transfer analysis of the first step. In these cases the maximum heat fluxes tested are shown. The agreement is very good at the higher values of quality for the mass velocity of 70,000. At lower qualities a fairly large discrepancy exists. Discrepancies exist also for the higher mass fluxes at all values of quality.

One reason for these discrepancies is that the contribution to the heat transfer by the liquid in the first step of the two step process is not considered. It was assumed that the droplets did not participate in absorbing heat from the tube wall either directly by evaporation at the tube

surface or indirectly by agitating the boundary layer, thus increasing the heat transfer coefficient.

Both the direct evaporation and the increase in the vapor heat transfer coefficient will produce the desired trends in the calculation for the departure from equilibrium from the test data. That is, the calculated symbols in figure 19 would be adjusted downward. In the first case, less heat is transferred to the vapor,

$$(q/A)_{\substack{\text{non-equilibrium}\\ \text{vapor phase}}} = (q/A)_{\text{total}} - (q/A)_{\text{evaporation}},$$

hence a further reduction in the thermal driving potential $(T_w - T_v)$ is required and a greater departure from equilibrium would be calculated. In the second case, the increase heat transfer coefficient also requires a reduction in the calculated thermal driving potential.

The core flow calculations will only be affected in the first case; the extra evaporation that occurs at the wall must be added to the evaporation in the core. The net effect will be to reduce the predicted departure from equilibrium as calculated in the core flow analysis. That is, the dashed curves in figure 19 will be adjusted upwards. This result is desirable in the case of high mass fluxes, where it was found previously that a sizable departure from equilibrium is still predicted from the core flow analysis even though trends in the experimental data indicate that it should not occur.

Thus it is evident that at least the additional evaporation heat transfer must be considered in the analysis.

Since little information is available on the effect of the presence of the liquid on the heat transfer process at the wall, it would not be fruitful to propose any elaborate model that would take into account the separate effects of both the evaporation and the augmentation of the heat transfer to the vapor. Independent experiments would be necessary to separate these two processes of heat transfer before each could be evaluated. Experiments might be made with single droplets falling down a heated surface that is slightly inclined from the vertical, from which the direct heat transfer to the droplets may be estimated. The effect of the presence of the lqiuid on the heat transfer to the vapor might be obtained from experiments on non-evaporating, non-wetting, two-phase flow with heat addition.

Although the above information is lacking, a very simple model is proposed here so that some understanding as to the effect of the increased heat transfer can be gained. The following model takes into account only the additional evaporation heat transfer and contains only one arbitrary constant that can be evaluated from the test data.

Addition of wall evaporation term to core flow analysis

It is assumed that the droplets in the core flow are uniformly distributed (N drops/ft^3) within the tube so that a uniform surface distribution of droplets is presented at the tube wall. This distribution (N_2 drop/ft^2) can be

obtained from

$$N_2 = K_1 N^{2/3} \qquad 49$$

where N is obtained from equation 13 and F_1 is an arbitrary constant that takes into account the thickness of the layer of droplets facing the tube wall (the region of influence of the tube wall).

It is assumed that the heat transfer between these droplets and the wall can be described in the same manner as that for a droplet sitting on a hot surface. Hamill and Baumeister * have proposed the following correlation.

$$h_{\delta,w} = 1.1 \left[\frac{k^3 H_{fg}' g \rho_l \rho_v}{\Delta T \mu (\pi \delta^3/6)^{1/3}} \right]^{1/4}$$

where

$$H_{fg}' = H_{fg} \left[1 + \frac{7}{20} \frac{C_p \Delta T}{H_{fg}} \right]^{-3} \qquad 50$$

and

$$\Delta T = T_w - T_{sat}$$

and where the properties are evaluated at the film temperature $(T_w + T_{sat})/2$.

Since the mechanism for holding the droplets next to the wall is different in the case of vertical turbulent

* K. J. Baumeister, T. D. Hamill, and G. J. Schoessow, A Generalized Correlation of Vaporization Times of Drops in Film Boiling on a Flat Plate, US-A.I.Ch.E - No. 120, Third International Heat Transfer Conference and Exhibit, August 7 - 12, 1966.

flow, the roll that g plays in equation 50 will not be the same. For simplicity, it is assumed that any differences can be absorbed in an arbitrary constant F_2 that replaces the constant 1.1 in equation 50. Since only the vapor density is a strong function of pressure, the other terms being mainly a function of the tube wall temperature, the heat transfer coefficient for nitrogen may be written as

$$h_{\delta,W} = K_2\ 59.4\ \ (P/14.7)^{1/4}\ \ (1/\delta)^{1/4}\ \ (T_w - T_{sat})^{-0.32} \qquad 51$$

By appropriately applying equations 13, 49, and 50, the additional heat flux from the tube wall becomes

$$(q/A)_{evaporation} = K_1 K_2\ \ 59.4\ \left[\frac{G_T\ (1 - X_A)\ \ 6}{\rho_\ell\ V_\ell}\right]^{2/3} \qquad 52$$

$$(P/14.7)^{1/4}\ \ (1/\delta)^{1/4}\ \ (T_w - T_{sat})^{0.63}$$

where $K_1 K_2$ is the resulting arbitrary constant. Note that the functional form is a desirable one with respect to mass flux and quality. The wall evaporation term becomes significant at high mass velocities and at low qualities.

Since the core flow is turbulent, with droplets moving to and from the wall, the amount of evaporation occuring at the wall can be considered to be spread evenly over the droplets in the core flow. The extra evaporation rate ($d\delta/dt$) for the droplet in the core can be obtained from the heat balance

$$(q/A)_{\substack{\text{evapor-}\\\text{ation}}} \pi D = N \pi \frac{D^2}{4} \rho_\ell H_{fg} \frac{3\pi\delta^2}{6} \frac{d\delta}{dt} \qquad 53$$

and then added to that in equation 42.

The total heat flux from the tube wall is obtained by adding equation 52 to the heat that is transferred to the superheated vapor,

$$(q/A)_{\substack{\text{non-equilibrium}\\\text{vapor phase}}} = \frac{0.019k}{D} \left[\frac{\rho_v V_v D}{\mu}\right]^{0.8} Pr^{0.4} (T_w - T_v) \qquad 54$$

Equation 54 is basically the same as equation 24; the constant 0.035 and the exponent 0.743 could equally well be used here for the range of the Reynolds numbers experienced in this study. The use of $\rho_v V_v$ instead of $G_T X_A$ in the Reynolds number is more correct here, but makes little difference since the void fraction is close to unity except in the very low quality region.

Since the core flow analysis and the heat transfer analysis are now dependent on one another via equations 52 and 53, the intermediate type comparison of the predicted departure from equilibrium quality to the calculated departure cannot be easily made. It is more expedient to make the comparison between the predicted tube wall temperatures and measured ones.

Calculation procedure

The predicted tube wall temperatures are probably calculated the easiest by breaking the tube length into elements

which are one thermocouple spacing in length starting at the entrance of the tube (thermocouple located at the center of the element). The heat flux over an element is assumed to be constant. The core flow integrations are started at the beginning of an element which is close to the entrance of the tube and whose flow conditions are consistant with those stated on pages 51 and 52. With the core flow conditions (T_v, X_A, V_ℓ , V_v, δ) and the total heat flux given, the predicted tube wall temperature for the element can be obtained by iterating equations 52 and 54. The extra evaporation rate ($d\delta/dt$) occuring within the element can then be obtained from equation 53. The core flow equations which contain the additional evaporation rate are then integrated up to the beginning of the next element, where the wall calculations are again made to obtain the next predicted tube wall temperature and additional evaporation rate.

Results of the modified core flow analysis

A comparison of the predicted tube wall temperatures with the measured ones are shown in figure 33 for three representative test conditions. Two values for the constant K_1K_2 (zero and 0.2) are shown.

Better agreement exists between the predicted and the measured temperatures when the optimum value of F_1F_2 equal to 0.2 is used. The predicted temperature profiles with F_1F_2 equal to zero are the profiles that one would get by using the original core flow analysis and tube wall heat

transfer calculations. The large discrepancy in the temperature profile in the low quality region for F_1F_2 = zero is due to both the discrepancy in the quality predicted from the core flow analysis and the fact that the vapor heat transfer coefficient approaches zero at low qualities.

It is obvious from these results that a wall evaporation term must be included in the analysis. Further experimental and analytical work should be directed towards the evaluation of this term and also the evaluation of the effect the liquid has on the heat transfer to the vapor.

2.5 Correlations

Several correlating techniques in the literature were tested to see if they could successfully correlate the data of this study even though it is known that non-equilibrium does exist. Miropolski's correlation is of the form shown by the line of demarkation in figure 34 when his y factor is not considered. For liquid nitrogen at 25 psia the value of y is negative for qualities up to 90%, hence cannot be used. The nitrogen data of this study is also compared to the correlating techniques of Hendricks (11) and that of von Glahn (36) in figures 35 and 36. In these cases equilibrium conditions are assumed. In figure 35 a portion of the abscissa is scaled off to indicate the equilibrium superheating region. A large amount of scatter is seen to occur with both correlating techniques.

2.6 Minimum heat flux

An estimate of the minimum heat flux necessary to maintain film boiling in vertical flow of nitrogen can be gotten from the data of Laverty (2) and the experience of this study. The following are the lowest heat fluxes tested by Laverty.

G	q/A
70,000	3700
115,000	5300
160,000	8100
210,000	8100

In the present study it was found that stable flim boiling could not be maintained at the following desired data points.

G	q/A	D
70,000	3300	0.228
190,000	5000	0.323

These points were obtained under a hot inlet flange condition so the collapse of the film occurred within the tube. If the flange were cold, film boiling could not be maintained for many of the other runs in this study (see Appendix A, Boiler Test Sections).

CHAPTER 3

SUMMARY AND CONCLUSIONS

1. The large departure from thermal equilibrium in dispersed flow film boiling has been confirmed in this study. Efforts in several directions have yielded independent evidence of this phenomenon, that agree with each other.

a) Heat transfer tests have yielded film boiling and superheating heat transfer coefficients based on equilibrium conditions that are much lower than single phase heat transfer coefficients based on an equivalent flow rate of pure vapor. When it is assumed that the liquid plays no role in the heat transfer at the tube wall, and an appropriate single phase heat transfer correlation is applied to the measured heat transfer rate and tube wall temperature, significant amounts of vapor superheat (hence a reduction in the amount of vapor generated) result. Departures of up to 50% in vapor quality are calculated. The calculated departure from equilibrium occurs as far out as 300% equilibrium quality in the superheating region.

b) Visual observations of the two phase flow issuing from the test sections confirm the existance of non-equilibrium in the superheating region. The observed points at which complete evaporation occurs are in agreement with the points calculated in the heat transfer analysis discussed in paragraph a) above.

c) Measured values of actual quality by means of the helium tracer gas technique agree favorably with the

calculated values over a portion of the test conditions.

d) The departure from equilibrium predicted by analyzing the kinematics and heat transfer of the core flow also agrees with the calculated values over a portion of the range of test conditions.

2. The departure from equilibrium is mainly dependent on the mass flux, and to a smaller degree on the heat flux.

3. The effect of tube diameter on the departure from equilibrium is small.

4. Analysis of the core flow shows that a wall evaporation heat transfer term is needed at high mass fluxes and at low qualities.

5. In an analysis of the kinematics and heat transfer of the core flow:

a) the drag coefficient for the droplets should be at least as large as the standard steady state drag coefficient for spheres when the droplet accelerations are small (less than 500 ft/sec^2). At higher acceleration rates (above 5000 ft/sec^2) Ingebo's drag coefficient should be used. A weighted average of the two can perhaps be used for moderate acceleration rates.

b) the droplet heat transfer coefficient can be reasonably estimated from

$$Nu_\delta = 2 + 0.55\ Re_\delta^{0.5}\ Pr^{1/3} .$$

c) the droplet breakup process along the tube is governed by a critical Weber number criterion where the permissible average droplet size is defined by

$$\delta \leq 7.5 \ (\sigma / \rho_v \Delta V^2).$$

A reasonable estimate for the departure from equilibrium can be obtained by a core flow analysis for low mass fluxes and high qualities.

6. In estimating the departure from equilibrium from q/A versus Δ T data, only the heat transfer correlation that accurately predicts heat transfer rates for the vapor phase for the fluid in question should be used.

7. The tracer gas technique is a useful technique for determining the departure from equilibrium. To further improve the performance of the probe, it is recommended that a heating device be installed within the probe to insure that the probe remains dry.

APPENDIX A

APPARATUS, INSTRUMENTATION, AND LIMITATIONS

Boiler Test Sections

The four boiler test sections are electrically heated round tubes of 304 stainless steel in which the I^2R heating occurs in the walls. The test sections were sized to produce an overall resistance of approximately 0.1 ohm and 0.05 ohm for the long and short tubes respectively. The dimensions of the test sections are given below in inches.

TEST SECTION	ID	WALL THICKNESS	LENGTH
1	0.323	0.028	47.7
2	0.323	0.028	96.0
3	0.462	0.020	96.0
4	0.228	0.042	96.0

The test sections were fitted through brass block flanges (2-1/2 X 1-1/4 X 3/8 inch) at both ends of the test section and silver soldered in place. The flanges serve as electrodes to which braided copper straps were firmly bolted. 0.040 inch pressure tap holes and voltage tap bolts were also provided on both flanges. A third pressure tap of 16 gauge stainless steel tubing was silver soldered to the tube half way up the test section.

An auxiliary heater was provided on the bottom flange to prevent collapse of the vapor film and the subsequent chilling of the flange since axial conduction to a cold flange initiates collapse in the tube. The collapse would

be further aggrevated by a reduction in heat flux ahead of the collapsing film due to the reduction in local tube resistivity with reduction in local temperature. In addition to preventing film collapse, the flange was maintained near room temperature to minimize conduction along the electrode strap. Up to 40 watts depending on tube temperature and flow rate were sufficient to maintain this condition.

A spring loaded yoke at the top of the test section was used to position the tube vertically and to take up thermal growth. Pins protruding from both sides of the flange carried the yoke load in order to eliminate bending moments in the tube.

Copper-constantan thermocouples were located at 4 inch intervals along the tube starting 2 inches from the bottom flange. The junctions were first formed in an arc welder, then lightly spot welded to the tube wall. The lead wires were wrapped three times around the tube circumference and the entire thermocouple assembly was then cemented to the tube with Sauereisen cement. Prior to wrapping the thermocouples around the tube, a small piece of glass tape was inserted under the short bare section of wire leading to the junction as a precaution to short circuting any tube current through the thermocouple wire. The thermocouple lead wire terminated at groups of 12-prong Cinch-Jones plugs which acted as the reference junction at room temperature.

Flow Apparatus

Liquid nitrogen is supplied to the test section from a pressurized liquid nitrogen dewar containing 50 liters, as shown in figure 38. The pressure head is obtained from a regulated supply of helium gas and is normally set at 15 to 18 psig. The pressurizing flow can be interrupted by a DC solenoid valve located between the He cylinder and the nitrogen dewar, which can be tripped by a switch in an emergency or during shut down. The dewar pressure can be relieved by a quick acting manual valve. The liquid is blown up through a 3/8 inch OD copper receiving tube which is suspended to the bottom of the tank through the neck of the dewar. The flow is led from the receiving tube to a 3/8 inch OD copper tube which carries the liquid back down to the subcooler assembly located close to the laboratory floor. A 1/2 inch OD copper tube surrounds the transfer tube to form an annulus through which a cooling nitrogen bleed flow is ducted. This arrangement thermally shields the transfer tube from ambient conditions so that boiling can not occur there and cause vapor locking in the valves downstream. The receiving tube is attached to the transfer tube by a flare fitting to allow removal and insertion of the receiving tube in the dewar. The flow is then led from the transfer tube to the subcooler which consists of a 5 foot coiled tube-in-tube heat exchanger made of 3/8 inch OD and 1/2 inch OD type L copper tubing. At the entrance of the subcooler a small portion of the flow is

throttled through a 1/16 inch Hoke valve into the annulus of the subcooler to provide a cooling bleed flow. The main flow is led through the center tube of the subcooler where it becomes slightly subcooled. The subcooler terminates at a brass block which serves as a mounting bracket for the subcooler assembly. The main flow is then led from the brass block to the 1/8 inch main control valve (Hoke). The bleed flow is also channelled through the block to provide a heat sink between the main flow channel and the attachment points. The bleed flow is then piped back to the annulus of the transfer tube and from there through a back pressure control valve to a Welch 1397B mechanical vaccuum pump. Prior to entering the pump, the vapor is heated in the annulus of a tube-in-tube heat exchanger. The bleed flow back pressure is normally 20 inch Hg vaccuum. After the control valve, the main flow is led to a 1/4 inch threaded tee which turns the flow vertically into a 5 inch long 3/8 inch OD straight inlet section upstream of the test section. An immersion thermocouple inserted up into the inlet tube through the other end of the tee serves to measure the inlet temperature of the liquid nitrogen. The inlet tube terminates at a steel flange onto which the test sections or helium injector were mounted. Micarta spacers with a flow channel through their center were provided to thermally and electrically insulate the test section inlet flange from the lower flange. The three bolts securing the flanges together were insulated from the test

section flange by teflon spacers and micarta washers.

On leaving the main test section the flow entered either a probe section and then an electrically heated glass visual section or in some cases entered the glass section directly when the probes were omitted. The glass section was electrically insulated from the test flange by locating the glass tube concentrically in a bored out over size brass Swagelok fitting with teflon ferrels and nut. A Swagelok union made of teflon joined the downstream end of the visual section to a 1/2 inch OD exit tube which carried the flow to the after-heaters. Copper bellows were provided at each end of the exit tube to allow for thermal expansion of the test section and any missalignment of the test section with the after-heater.

The two after-heaters (coolers) are tube-in-tube heat exchangers 6 foot long made from 7/8 inch OD and 1-1/8 inch OD type L copper tubing. The nitrogen flow passed through the inner tube and steam or water was passed through the annulus. At high N_2 flow rates or low heat fluxes, steam was used to evaporate the remaining liquid and super heat the vapor to approximately room temperature. At low flow rates or high heat fluxes with liquid N_2 or during tests with gaseous nitrogen, water was used to bring the vapor close to ambient conditions. The second heat exchanger could be bypassed by a 6 foot length of 7/8 inch OD copper tubing exposed to the air to allow for greater control of the vapor temperature prior to passing the flow through the flow meters.

A 3/4 inch gate valve upstream of the rotometers was provided to obtain the back pressure necessary to maintain a 25 psia test section inlet pressure. The entire system between the dewar and the visual section was thermally insulated in Santocel powder. The Santocel powder was contained by a 2-1/2 inch cardboard tube encasing the transfer tube heat exchanger, by a wooden box containing the subcooler and valves and by a 3 inch vertical plexiglass tube encasing the test section.

Power

115 volt and 230 volt 60 cycle laboratory power was used for heating the 4 foot and 8 foot test sections respectively. The power to the 4 foot test section was controlled by a 5 KVA General Radio Variac which was capable of supplying 0 to 135 volts to a 3 KVA General Electric transformer model 9T1Y113. The transformer was wired to produce a 10 to 1 reduction in voltage to match the power requirements of the short tube. Power to the 8 foot test section was controlled by one branch of a 230 volt 18 KVA 3Ø American Transformer Company Transtat which was capable of supplying 0 to 230 volts to the primary of a 5 KVA General Electric transformer model 61G76. This transformer was also wired to produce a 10 to 1 reduction in voltage. Either two strands of #2 welding cable or a single strand of #3 were used to carry the secondary current (up to 240 amps) to the test section. The laboratory power was connected to the system via a power

relay that could be tripped in the event of an emergency and during shut down.

The power to the inlet flange heater, probe heater blocks and the electrically heated glass section were each controlled by small 115 volt variacs capable of supplying up to 2 amps. These variacs were connected directly to the 115 volt emergency switch that operated the power relay so that all power could be turned off simultaneously.

Instrumentation

Test section pressure Four U-tube manometers, three containing mercury and one containing Miriam fluid were available for pressure measurement. The inlet gage pressure, the pressure drop to the mid-point of the tube, and the total pressure drop along the entire tube were continuously monotored on the 3 Hg manometers. The Miriam fluid manometer was used to obtain greater accuracy when pressure drops were smaller than 10 cm Hg.

Test section wall temperature Since the Brown recorder (Minneapolis-Honewell Model 153X52V16) contained only 16 channels, two groups of twelve odd and even thermocouples of the 24 along the tube were recorded separately. The change from odd to even was facilitated by the use of the Cinch-Jones plugs which formed the cold junction for the wall thermocouples. A copper-constantan thermocouple with an ice bath for a cold junction was placed in the immediate vicinity of the plugs in order to obtain the appropriate

millivolt correction for the wall thermocouples. This correction was continuously monitored on the recorder.

Before tests were run, the output of the wall thermocouples were checked against the output of a calibrating thermocouple suspended within the tube adjacent to the wall thermocouple in question. The outputs agreed to within three degrees (the wall temperature being the lower of the two as expected) except for the end thermocouples where the axial conduction and internal convection losses become important. The calibrating thermocouple was taken from the same roll of wire that was used to thermocouple each test section. Thermocouple checks were run at approximately 800° to 900° R. The calibrating thermocouples were checked against the melting point of tin (909°R) and was found to be within 5 R°. The recorder which has a range of 0 - 10 mv was wired to a switching network so that negative potentials and potentials up to approximately 19.3 mv could be read. For the latter an iron-constantan thermocouple with its cold junction in liquid nitrogen and its leads at room temperature was used to produce a bucking voltage of approximately 9.3 mv. Its output was monitored whenever it was used.

All the thermocouple outputs could be read on a Leeds and Northrup precision potentiometer as well in order to check the accuracy of the recorder from time to time and to obtain readings outside the range of the recorder. This was facilitated by a switching panel. The switching panel also

allowed other temperature measurements to be recorded on the last channel of the recorder. In addition to the 24 thermocouples along the tube, another was located at the inlet flange and was monitored in adjusting the power to the auxiliary heater.

Inlet and exit temperature The subcooled inlet temperature was measured with a copper-constantan thermocouple silver soldered into the end of a 0.065 inch stainless tube situated inside the inlet tube. Liquid nitrogen at atmosphere pressure was used for the reference junction to obtain greater accuracy in determining the amount of subcooling. Outputs of + 0.08 to - 0.01 mv (0 to 10° F subcooling at 25 psia) were measured on the precision potentiometer. The accuracy of the measurement is estimated to be within 0.01 mv (approximately 1 R°).

A copper-constantan thermocouple was inserted inside the visual section approximately 10 diameters downstream of the test section exit for the purpose of checking the accuracy of the heat balances. The lead wire was bunched up to form a spider which held the junction in the middle of the tube. The readings from this thermocouple are reliable only for those runs in which very little or no liquid is present. Power to the visual section was turned off prior to noting the readings. Thermal radiation loss from the thermocouple was estimated to result in an error of less than 1 R° assuming the glass to be opaque to low temperature radiation.

Power Power to the test section was obtained by measuring the voltage drop between the flanges with a Weston Model 433 AC voltmeter containing a dual range of 0-10 and 0-20 volts and the current with a Weston Model 115 AC ammeter containing a range of 0-250 amps. The voltmeter was calibrated and found to be accurate within $\pm$ 0.01 volt for the lower range and $\pm$ 0.02 volt for the upper range. The ammeter was calibrated and found to have an accuracy of $\pm$ 1/2% in the range of 100-250 amps in which most data was taken. Calibrations were made against NBS certified equipment. Read out error due to interpolation is estimated to be within 0.02/0.04 volts and 0.4 amps. The calibration was checked before and after the experimental program.

Power to the inlet heater was obtained by voltage and current measurements with panel type instruments. These were not calibrated since the power generated is very small compared to the power dissipated in the test section. Probe heater and glass section currents were measured so that their proper operating conditions could be monitored throughout the tests.

The tube wall thermocouples were used as voltage taps in checking for any nonuniformities in power dissipation along the tube during heat loss tests at uniform tube wall temperature. The voltage gradient measured between adjacent thermocouples with a VTVM was found to be uniform except at the ends where a reduction in tube wall resistivity occurs.

This was probably due to overheating the tube while silver soldering the flanges. Since the degradation of resistivity is small (approximately 15%) and is confined to the first 2 inches at each end of the tube, correction for this was considered unnecessary.

Nitrogen flow rate Two Brook Model 10-1110 flow meters in parallel, whose full scale readings are 80 and 118 lbm/hr at 70° and 14.7 psia, were available for measuring the nitrogen flow rate. The first contained a 25-1 tube; the second a 25-3 tube. Both were calibrated to 1% full scale. The rotameter inlet temperature and exit pressure were maintained as close to 70° and 14.7 psia as possible so that only small density corrections had to be made. The vapor temperature was measured by a mercury thermometer located just upstream of the flow meters. The flow meters were usually vented to atmosphere, but during tests with the concentration probe a slight back pressure (1cm Hg) was necessary to provide an adequate sample B flow rate.

Helium Concentration Apparatus

The helium concentration apparatus consists of a helium gas injector located at the test section inlet, one of two vapor sampling probes mounted on test section exit flange and a thermal conductivity cell used to measure the concentration of helium in the vapor sample.

Injector The helium injector shown in figure 39 consists of a 5 inch long .065 inch OD stainless steel tube inserted

into the entrance of the test section. The injector is movable so that the helium gas can be injected into the nitrogen flow at any location across the diameter of the test section. This capability was provided in order to evaluate the uniformity of mixing that takes place in the test section. The injector body is mounted directly on the lower flange and separated from the inlet flange by a micarta spacer. O-ring seals are provided between all faces. Helium gas is supplied from a separate cylinder regulated at 30 psig, and metered through a needle valve. The 20 psi pressure drop across the control valve is required to prevent He flow oscillations with the small fluctuations in test section pressure.

Probe A stationary and movable probe, shown in figures 40 and 41 respectively, were mounted on the test section exit flange. The stationary probe consists of an 0.095 inch OD brass tube located vertically on the axis of the test section. A small cone shaped baffle at the tip of the probe was provided to deflect the droplets away from the .050 inch ports drilled in the brass tube behind the baffle. The movable probe consisted of an 0.065 inch OD stainless steel tube located across the diameter of the flow area. The probe port is a 0.040 inch hole drilled in the side of the stainless tube, and is capable of traversing the diameter and rotating to face upstream or downstream. The radial position of the port is determined with the aid of a 1 inch micrometer.

The micrometer end of the probe tube is blanked off by a small handle which serves to indicate the rotational position of the port. The other end opens into a discharge tube. The probe tube is sealed by teflon sealants which are kept plyable with heat provided by the heater blocks clamped to the probe flange.

Thermal conductivity cell The apparatus for determining the concentration of helium in the vapor sample is shown schematically in figure 42. The main component is a Gow-Mac model 30TH2GBT thermal conductivity cell which is a resistance bridge containing two thermistors, one immersed in the sample gas, the other in a reference gas (prepurified nitrogen). The bridge becomes unbalanced and a signal is generated when the thermal conductivities of the two gasses differ. For low concentrations of helium in nitrogen the cell output is linear with concentration and is approximately 60 mv per 1% helium in nitrogen. The cell in an "on stream" type normally requiring a continuous flow of sample and reference gas of approximately 400 cc/min. The cell however was found to operate successfully at flow rates as low as 50 cc/min.

Prior to running a test prepurified nitrogen was passed through the sample side of the cell so that the bridge could be balanced. Known samples of 1.12% and 2.13% helium in nitrogen were then used to adjust the output voltage level of the cell and to check its linearity. In order to know

the amount of helium injected in the test section during tests a concentration sample B was taken after the rotameters where well mixed pure vapor exists. This method is more accurate than measuring the helium injection rate directly. The outputs for sample B and pure nitrogen were monitored occasionally during tests so that any changes in helium flow rate and cell calibration could be rectified. A flow selector valve was provided for this purpose. Part of the sample A flow could be bypassed through a separate flow meter when probe flow rates were greater than the design flow rate of the thermal conductivity cell.

The cell output was recorded on a Model 320 Sandborn recorder.

Experimental Limitations

In general the upper limits for mass and heat flux are dictated by the capabilities of the apparatus; the lower limits are dependent on the accuracy of the flow measurements and heat loss calibration. The upper limits on heat flux and mass flux for each test section are dependent on one of the following conditions that may occur:

1. Power limitation
2. High tube wall temperatures with large gradients near the entrance of the tube. Temperatures much larger than 1200° R were avoided to preclude any possibility of damage to the tube in the region between the flange and the first thermocouple.

3. Exit vapor temperatures greater than 850° R were avoided to prevent melting the soft soldered joints downstream of the test section.

4. Large flow system pressure drops that would require inlet pressures greater than 25 psia, consequently an increase in dewar supply pressure. The dewar supply pressure is limited to 20 psig for reasons of safety.

5. Maximum flow rate of 150 lbm/hr. This is dictated by the time needed to set up and record a single run and the amount of nitrogen available.

APPENDIX B

DATA REDUCTION

The data of both the film boiling runs and the single phase vapor runs were reduced with the aid of an IBM 7094 computer. The data reduction involved the following calculations at each thermocouple location.

Local heat flux The local heat flux reported in table was obtained by

$$(q/A)_{net} = 3.413\ (VI/A) \cdot (R/R_{avg}) - (q/A)_{loss}\ , \qquad (B1)$$

where R is the tube resistance evaluated at the local tube wall temperature and R_{avg} is the average tube resistance obtained by averaging all the calculated values of R along the tube. These values were obtained from linear curve fits to the measured data of the film boiling runs shown in figure 43. Resistance values obtained in uniform temperature heat loss calibration runs were in agreement with these values. This resistance ratio correction was necessary since variations in resistances up to 24% occur along the tube in one run, although the variation in most of the runs is less than 5%.

The local radial heat losses were evaluated by second order curve fits to the heat loss data shown in figure 44. Below room temperature the heat gain is assumed to be linear. Axial conduction in the test section and insulation is negligible.

Bulk temperature and quality (film boiling) The equilibrium quality and bulk temperature variation along the tube were determined by

$$X = (H - H_{\ell\ sat})/H_{fg} \tag{B2}$$

and

$$T_b = T_{sat} + X\ H_{fg}/C_{p\ell} \quad \text{for} \quad X < 0$$

$$T_b = T_{sat} \quad 0 \leq X \leq 1.0 \tag{B3}$$

$$T_b = T_{sat} + (H - H_{V\ sat})/C_{pv} \quad X > 1.0$$

where H is the enthalpy of the mixture calculated by a heat balance along the tube. The inlet enthalpy was corrected for the amount of subcooling and for the heat supplied to the inlet flange.

$$H_1 = H_{\ell\ sat} - C_{p\ell}\,\Delta T_{sc} + Q_1/W \tag{B4}$$

$$H_i = H_{i-1} + (q/A)_i + (q/A)_{i-1} \cdot (\pi D \Delta x/2W) \tag{B5}$$

In evaluating T_b an estimate was first obtained by using the average C_p between the saturation temperature and 540° R (ie; $C_p = f(P)$ only). The final value of T_b was obtained by using a curve fit of the average specific heat ($C_p = f(T,P)$) evaluated at the first estimate of T_b. The error in the final value of T_b thus calculated is less than 1°R. The saturation properties, T_{sat}, $H_{\ell\ sat}$, $H_{V\ sat}$ and average C_p were taken or calculated from reference 37. The curve fits for T_{sat}, $H_{\ell\ sat}$, and $H_{V\ sat}$ were within 0.05 R°

and 0.03 Btu/lbm, which represents an error of 0.1 R^o in the calculation of T_b for the range of pressures used in this study.

Bulk temperature (single phase vapor flow) The bulk temperature for the pure vapor tests was determined by

$$T_b = T_{inlet} + \Delta H/C_p \tag{B6}$$

where $C_p = 0.248$ Btu/lbm/^oR

Kinetic energy Kinetic energy is neglected in these calculations since the difference between the bulk temperature calculated and the adiabatic wall temperature, which should be used as the sink temperature in high velocity flow heat transfer, is small. The maximum value of kinetic energy encountered in this study amounts to 35 R^o, which presents a maximum error of 3.5 R^o for a recovery factor of 0.9. In most cases the kinetic energy amounts to less than 10 R^o or an error of less than 1 R^o.

Inside tube wall temperature The inside wall temperature was obtained by

$$T_i = T_o - (q/A)\ (D_o - D_i)/4k_{ss} \tag{B7}$$

The last term is a valid expression for the tube wall temperature drop since the diameter ratios are close to unity, and the heat loss and wall temperature drop are small ($\Delta T_w < 4R^o$).

Heat transfer coefficients The evaluation of the calculated quality reported in section 2.2.4 and the determination of the heat transfer correlation reported in section 2.5 were done with the aid of the computer. Thermal conductivity, viscosity, and Prandtl numbers for nitrogen at 1 atm were obtained from references 38 and 39. Curve fits of this data were within 2%.

APPENDIX C

INTEGRATION OF HELIUM CONCENTRATION PROFILE

When the helium concentration profiles across the diameter of the tube are not uniform, the determination of the actual quality requires integrations for the conservation of helium, nitrogen, and energy.

Conservation of helium

$$W_{He} = 2\pi \int_0^{r_o} C_A(r)\,\rho_{He}(r)V(r)\,r\,dr$$

$$= (C_B/(1-C_B))\,(m_{He}/m_{N2})\,W_{N2\ total}\ , \qquad (C1)$$

where ρ_{He} is evaluated at the local temperature T(r) and total pressure P. $C_A(r)$ is the volume fraction of helium (concentration) in the test section and C_B is the well mixed helium concentration at the rotameter exhaust.

Conservation of nitrogen

$$W_{N2} = 2\pi \int_0^{r_o} (1-C_A)\,\rho_{N_2}(r)\,V(r)\,r\,dr$$

$$= X_A\,W_{N_2\ total} \qquad (C2)$$

where X_A is the vapor quality, which is the final desired quantity is these calculations.

Concentration of energy

$$X_E\,H_{fg}\,W_{N_2\ total} + 2\pi \int_0^{r_o} C_{pHe}(T_{amb}-T(r))C_A(r)V(r)rdr$$

$$= 2\pi \int_0^{r_o} \left[H_{fg} + C_{p_{N2}}(T(r)-T_{sat})\right]\,(1-C_A(r))\,\rho_{N2}(r)V(r)rdr \qquad (C3)$$

where the first and second terms on the left hand side of

equation are the power input to the test section in terms of equilibrium quality and the enthalpy rise contributed by the injected helium. The term on the right side is the enthalpy rise of the nitrogen vapor existing in the tube. When the perfect gas laws,

$$\rho_{N_2} = P/R_{N_2}T \ ,$$

$$\rho_{He} = P/R_{He}\ T = (m_{He}/m_{N_2})\ P/R_{N_2}T \ ,$$

$$Cp_{He} = (m_{N_2}/m_{He})\ Cp_{N_2} \ ,$$

and the assumed concentration, velocity, and temperature profiles,

$$(C_A/C_B = (C_A/C_B)_{max}\ \gamma^{1/m} \ ,$$

$$V(a) = V_{max}\ \gamma^{1/n} \ ,$$

$$(T(r) - T_w) = (T_{\ell} - T_w)\ \gamma^{1/n} \ ,$$

$$= T_w \beta\ \gamma^{1/n} \ ,$$

where $\gamma = (1 - r/r_o)$ and $\beta = (T_{\ell} - T_w)/T_w$ are inserted, the above equations become

$$\left[\frac{(1 - C_B)\ 2\pi P\ (C_A/C_B)_{max}\ V_{max}\ r_o^2}{R_{N_2}\ W_T\ T_w}\right] f_1\ (m,n,\beta) = 1 \qquad (C4)$$

$$\left[\frac{2\pi P\ V_{max}\ r_o^2}{R\ W_T\ T_w\ X_A}\right]\left[f_2(n,\beta) - C_B(C_A/C_B)_{max}\ f_1(m,n,\beta)\right] = 1 \qquad (C5)$$

$$\left[\frac{2\pi Cp_{N_2}\ P\ V_{max}\ r_o^2}{h_{fg}\ R\ W_T\ [X_E - X_A\phi_1 + \phi_2 C_B/(1 - C_B)]}\right] f_3\ (n) = 1 \qquad (C6)$$

where

$$f_1(m,n,\beta) = \int_0^1 \frac{\gamma^{1/m}\,\gamma^{1/n}(1-\gamma)\,d\gamma}{1-\beta\gamma^{1/m}}$$

$$f_2(n,\beta) = \int_0^1 \frac{\gamma^{1/m}(1-\gamma)\,d\gamma}{1-\beta\gamma^{1/m}}$$

$$f_3(n) = \int_0^1 \gamma^{1/m}(1-\gamma)\,d\gamma$$

$$\phi_1 = 1 - Cp\ T_{sat}/H_{fg}$$

$$\phi_2 = Cp\ T_{amb}/H_{fg}$$

When equation C4 is divided into equations C5 and C6 the following equations for X_A result.

$$X_A = \frac{1}{1 - C_B}\left[\frac{F_1(m,n,\beta)}{(C_A/C_B)_{max}} - C_B\right], \qquad (C7)$$

$$X_A = \frac{1}{\phi_1}\left[X_E + \frac{C_B}{1 - C_B}\,\phi_2\right] - \frac{\phi_3\,F_2(m,n,\beta)}{\phi_1\,(1 - C_B)(C_A/C_B)_{max}}, \qquad (C8)$$

where $\phi_3 = Cp\ T_w/H_{fg}$

$$F_1(m,n,\beta) = f_2(n,\beta)/f_1(m,n,\beta)\ ,$$

$$F_2(m,n,\beta) = f_3(n)/f_1(m,m,\beta)\ .$$

Once m and n are chosen, equations C7 and C8 are iterated to obtain X_A and β. The value for β must yield $T_{\ell} \geq T_{sat}$.

The values of F_1 and F_2 are shown in figure 45 for $1/m = 1/9$ and $1/n = 1/3$, $1/5$, and $1/7$. F_1 can be considered the approximate correction to actual quality calculated in equation 31 of section 2.3.4.

APPENDIX D

ACCURACY OF TESTS

Flow The two flow meters were calibrated to ± 1% full scale accuracy which amounts to a possible error of ± 0.8 and ± 1.2 lbm/hr in flow measurement. This gives an error of ± 1.5% and ± 3.5% for the maximum and minimum flow rates used in the pure vapor tests; an error of ± 1.1% to ± 2.0% for the maximum and minimum flow rates in the larger diameter tube, and a maximum error of ± 4% for the minimum flow rate with the small diameter tube.

Another source of error in flow rate is due to flow instabilities. In most cases they were less than ± 1%, some being indetectable; the worst cases were as high as ± 2%. Since these fluctuations were fairly uniform and of sufficiently high frequency, the average reading was taken to be an accurate measure of the flow rate.

Heat input The voltmeter and ammeter calibration and readout accuracy noted in Appendix A produced a maximum error of approximately 2% for heat input and heat flux at the lowest heat flux, 3500 Btu/hr/ft^2 in run #1 and a maximum error of approximately 1% for the highest heat flux of 25,000 Btu/hr/ft^2.

Heat loss The average heat losses through the insulation are less than 3% of the total heat input, although local values are as high as 5%. Since this correction to the heat input and heat fluxes is small, the errors involved in obtaining the losses are negligible with respect to

the total heat flux.

Inlet subcooling The error in measuring the inlet subcooling is estimated to be $\pm$ 1R°, which represents an error of $\pm$ 1/2% in the calculation of quality or $\pm$ 2R° in the calculation of bulk vapor temperature in the superheating region.

Heat balance An indication of the accuracy of the heat balances is afforded by the exit temperature measurements in the pure vapor tests and in the film boiling tests where little or no liquid was present. The errors for these runs are given below.

Run	Error	Run	Error
4	0.7%	299	3.4%
5	1.2%	284	1.0%
6	2.7%	288	3.0%
258	1.4%	292	0.7%
259	0.3%	293	1.2%
261	2.7%	294	2.8%

Surface Temperature The total maximum error in thermocouple output is estimated to be approximately 8 R° at 900°R (5 R° error inherent in the wire and a measured 3 R° error due to installation technique) which represents an error of about 1% in wall superheat at that temperature.

Pressure measurements The inlet pressure is known to be within $\pm$ 1/2% due to pressure fluctuations that were within 1/2 cm Hg in most cases. In a few cases the pressure fluctuations were as large as $\pm$ 2 cm Hg. The accuracy of the pressure drop measurements are estimated to be within $\pm$ 2% or 0.03 psi whichever is larger.

Reproducibility The excellent reproducibility of the film boiling data is indicated by the runs with the long and short 0.323 inch ID test sections. The temperature profiles for the same test conditions (flow rate and test section current) are coincident except in the neighborhood of the test section entrance. The reproducibility is also evident in the measured pressure drops over the first four feet on both the long and short 0.323 inch ID test sections. They agree within 0.05 psi except in the case of run 207-260.

RUN		1	2	3	4
D	INCHES	.323	.323	.323	.323
G	LBM/HR/FT**2	41929.602	76725.952	76725.952	70153.799
V	VOLTS	4.100	4.050	6.020	4.880
I	AMPS	86.000	88.000	123.000	104.000
P	PSIA	25.020	25.020	25.020	24.749
ΔP1	PSI	.273	.788	.886	.712
ΔP2	PSI	.610	1.645	1.945	1.511
TINLET R		534.000	518.000	509.000	510.000
TEXIT MEAS R		0.	0.	0.	682.000
TEXIT CALC R		728.807	628.126	736.432	680.893

I	X INCH	TWALL INSIDE R	Q/A BTU/HR/ FT**2	BULK TEMP R	TWALL INSIDE R	Q/A BTU/HR/ FT**2	BULK TEMP R	TWALL INSIDE R	Q/A BTU/HR/ FT**2	BULK TEMP R	TWALL INSIDE R	Q/A BTU/HR/ FT**2	BULK TEMP R
1	00	00	00	534	00	00	518	00	00	509	00	00	510
2	2	621	3341	542	580	3479	523	629	6984	518	599	4871	517
3	6	650	3371	558	597	3500	532	664	7086	536	626	4923	531
4	10	672	3392	574	611	3517	541	690	7160	555	642	4953	545
5	14	690	3409	590	621	3529	550	713	7224	574	659	4984	559
6	18	705	3422	606	630	3539	559	733	7279	592	674	5011	573
7	22	724	3437	623	642	3553	568	749	7321	611	689	5037	588
8	26	739	3449	639	651	3562	578	773	7384	631	704	5062	602
9	30	755	3460	656	661	3573	587	793	7435	650	719	5087	616
10	34	771	3471	672	670	3583	596	811	7480	669	733	5110	631
11	38	788	3482	689	680	3593	605	832	7531	689	749	5136	645
12	42	802	3490	705	689	3602	615	850	7574	708	762	5155	660
13	46	817	3498	722	698	3611	624	869	7617	728	777	5178	675
14	48	00	00	729	00	00	628	00	00	736	00	00	681

TABLE I PURE VAPOR TESTS

RUN		5	6
D	INCHES	.323	.323
G	LBM/HR/FT**2	70220.074	119542.049
V	VOLTS	7.230	7.030
I	AMPS	140.500	146.000
P	PSIA	24.807	24.749
ΔP1	PSI	.857	2.109
ΔP2	PSI	1.825	4.799
TINLET R		502.000	492.000
TEXIT MEAS R		844.000	702.000
TEXIT CALC R		840.087	696.430

I	X INCH	TWALL INSIDE R	Q/A BTU/HR/ FT**2	BULK TEMP R	TWALL INSIDE R	Q/A BTU/HR/ FT**2	BULK TEMP R
1	00	00	00	502	00	00	492
2	2	674	9286	515	609	9760	500
3	6	734	9520	542	644	9917	517
4	10	767	9644	569	665	10010	533
5	14	799	9762	597	686	10102	550
6	18	830	9873	625	705	10185	567
7	22	860	9978	653	724	10266	584
8	26	888	10072	681	741	10338	601
9	30	917	10167	710	759	10413	618
10	34	945	10256	739	776	10483	636
11	38	974	10345	768	794	10556	653
12	42	1002	10428	798	811	10624	671
13	46	1029	10505	827	829	10696	689
14	48	00	00	840	00	00	696

TABLE I (CONT.)

RUN		201	206	207	208
D	INCHES	.323	.323	.323	.323
G	LBM/HR/FT**2	127951.416	68317.798	69692.408	71153.255
V	VOLTS	10.050	10.500	7.020	4.600
I	AMPS	201.500	193.000	144.500	108.500
P	PSIA	25.136	24.710	24.865	24.478
ΔP1	PSI	.592	.406	.232	.155
ΔP2	PSI	1.496	1.161	.522	.277
ΔTSUB	R	5.300	4.770	4.770	6.360
Q1	WATTS	1.580	9.600	23.900	42.000
TSAT1	R	148.041	147.745	147.853	147.582
TEXIT MEAS	R	0.	0.	0.	0.
TEXIT CALC	R	178.427	495.209	157.566	147.386
EXIT QUALITY		1.099	2.054	1.032	.514

I	X INCH	TWALL INSIDE R	Q/A BTU/HR/ FT**2	BULK TEMP R	TWALL INSIDE R	Q/A BTU/HR/ FT**2	BULK TEMP R	TWALL INSIDE R	Q/A BTU/HR/ FT**2	BULK TEMP R	TWALL INSIDE R	Q/A BTU/HR/ FT**2	BULK TEMP R
1	00	00	00	143	00	00	145	00	00	147	00	00	148
2	2	1165	23016	148	1197	20933	148	678	9863	148	532	5117	148
3	6	1044	22110	148	1184	20853	148	732	10089	148	433	4900	148
4	10	894	20894	148	1102	20325	148	744	10138	148	455	4948	148
5	14	845	20481	148	1065	20079	148	754	10179	148	479	5001	148
6	18	820	20267	148	1035	19875	148	760	10203	148	498	5043	147
7	22	800	20095	148	1013	19723	147	764	10219	148	518	5087	147
8	26	779	19912	148	995	19598	189	761	10207	148	533	5120	147
9	30	753	19685	147	982	19506	245	759	10199	148	545	5146	147
10	34	730	19482	147	979	19485	301	756	10187	148	549	5155	147
11	38	704	19250	147	982	19506	357	749	10159	148	559	5177	147
12	42	688	19089	147	996	19605	414	744	10138	148	567	5195	147
13	46	668	18927	167	1011	19710	471	739	10118	148	569	5200	147
14	48	00	00	178	00	00	495	00	00	158	00	00	147
		FINE DROPLETS SIMILAR TO FIG 16 E			VERY FINE DROPLETS SIMILAR TO FIG 16 D			DROPLETS SIMILAR TO FIG 15 D			LARGE DROPLETS SIMILAR TO FIG 15 A		

TABLE II FILM BOILING TESTS

RUN		209	210	211	212
D	INCHES	.323	.323	.323	.323
G	LBM/HR/FT**2	69931.336	190059.227	190948.715	192035.746
V	VOLTS	8.900	11.000	9.720	8.220
I	AMPS	172.000	224.000	204.000	180.000
P	PSIA	24.826	24.865	24.865	24.749
ΔP1	PSI	.319	.890	.716	.522
ΔP2	PSI	.813	2.206	1.707	1.190
ΔTSUB	R	5.830	5.830	6.360	5.300
Q1	WATTS	8.900	2.700	4.000	5.900
TSAT1	R	147.826	147.853	147.853	147.772
TEXIT MEAS	R	0.	0.	0.	0.
TEXIT CALC	R	316.265	146.256	146.629	146.923
EXIT QUALITY		1.518	.896	.711	.527

I	X INCH	TWALL INSIDE R	Q/A BTU/HR/ FT**2	BULK TEMP R	TWALL INSIDE R	Q/A BTU/HR/ FT**2	BULK TEMP R	TWALL INSIDE R	Q/A BTU/HR/ FT**2	BULK TEMP R	TWALL INSIDE R	Q/A BTU/HR/ FT**2	BULK TEMP R
1	00	00	00	144	00	00	142	00	00	142	00	00	143
2	2	833	14808	148	1296	29847	148	1106	23246	148	866	16423	147
3	6	989	15682	148	1027	27274	148	969	22142	148	861	15390	148
4	10	951	15477	148	866	25589	148	799	20663	148	727	15497	148
5	14	932	15373	148	813	25014	148	740	20131	148	650	15030	148
6	18	919	15301	148	786	24718	147	715	19902	147	631	14825	148
7	22	908	15239	148	763	24464	147	698	19745	147	618	14732	147
8	26	895	15166	148	739	24197	147	680	19579	147	607	14653	147
9	30	884	15103	148	706	23827	147	658	19374	147	593	14552	147
10	34	874	15046	173	675	23477	147	636	19168	147	580	14459	147
11	38	866	15000	214	639	23068	147	610	18923	147	563	14335	147
12	42	863	14983	256	615	22793	147	517	18038	147	550	14241	147
13	46	863	14983	298	589	22494	146	566	18505	147	532	14110	147
14	48	00	00	316	00	00	146	00	00	147	00	00	147
		FINE DROPLETS SIMILAR TO FIG 16 A			SMALL DROPLETS			SMALL DROPLETS SIMILAR TO FIG 16 F			DROPLETS SIMILAR TO FIG 16 C		

TABLE II (CONT.)

RUN		213	214	215	227
D	INCHES	.323	.323	.323	.323
G	LBM/HR/FT**2	130319.106	125573.116	191760.254	131460.619
V	VOLTS	6.650	5.700	6.500	8.430
I	AMPS	148.000	132.000	150.000	179.000
P	PSIA	25.136	25.232	24.749	25.039
ΔP1	PSI	.325	.271	.420	.453
ΔP2	PSI	.695	.503	.865	1.070
ΔTSUB	R	4.770	4.770	5.300	7.420
Q1	WATTS	21.900	29.600	29.500	20.500
TSAT1	R	148.041	148.108	147.772	147.974
TEXIT MEAS	R	0.	0.	0.	0.
TEXIT CALC	R	147.556	147.759	147.158	147.219
EXIT QUALITY		.530	.421	.350	.791

I	X INCH	TWALL INSIDE R	Q/A BTU/HR/ FT**2	BJLK TEMP R	TWALL INSIDE R	Q/A BTU/HR/ FT**2	BULK TEMP R	TWALL INSIDE R	Q/A BTU/HR/ FT**2	BULK TEMP R	TWALL INSIDE R	Q/A BTU/HR/ FT**2	BULK TEMP R
1	00	00	00	145	00	00	146	00	00	144	00	00	142
2	2	650	10189	148	597	7879	148	709	10646	147	946	16708	148
3	6	675	10302	148	552	7716	148	654	10394	148	823	15937	148
4	10	638	10134	148	542	7680	148	608	10177	148	754	15482	148
5	14	613	10018	148	533	7647	148	562	9956	148	726	15293	148
6	18	599	9953	148	526	7622	148	537	9834	148	711	15191	148
7	22	595	9934	148	529	7633	148	527	9786	148	701	15123	148
8	26	590	9910	148	528	7629	148	519	9747	147	688	15034	148
9	30	584	9882	148	527	7626	148	512	9713	147	671	14917	148
10	34	580	9863	148	525	7618	148	505	9680	147	656	14813	147
11	38	570	9816	148	521	7604	148	497	9641	147	635	14666	147
12	42	564	9787	148	519	7597	148	491	9612	147	621	14567	147
13	46	554	9739	148	514	7579	148	489	9603	147	606	14462	147
14	48	00	00	148	00	00	148	00	00	147	00	00	147
		DROPLETS SIMILAR TO FIG 15 E			DROPLETS			DROPLETS SIMILAR TO FIG 15 F			DROPLETS SIMILAR TO FIG 16 B		

TABLE II (CONT.)

RUN		258	259	260	261
D	INCHES	.323	.323	.323	.323
G	LBM/HR/FT**2	188522.129	70439.183	69934.648	128404.299
V	VOLTS	21.000	18.450	14.250	19.700
I	AMPS	224.000	171.500	144.500	201.500
P	PSIA	25.542	25.213	24.923	25.058
ΔP1	PSI	2.225	.793	.735	1.548
ΔP2	PSI	8.959	2.806	1.703	5.515
ΔTSUB	R	4.240	5.300	5.300	5.300
Q1	WATTS	14.400	25.000	25.000	10.000
TSAT1	R	148.320	148.095	147.894	147.988
TEXIT	MEAS R	410.000	865.000	515.000	520.000
TEXIT	CALC R	401.534	861.824	506.387	538.809
EXIT	QUALITY	1.770	3.143	2.087	2.177

I	X INCH	TWALL INSIDE R	Q/A BTU/HR/ FT**2	BULK TEMP R	TWALL INSIDE R	Q/A BTU/HR/ FT**2	BULK TEMP R	TWALL INSIDE R	Q/A BTU/HR/ FT**2	BULK TEMP R	TWALL INSIDE R	Q/A BTU/HR/ FT**2	BULK TEMP R
1	C0	00	00	145	00	00	147	00	00	147	00	00	144
2	2	1196	29453	148	911	15413	148	615	9636	148	1165	23474	148
3	6	1034	27730	148	989	15876	148	738	10206	148	1047	22510	148
4	10	864	25814	148	942	15600	148	749	10255	148	892	21155	148
5	14	811	25195	148	922	15480	148	755	10281	148	830	20579	148
6	18	789	24935	148	910	15407	148	761	10308	148	809	20384	148
7	22	762	24615	148	895	15315	148	760	10303	148	788	20188	148
8	26	740	24352	148	886	15260	148	760	10303	148	768	20000	148
9	30	707	23956	148	872	15173	148	759	10299	148	748	19810	148
10	34	672	23532	148	864	15123	182	753	10273	148	724	19581	147
11	38	641	23154	147	854	15060	223	749	10255	147	700	19351	147
12	42	609	22761	147	853	15054	265	741	10219	147	678	19138	147
13	46	580	22403	147	848	15023	307	735	10192	147	658	18944	170
14	50	547	21993	147	847	15016	349	722	10134	174	645	18817	198
15	54	542	21931	157	857	15079	392	724	10143	202	633	18700	227
16	58	534	21832	179	875	15192	435	724	10143	231	635	18719	255
17	62	538	21882	202	890	15284	478	726	10152	259	637	18739	284
18	66	538	21882	224	908	15395	521	726	10152	288	647	18837	313
19	70	540	21907	247	911	15413	565	732	10179	316	656	18925	342
20	74	562	22180	270	963	15724	609	735	10192	345	672	19080	371
21	78	568	22254	293	995	15911	653	744	10233	374	689	19245	401
22	82	599	22638	317	1027	16093	699	752	10268	403	711	19457	431
23	86	608	22748	341	1064	16299	745	765	10325	432	734	19677	461
24	90	645	23202	365	1100	16494	791	769	10343	462	762	19943	492
25	94	656	23337	389	1143	16718	838	795	10456	491	789	20197	523
26	96	00	00	402	00	00	862	00	00	506	00	00	539
		FINE MIST BARELY VISIBLE			FEW FINE DROPLETS BARELY DETECTABLE			FINE DROPLETS SEE FIG 17 D			FINE MIST BARELY VISIBLE		

TABLE II (CONT.)

RUN		262	263	264	265
D	INCHES	.323	.323	.323	.323
G	LBM/HR/FT**2	70482.066	127308.489	129762.770	194358.613
V	VOLTS	9.520	16.400	13.050	18.550
I	AMPS	108.500	178.000	148.500	204.500
P	PSIA	25.136	25.136	25.136	24.845
ΔP1	PSI	.310	1.103	.697	1.741
ΔP2	PSI	.716	3.406	1.916	6.115
ΔTSUB	R	0.	6.360	6.360	7.420
Q1	WATTS	25.000	15.000	15.000	25.000
TSAT1	R	148.041	148.041	148.041	147.840
TEXIT MEAS	R	150.000	295.000	147.000	268.000
TEXIT CALC	R	175.732	350.367	163.631	266.686
EXIT QUALITY		1.089	1.621	1.054	1.372

I	X INCH	TWALL INSIDE R	Q/A BTU/HR/ FT**2	BULK TEMP R	TWALL INSIDE R	Q/A BTU/HR/ FT**2	BULK TEMP R	TWALL INSIDE R	Q/A BTU/HR/ FT**2	BULK TEMP R	TWALL INSIDE R	Q/A BTU/HR/ FT**2	BULK TEMP R
1	00	00	00	148	00	00	143	00	00	143	00	00	142
2	2	391	4877	148	880	16465	148	594	10031	147	1132	23863	148
3	6	401	4902	148	847	16238	148	644	10284	148	979	22536	148
4	10	439	4995	148	758	15609	148	620	10163	148	803	20886	148
5	14	459	5044	148	719	15326	148	598	10051	148	748	20352	148
6	18	491	5122	148	704	15216	148	587	9995	148	725	20126	148
7	22	504	5154	148	693	15134	148	649	10309	148	705	19929	148
8	26	529	5216	148	681	15046	148	579	9954	148	689	19770	147
9	30	532	5223	148	667	14942	148	577	9943	148	667	19550	147
10	34	544	5252	148	651	14822	148	569	9902	148	641	19289	147
11	38	553	5275	148	635	14702	147	566	9887	148	619	19067	147
12	42	558	5287	148	617	14566	147	555	9830	148	591	18783	147
13	46	561	5295	148	601	14444	147	549	9798	148	569	18558	147
14	50	559	5290	148	576	14253	147	529	9696	148	533	18189	146
15	54	562	5297	148	570	14207	147	529	9696	147	518	18036	146
16	58	565	5305	148	563	14153	147	519	9644	147	513	17985	146
17	62	565	5305	148	556	14099	167	514	9618	147	500	17852	146
18	66	565	5305	148	549	14045	188	504	9567	147	494	17791	146
19	70	565	5305	148	544	14007	209	499	9541	147	486	17710	152
20	74	565	5305	148	540	13976	231	492	9505	147	484	17689	169
21	78	565	5305	148	540	13976	252	485	9469	147	480	17648	186
22	82	565	5305	148	543	13999	274	479	9438	147	489	17740	204
23	86	562	5297	148	545	14015	296	474	9413	147	488	17730	222
24	90	562	5297	154	555	14092	317	470	9392	147	503	17883	240
25	94	562	5297	169	564	14161	339	466	9372	157	507	17924	258
26	96	00	00	176	00	00	350	00	00	164	00	00	267
		DROPLETS SEE FIG 17 A			FINE MIST			DROPLETS SEE FIG 17 B			FINE MIST		

TABLE II (CONT.)

RUN		266	267	268	299
D	INCHES	.323	.323	.323	.323
G	LBM/HR/FT**2	189559.758	129288.660	191691.332	129047.703
V	VOLTS	15.900	9.150	12.700	21.800
I	AMPS	180.000	112.500	150.000	212.500
P	PSIA	25.232	25.290	25.290	25.000
ΔP1	PSI	1.238	.464	.832	1.935
ΔP2	PSI	3.657	.948	2.167	6.772
ΔTSUB	R	6.890	4.240	4.240	9.540
Q1	WATTS	10.000	25.000	25.000	10.000
TSAT1	R	148.108	148.148	148.148	147.948
TEXIT MEAS	R	147.000	147.000	147.000	620.000
TEXIT CALC	R	163.791	147.486	146.603	647.654
EXIT QUALITY		1.058	.581	.711	2.494

I	X INCH	TWALL INSIDE R	Q/A BTU/HR/ FT**2	BULK TEMP R	TWALL INSIDE R	Q/A BTU/HR/ FT**2	BULK TEMP R	TWALL INSIDE R	Q/A BTU/HR/ FT**2	BULK TEMP R	TWALL INSIDE R	Q/A BTU/HR/ FT**2	BULK TEMP R
1	00	00	00	142	00	00	146	00	00	145	00	00	139
2	2	998	17500	146	352	5063	148	616	10311	148	1197	26886	148
3	6	900	16845	148	373	5119	148	644	10455	148	1047	25469	148
4	10	755	15815	148	397	5182	148	599	10223	148	922	24214	148
5	14	675	15219	148	407	5209	148	562	10029	148	892	23904	148
6	18	646	14999	148	417	5235	148	539	9908	148	855	23518	148
7	22	628	14861	148	424	5253	148	526	9840	148	830	23254	148
8	26	618	14784	148	431	5272	148	519	9803	148	810	23041	147
9	30	603	14669	148	437	5288	148	515	9783	148	784	22763	147
10	34	588	14553	148	440	5296	148	507	9741	148	757	22472	147
11	38	573	14436	147	446	5312	148	504	9725	148	732	22200	147
12	42	556	14303	147	448	5317	148	493	9667	148	707	21927	179
13	46	538	14163	147	449	5319	148	486	9631	148	690	21740	212
14	50	513	13968	147	449	5319	148	477	9583	148	672	21541	245
15	54	506	13914	147	448	5317	148	467	9531	147	682	21652	278
16	58	498	13852	147	448	5317	148	459	9489	147	692	21762	311
17	62	488	13774	147	448	5317	148	454	9463	147	710	21960	345
18	66	478	13696	147	446	5312	148	444	9411	147	727	22146	378
19	70	468	13618	147	444	5306	148	438	9379	147	752	22417	413
20	74	458	13541	146	441	5298	148	428	9327	147	777	22688	448
21	78	449	13471	146	437	5288	148	422	9295	147	805	22988	483
22	82	443	13424	146	436	5285	148	413	9248	147	834	23296	519
23	86	435	13362	146	431	5272	148	407	9217	147	867	23644	555
24	90	433	13346	146	431	5272	148	400	9180	147	899	23977	592
25	94	428	13307	157	429	5267	148	397	9164	147	932	24317	629
26	96	00	00	164	00	00	147	00	00	147	00	00	648
		DROPLETS			DROPLETS SEE FIG 17 B			DROPLETS SEE FIG 17 F			NO LIQUID		

TABLE II (CONT.)

RUN		271	272	274	275
D	INCHES	.462	.462	.462	.462
G	LBM/HR/FT**2	69712.723	70292.484	69051.722	128091.782
V	VOLTS	21.400	14.250	17.800	20.600
I	AMPS	192.000	143.000	168.000	200.000
P	PSIA	24.691	24.691	24.981	24.574
ΔP1	PSI	.462	.319	.348	.646
ΔP2	PSI	1.248	.617	.851	1.614
ΔTSUB	R	4.770	4.770	7.420	7.420
Q1	WATTS	22.500	30.000	40.000	25.000
TSAT1	R	147.732	147.732	147.934	147.650
TEXIT MEAS	R	530.000	150.000	360.000	230.000
TEXIT CALC	R	483.311	149.549	305.794	176.439
EXIT QUALITY		2.019	1.007	1.487	1.094

I	X INCH	TWALL INSIDE R	Q/A BTU/HR/ FT**2	BULK TEMP R	TWALL INSIDE R	Q/A BTU/HR/ FT**2	BULK TEMP R	TWALL INSIDE R	Q/A BTU/HR/ FT**2	BULK TEMP R	TWALL INSIDE R	Q/A BTU/HR/ FT**2	BULK TEMP R
1	00	00	00	145	00	00	146	00	00	144	00	00	141
2	2	819	13830	148	428	6667	148	584	9774	148	780	15004	146
3	6	902	14206	148	473	6788	148	671	10109	148	841	15324	148
4	10	922	14293	148	504	6871	148	704	10231	148	797	15094	148
5	14	934	14344	148	524	6925	148	738	10354	148	766	14929	148
6	18	941	14374	148	557	7014	148	754	10410	148	749	14837	148
7	22	936	14353	148	581	7080	148	776	10487	148	738	14777	147
8	26	935	14348	148	605	7145	148	782	10508	148	735	14761	147
9	30	926	14310	148	619	7182	148	765	10449	148	727	14717	147
10	34	919	14280	148	631	7214	148	792	10542	148	721	14684	147
11	38	909	14238	147	640	7237	148	795	10552	148	709	14618	147
12	42	899	14192	147	647	7255	148	789	10532	148	702	14579	147
13	46	891	14157	147	652	7268	148	790	10535	148	689	14507	147
14	50	882	14117	163	652	7268	147	781	10504	148	676	14434	147
15	54	875	14086	190	654	7273	147	779	10497	148	662	14355	147
16	58	871	14068	217	654	7273	147	772	10473	148	652	14298	147
17	62	868	14055	245	654	7273	147	771	10470	148	638	14218	147
18	66	865	14041	273	651	7265	147	761	10435	153	627	14155	147
19	70	864	14037	300	649	7260	147	746	10382	172	612	14069	147
20	74	869	14059	328	645	7250	147	751	10400	193	603	14016	147
21	78	874	14081	356	643	7245	147	752	10403	213	589	13935	147
22	82	882	14117	384	640	7237	147	747	10386	233	583	13900	147
23	86	886	14135	412	636	7227	147	747	10386	254	571	13829	147
24	90	904	14214	441	634	7221	147	745	10379	275	566	13800	155
25	94	913	14254	469	629	7208	147	747	10386	295	554	13729	169
26	96	00	00	483	00	00	150	00	00	306	00	00	176
		FINE MIST			DROPLETS			FINE DROPLETS			FINE DROPLETS		

TABLE II (CONT.)

RUN		282	284	288	289
D	INCHES	.228	.228	.228	.228
G	LBM/HR/FT**2	69690.775	129047.703	129047.703	69774.482
V	VOLTS	11.690	14.600	12.500	9.270
I	AMPS	129.000	170.000	153.000	110.000
P	PSIA	25.000	25.348	25.000	24.903
ΔP1	PSI	.871	2.187	1.684	.571
ΔP2	PSI	3.367	10.352	6.637	1.916
ΔTSUB	R	8.480	9.540	9.540	6.360
Q1	WATTS	25.000	25.000	25.000	20.000
TSAT1	R	147.948	148.188	147.948	147.880
TEXIT MEAS	R	810.000	698.000	530.000	427.000
TEXIT CALC	R	819.470	716.773	509.633	503.858
EXIT QUALITY		3.014	2.684	2.089	2.079

I	X INCH	TWALL INSIDE R	Q/A BTU/HR/ FT**2	BULK TEMP R	TWALL INSIDE R	Q/A BTU/HR/ FT**2	BULK TEMP R	TWALL INSIDE R	Q/A BTU/HR/ FT**2	BULK TEMP R	TWALL INSIDE R	Q/A BTU/HR/ FT**2	BULK TEMP R
1	00	00	00	148	00	00	143	00	00	143	00	00	148
2	2	731	10094	148	1062	20205	148	947	15587	148	544	6787	148
3	6	778	10296	148	887	18831	148	815	14764	148	600	6965	148
4	10	773	10274	148	773	17897	148	752	14356	148	628	7052	148
5	14	768	10253	148	737	17595	148	688	13925	148	645	7103	148
6	18	763	10232	148	715	17409	148	668	13790	148	654	7130	148
7	22	758	10211	148	697	17256	148	648	13655	148	659	7145	148
8	26	752	10185	148	675	17069	148	633	13553	148	661	7151	148
9	30	748	10168	148	657	16914	148	618	13450	147	661	7151	148
10	34	743	10146	165	637	16742	148	603	13347	147	661	7151	148
11	38	743	10146	204	624	16629	171	588	13243	147	660	7148	148
12	42	744	10151	244	614	16542	206	580	13188	147	661	7151	148
13	46	745	10155	285	607	16481	241	562	13063	152	659	7145	148
14	50	738	10125	326	594	16368	277	553	13000	179	644	7100	172
15	54	754	10193	366	609	16499	312	543	12931	207	651	7121	200
16	58	768	10253	408	623	16620	348	543	12931	234	654	7130	228
17	62	783	10317	449	642	16785	385	543	12931	262	659	7145	256
18	66	803	10401	491	666	16991	421	553	13000	290	664	7160	285
19	70	825	10492	533	693	17222	459	563	13070	318	671	7181	313
20	74	851	10598	576	723	17477	497	578	13174	347	677	7199	342
21	78	879	10710	619	760	17788	535	594	13285	376	689	7234	371
22	82	911	10836	663	793	18063	574	620	13464	405	697	7258	400
23	86	946	10970	707	834	18401	614	638	13587	434	711	7298	430
24	90	980	11098	752	870	18694	655	663	13756	464	723	7333	459
25	94	1014	11222	797	917	19071	696	689	13931	494	739	7378	489
26	96	00	00	819	00	00	717	00	00	510	00	00	504
		FEW FINE DROPLETS			NO DROPLETS			BARELY DETECTABLE LIQUID			DROPLETS		

TABLE II (CONT.)

RUN		290	291	292	293
D	INCHES	.228	.228	.228	.228
G	LBM/HR/FT**2	69555.256	129483.896	129345.780	188774.924
V	VOLTS	7.370	6.820	13.250	14.100
I	AMPS	94.000	114.500	158.800	177.000
P	PSIA	24.536	24.903	25.058	26.800
ΔP1	PSI	.420	.764	1.780	2.515
ΔP2	PSI	1.190	2.277	7.546	11.900
ΔTSUB	R	8.480	8.890	9.010	9.540
Q1	WATTS	20.000	27.000	27.000	15.000
TSAT1	R	147.623	147.880	147.988	149.162
TEXIT MEAS	R	150.000	150.000	585.000	440.000
TEXIT CALC	R	286.243	146.231	579.758	432.662
EXIT QUALITY		1.428	.877	2.293	1.859

I	X INCH	TWALL INSIDE R	Q/A BTU/HR/ FT**2	BULK TEMP R	TWALL INSIDE R	Q/A BTU/HR/ FT**2	BULK TEMP R	TWALL INSIDE R	Q/A BTU/HR/ FT**2	BULK TEMP R	TWALL INSIDE R	Q/A BTU/HR/ FT**2	BULK TEMP R
1	00	00	00	146	00	00	146	00	00	144	00	00	142
2	2	399	4611	148	497	5683	148	948	16939	148	1037	21973	149
3	6	439	4691	148	534	5778	148	829	16121	148	860	20415	149
4	10	481	4775	148	524	5752	148	730	15413	148	707	18993	149
5	14	509	4832	148	519	5739	148	695	15157	148	665	18596	149
6	18	532	4878	148	511	5719	148	678	15032	148	642	18377	149
7	22	549	4912	148	513	5724	148	663	14921	148	623	18195	149
8	26	564	4943	147	508	5711	148	647	14802	148	600	17974	149
9	30	569	4953	147	509	5713	148	629	14668	148	579	17771	149
10	34	577	4969	147	503	5698	148	613	14547	147	555	17538	148
11	38	579	4973	147	503	5698	147	599	14442	147	539	17382	148
12	42	584	4983	147	494	5675	147	588	14359	153	515	17150	148
13	46	582	4979	147	491	5667	147	577	14275	183	493	16936	148
14	50	572	4959	147	466	5603	147	558	14123	213	466	16675	147
15	54	576	4967	147	452	5567	147	565	14176	243	469	16704	168
16	58	580	4975	147	466	5603	147	571	14222	273	467	16684	192
17	62	580	4975	147	463	5596	147	577	14275	304	468	16694	216
18	66	583	4981	147	456	5578	147	589	14366	335	471	16723	241
19	70	583	4981	158	455	5575	147	605	14487	366	479	16801	265
20	74	588	4991	177	449	5560	147	624	14630	398	491	16917	290
21	78	588	4991	197	447	5555	147	648	14810	430	507	17072	315
22	82	593	5001	216	439	5534	147	673	14995	463	526	17256	341
23	86	594	5003	236	440	5537	147	702	15209	495	548	17470	366
24	90	599	5013	256	435	5524	146	732	15428	529	576	17742	393
25	94	601	5017	276	435	5524	146	763	15652	563	599	17964	419
26	96	00	00	286	00	00	146	00	00	580	00	00	433
		DROPLETS			DROPLETS			NO LIQUID			NO LIQUID		

TABLE II (CONT.)

RUN		294	295	296
D	INCHES	.228	.228	.228
G	LBM/HR/FT**2	189309.447	189668.328	190574.531
V	VOLTS	13.000	12.000	10.250
I	AMPS	168.000	157.000	138.000
P	PSIA	24.961	24.903	24.903
ΔP1	PSI	2.709	1.935	1.354
ΔP2	PSI	9.675	7.353	4.315
ΔTSUB	R	9.540	9.540	9.540
Q1	WATTS	15.000	15.000	15.000
TSAT1	R	147.921	147.880	147.880
TEXIT MEAS	R	365.000	288.000	150.000
TEXIT CALC	R	350.913	275.036	158.332
EXIT QUALITY		1.622	1.398	1.043

I	X INCH	TWALL INSIDE R	Q/A BTU/HR/ FT**2	BULK TEMP R	TWALL INSIDE R	Q/A BTU/HR/ FT**2	BULK TEMP R	TWALL INSIDE R	Q/A BTU/HR/ FT**2	BULK TEMP R
1	00	00	00	140	00	00	140	00	00	140
2	2	517	18761	147	866	16062	146	798	11946	145
3	6	607	17885	148	775	15435	148	688	11381	148
4	10	674	16787	148	650	14542	148	518	10457	148
5	14	632	16432	148	603	14190	148	549	10628	148
6	18	611	16253	148	586	14064	148	528	10512	148
7	22	594	16107	147	569	13937	148	515	10441	148
8	26	576	15953	147	556	13840	147	504	10380	148
9	30	551	15737	147	538	13706	147	496	10336	147
10	34	532	15573	147	517	13550	147	486	10281	147
11	38	510	15383	147	500	13423	147	477	10231	147
12	42	492	15228	146	485	13312	147	463	10154	147
13	46	465	14995	146	466	13170	147	449	10077	147
14	50	443	14806	146	435	12940	146	419	9912	147
15	54	443	14806	145	434	12932	146	422	9928	147
16	58	439	14771	145	428	12888	146	415	9890	147
17	62	435	14737	165	420	12828	146	408	9851	146
18	66	434	14728	186	417	12806	145	400	9807	146
19	70	435	14737	207	410	12754	154	393	9769	146
20	74	440	14780	229	411	12761	172	387	9736	146
21	78	447	14840	250	408	12739	191	381	9703	146
22	82	457	14926	272	413	12776	209	375	9670	145
23	86	477	15099	294	418	12813	228	372	9653	145
24	90	491	15219	317	427	12880	247	368	9631	145
25	94	507	15357	340	434	12932	266	366	9620	152
26	96	00	00	351	00	00	275	00	00	158
		FINE MIST BARELY VISIBLE			FINE MIST			FINE MIST		

TABLE II (CONT.)

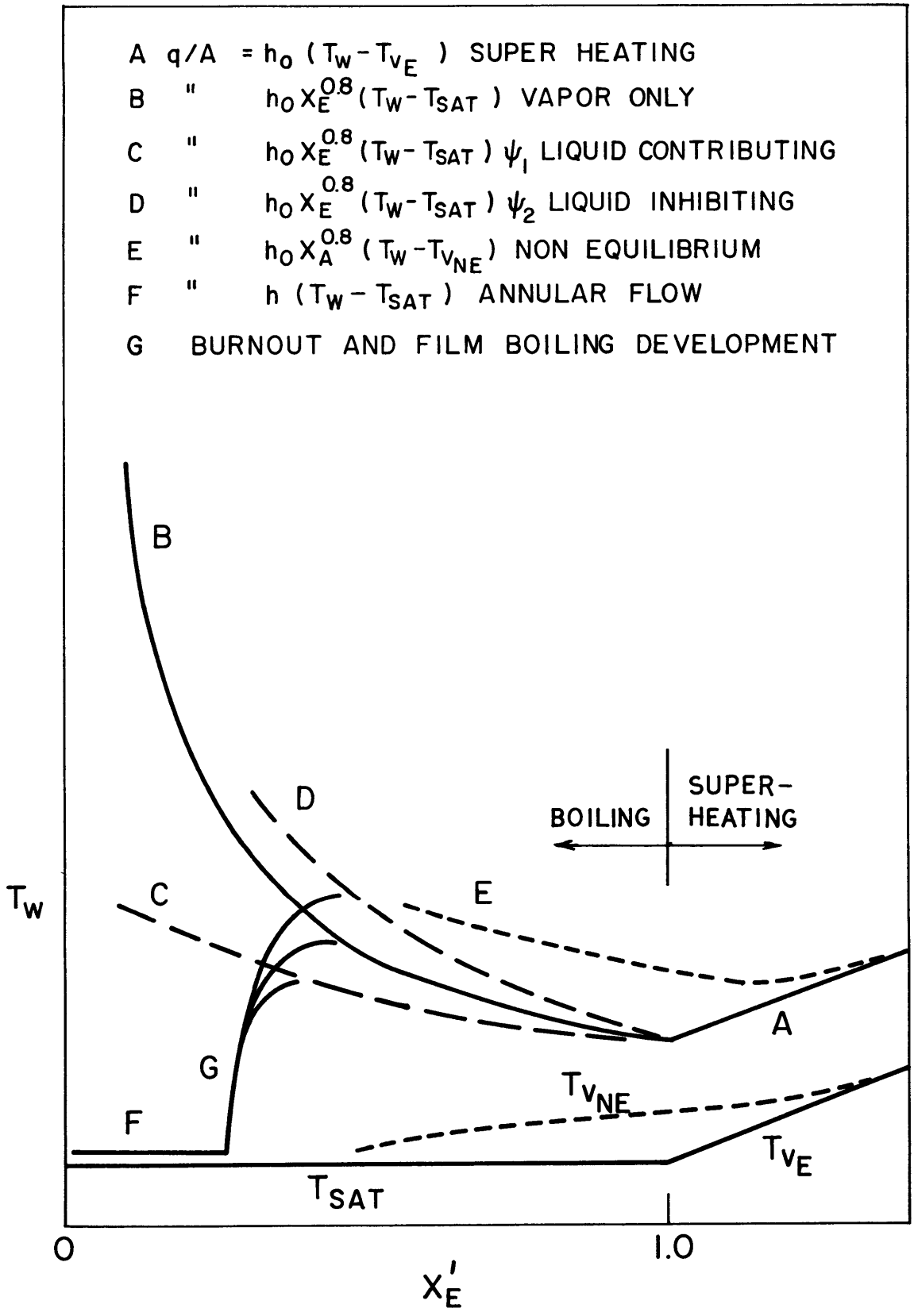

FIG. 1 TYPICAL TUBE WALL TEMPERATURE PROFILES IN FILM BOILING

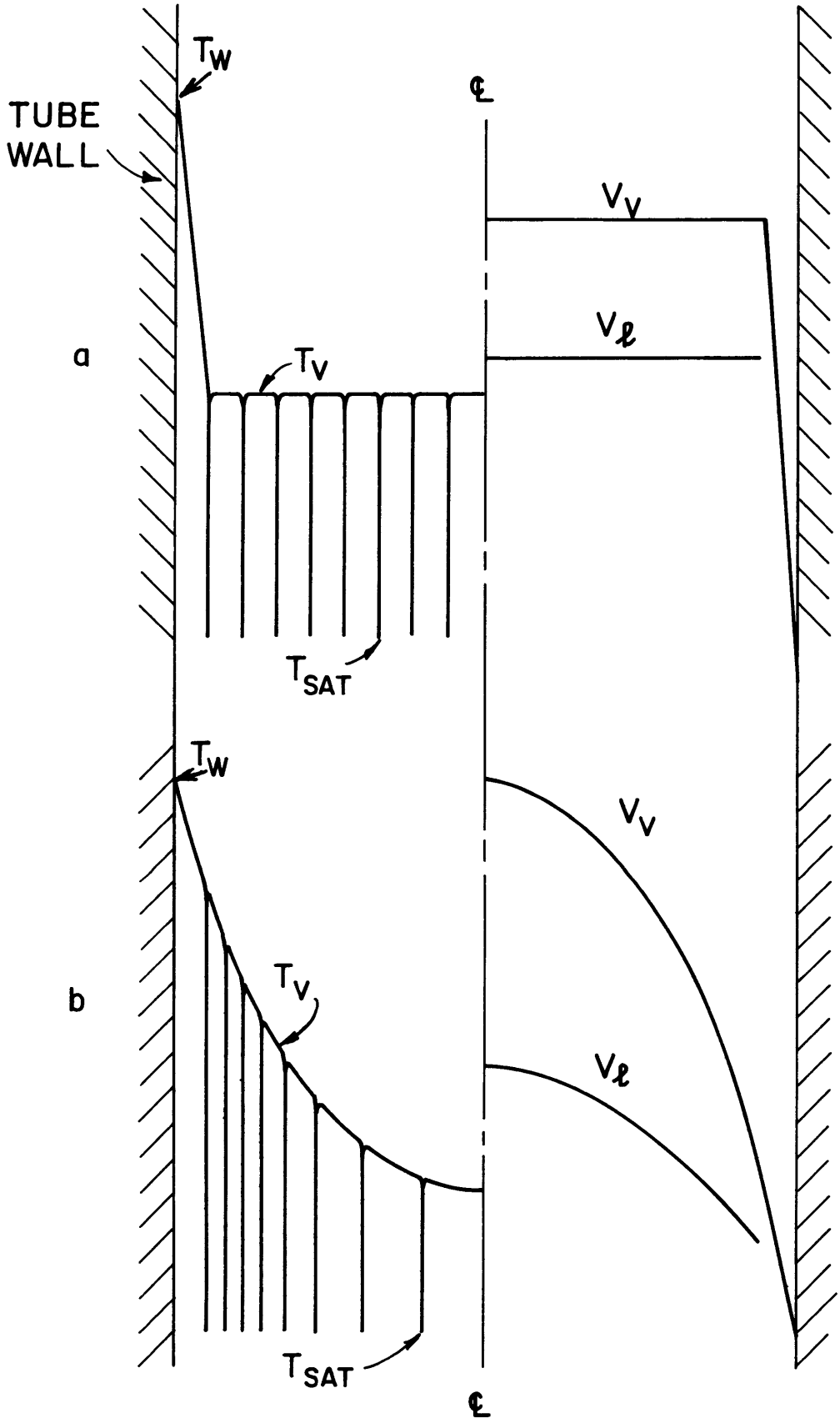

FIG. 2 FLOW MODELS FOR DISPERSED FLOW FILM BOILING

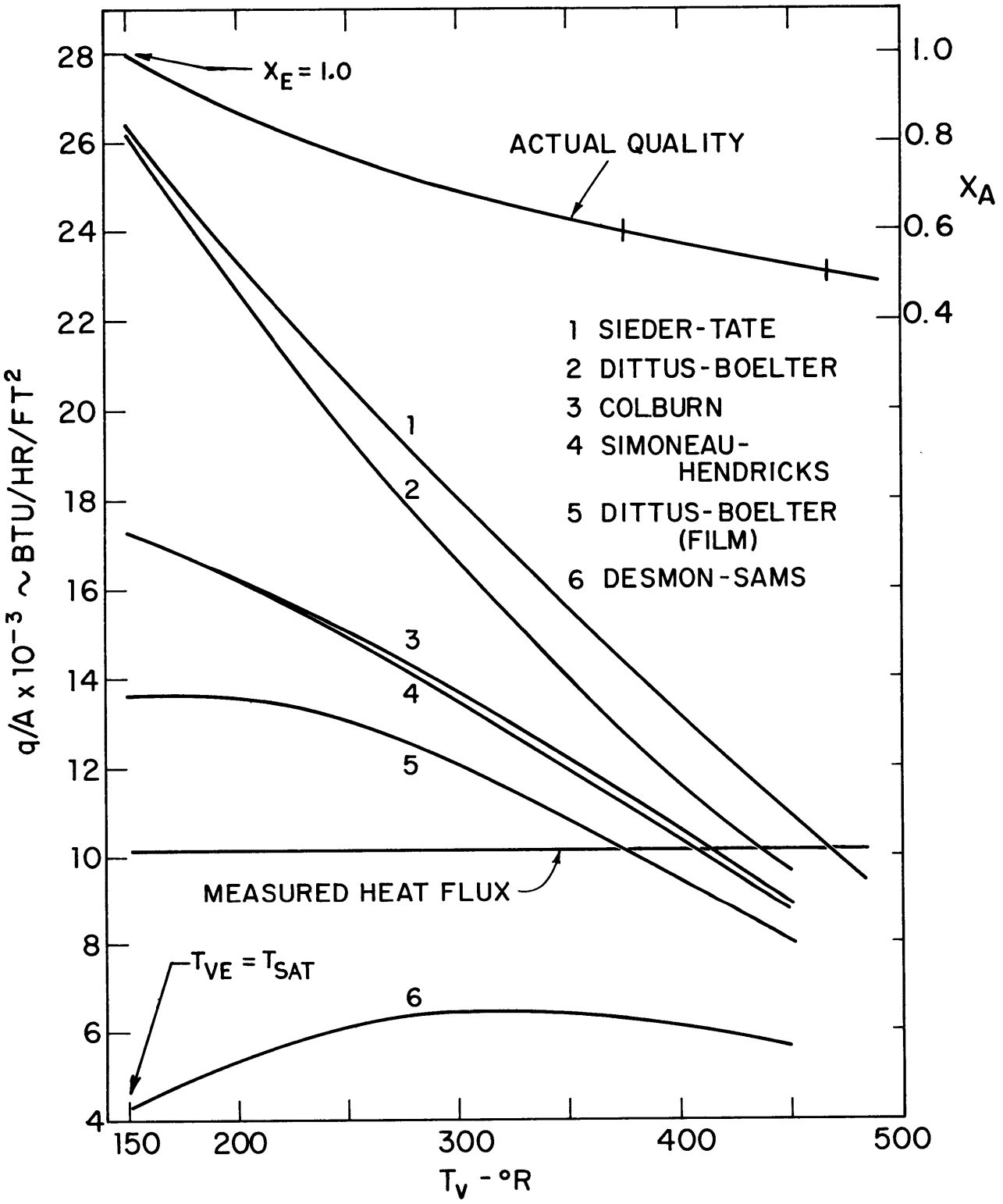

FIG. 3 VARIATION IN DEPARTURE FROM EQUILIBRIUM CALCULATED BY VARIOUS CORRELATIONS AT STATION 13 OF RUN 260

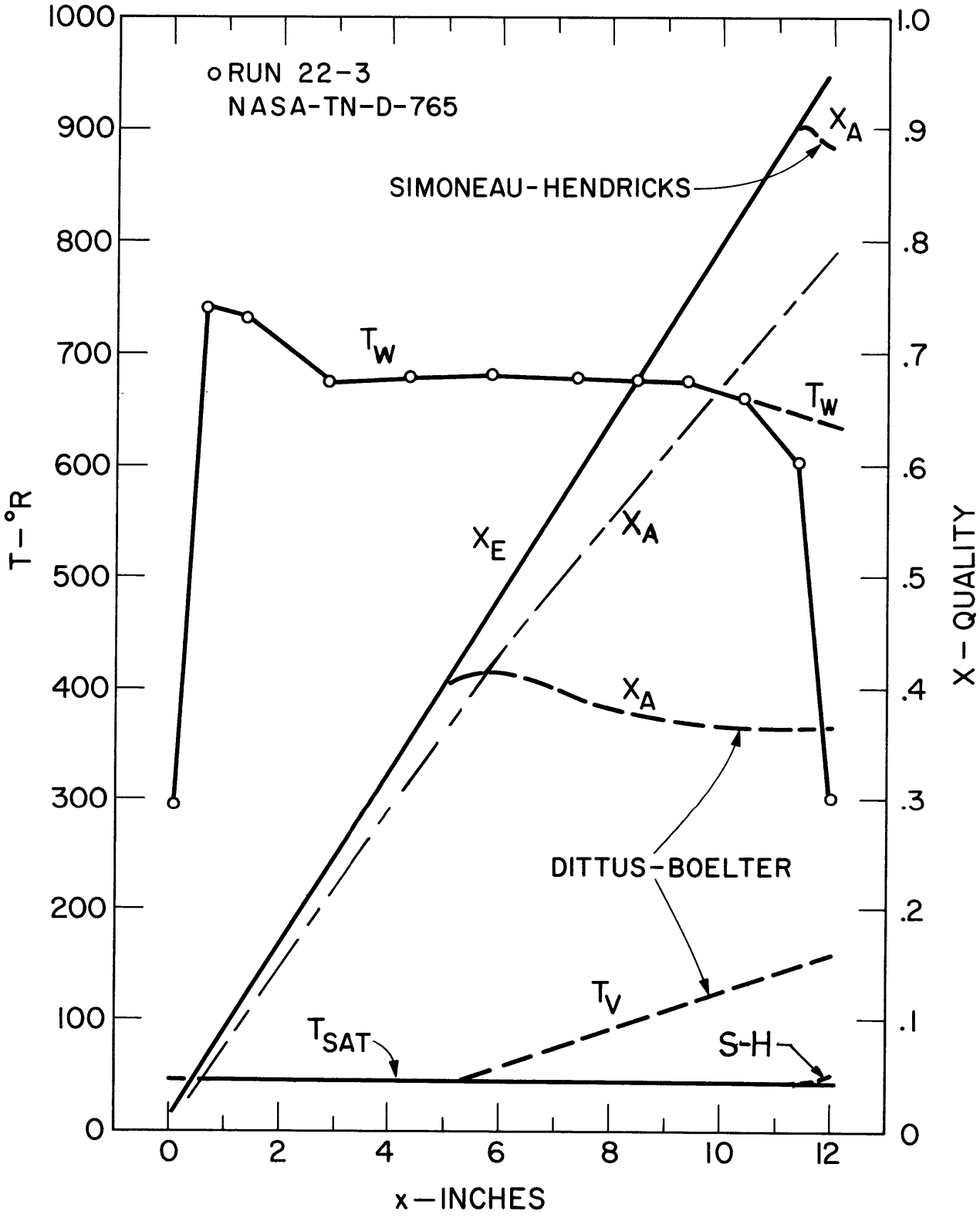

FIG. 4 CALCULATED DEPARTURE FROM EQUILIBRIUM FOR H_2 FILM BOILING

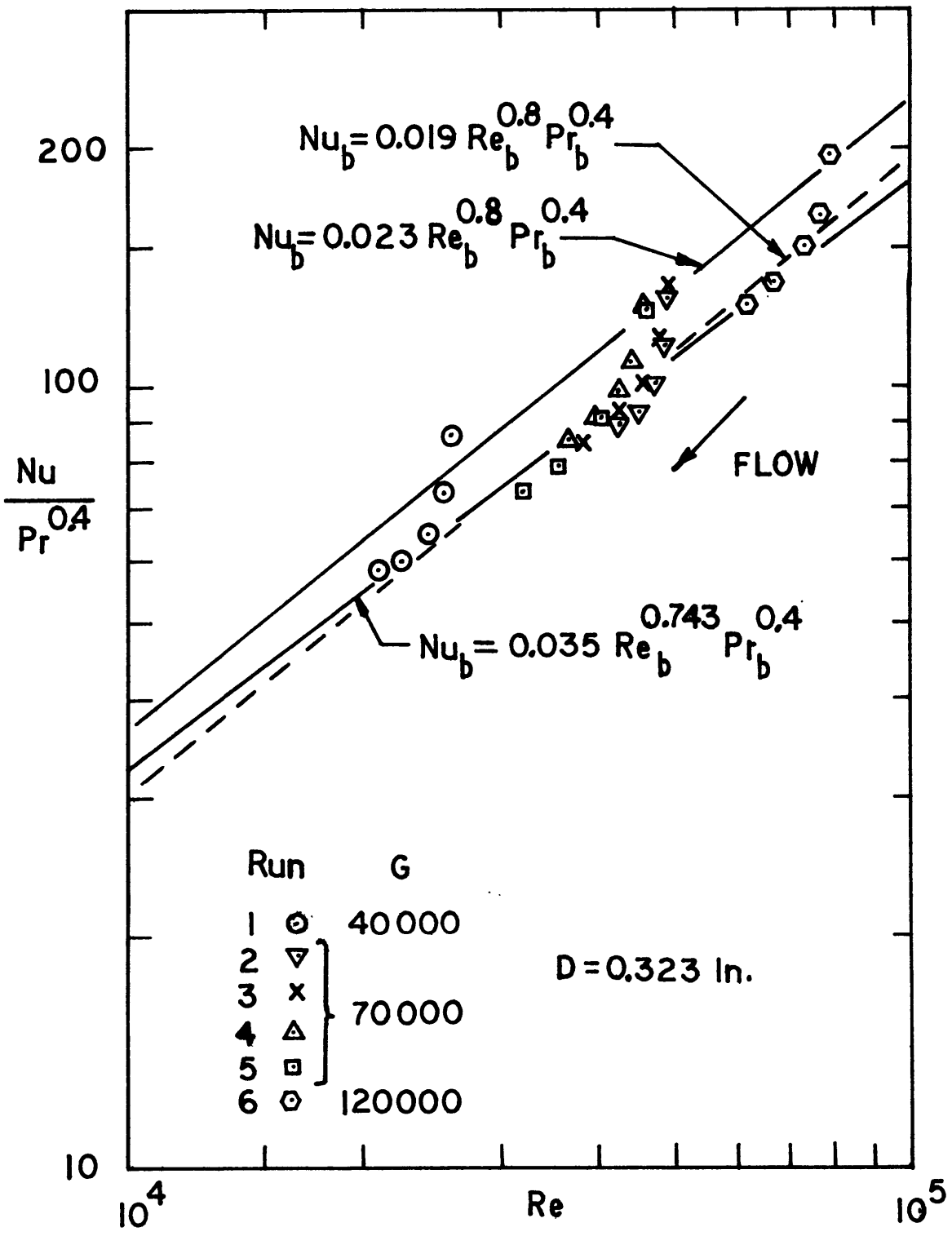

FIG. 5 RESULTS OF PURE VAPOR HEAT TRANSFER TESTS

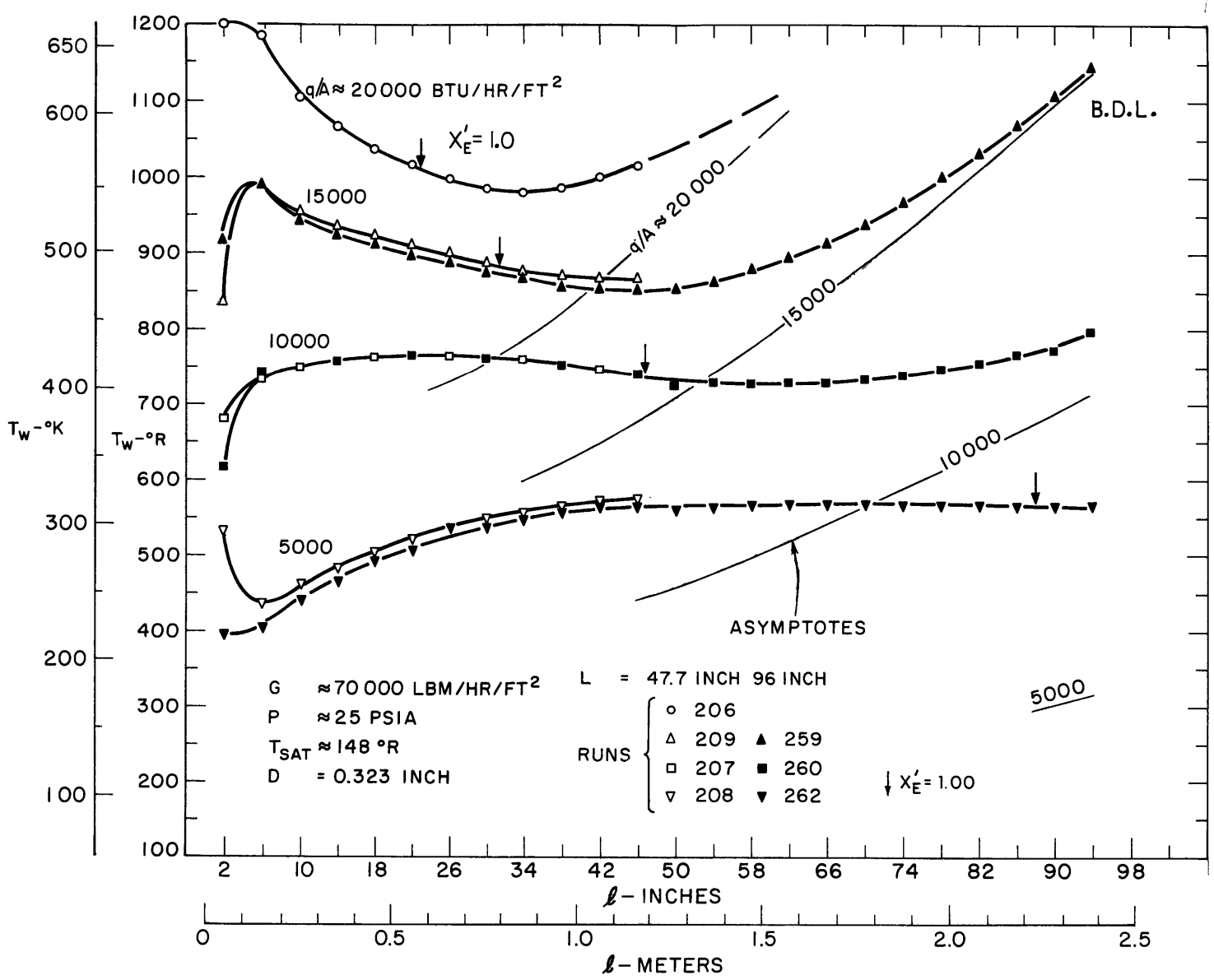

FIG. 6 TUBE WALL TEMPERATURE PROFILES - 0.323 INCH ID TUBE

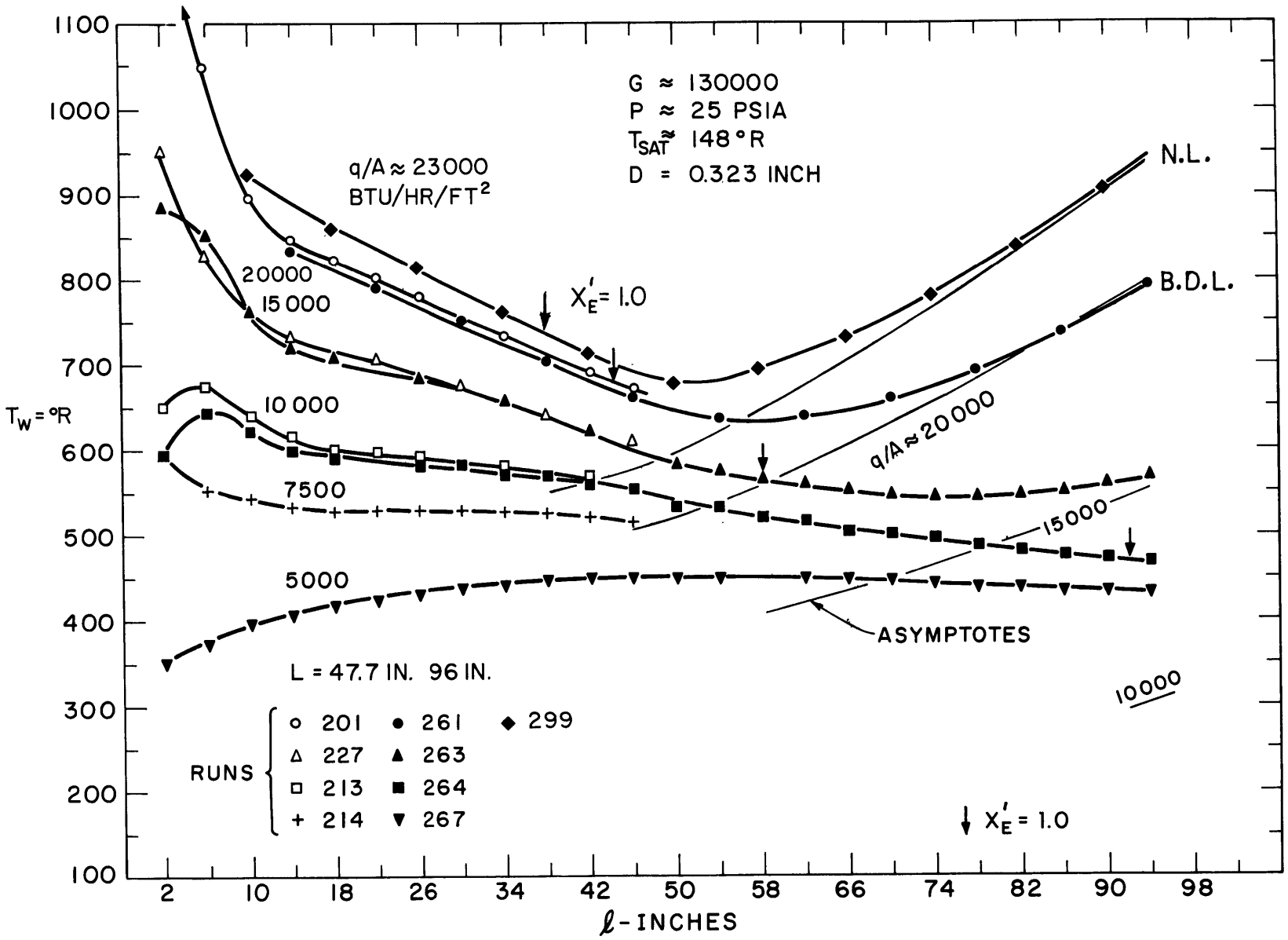

FIG. 7 TUBE WALL TEMPERATURE PROFILES - 0.323 INCH ID TUBE

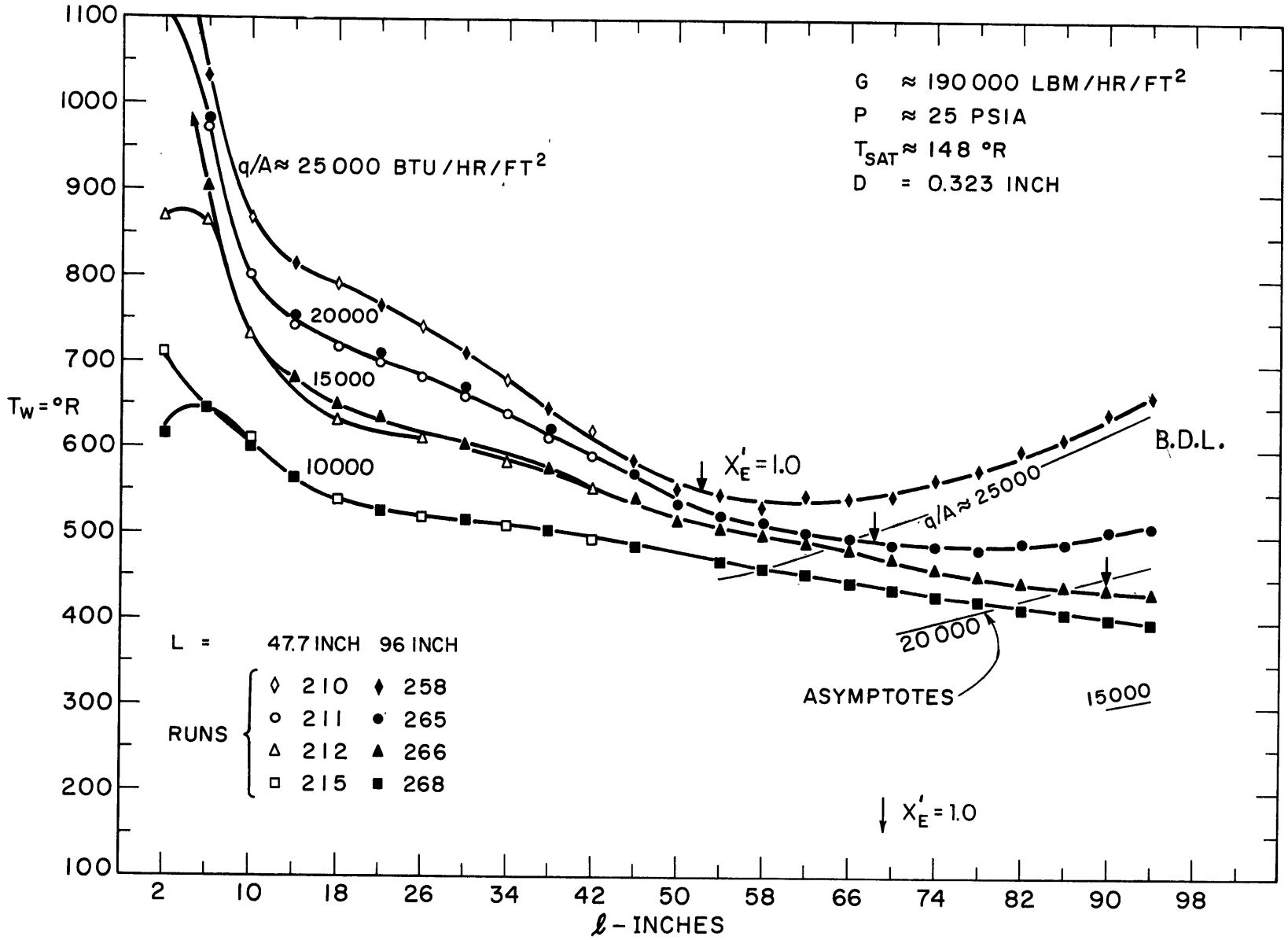

FIG. 8 TUBE WALL TEMPERATURE PROFILES - 0.323 INCH ID TUBE

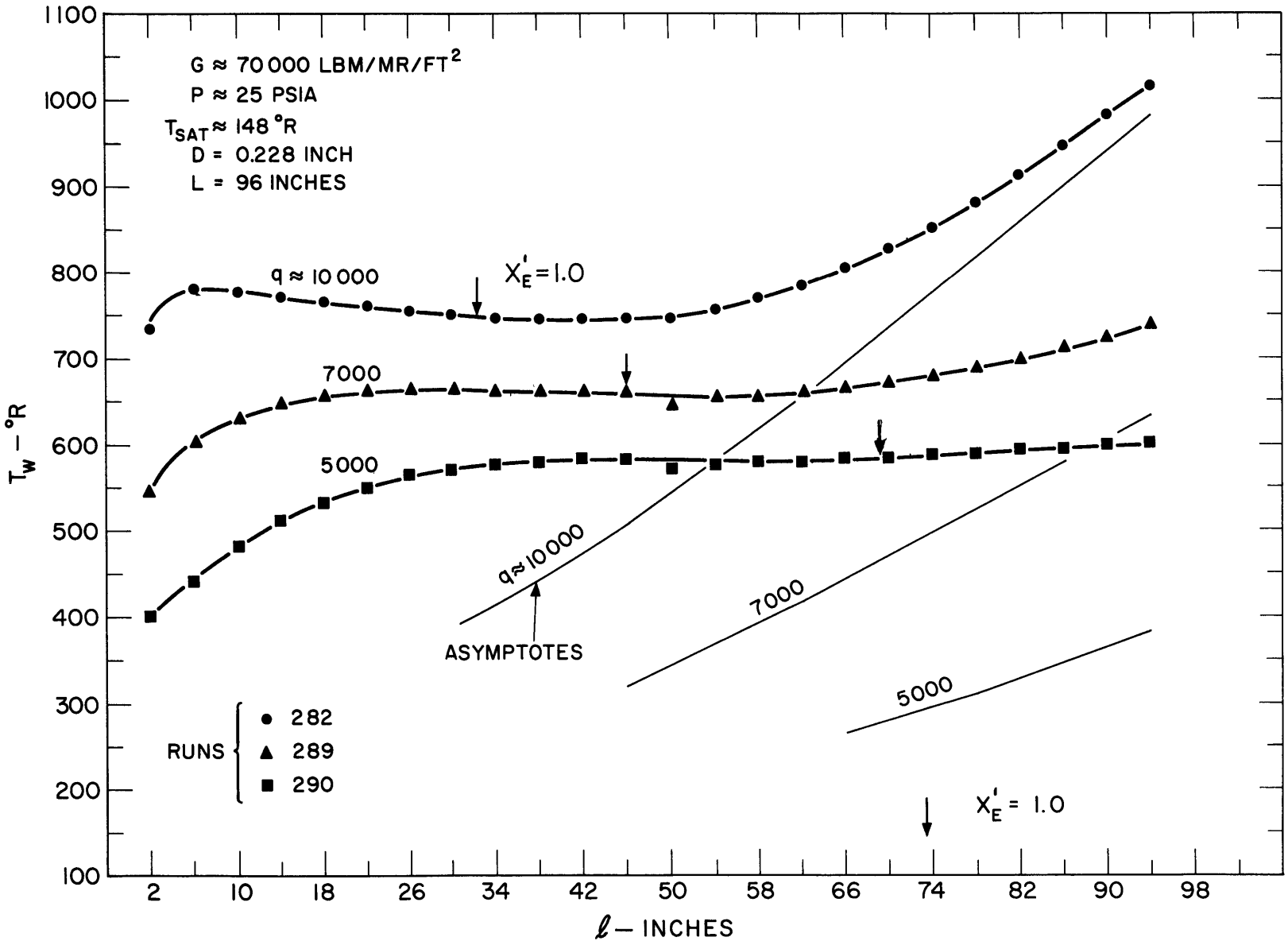

FIG. 9 TUBE WALL TEMPERATURE PROFILES - 0.228 INCH ID TUBE

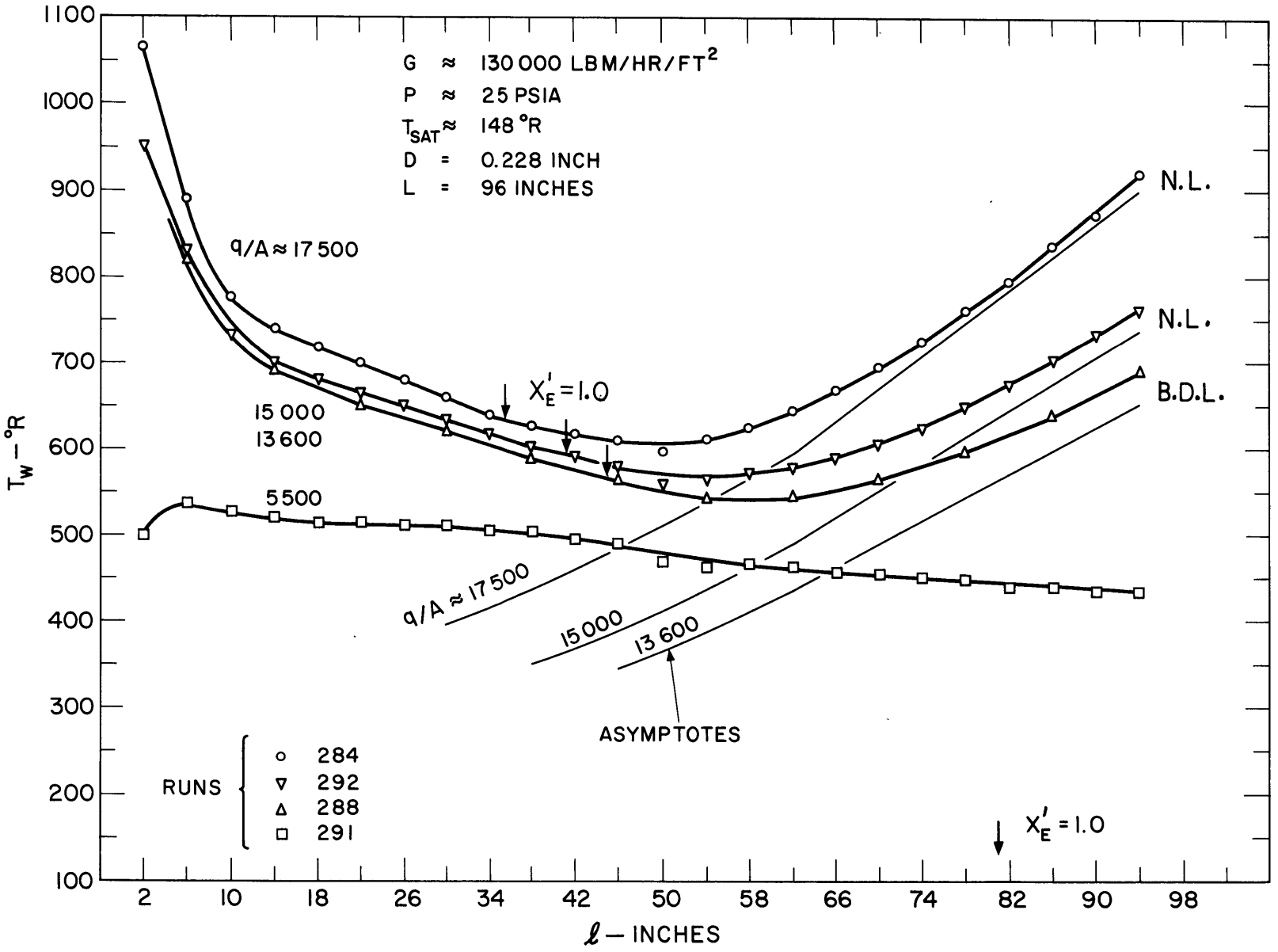

FIG. 10 TUBE WALL TEMPERATURE PROFILES - 0.228 INCH ID TUBE

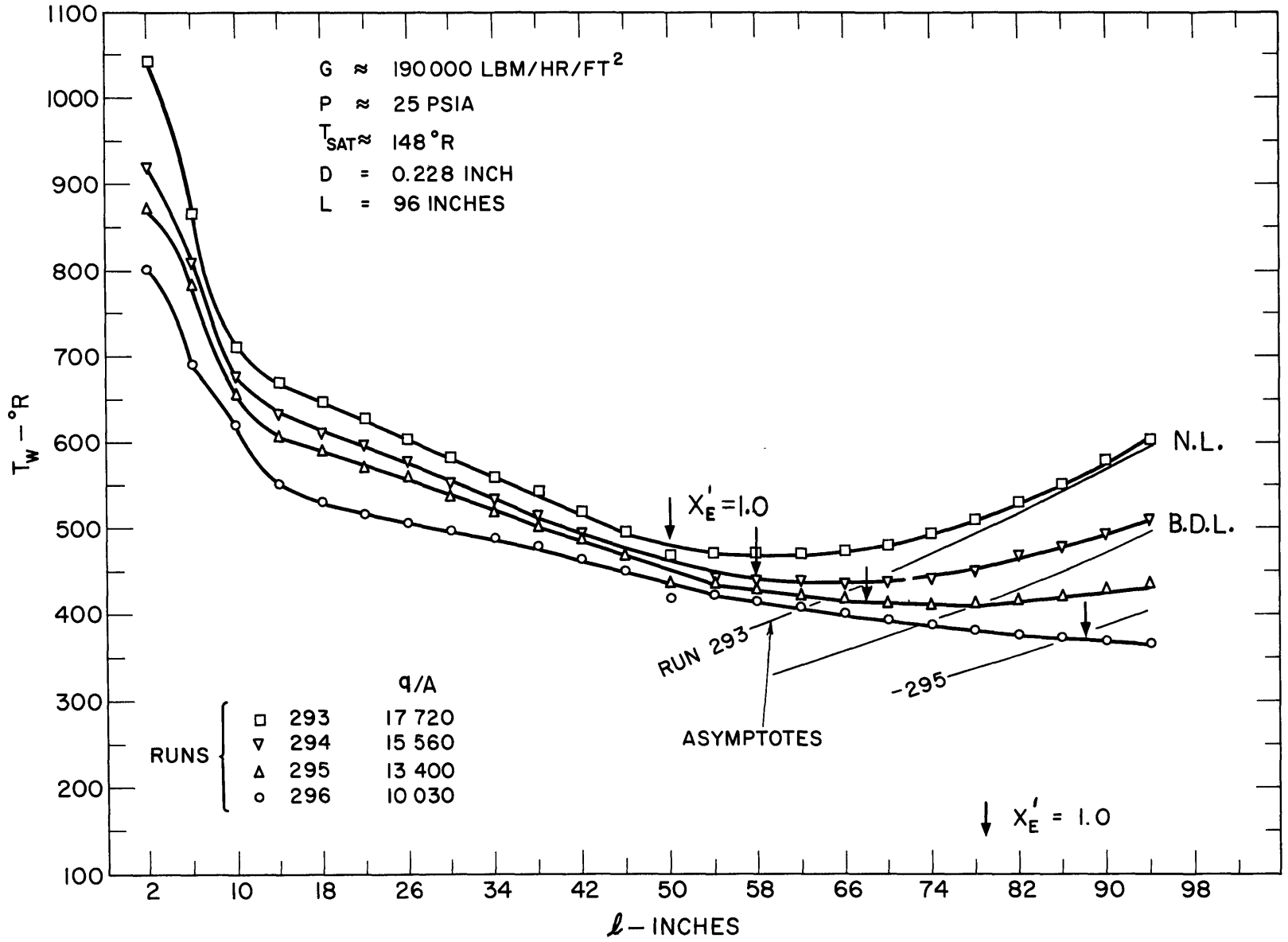

FIG. 11 TUBE WALL TEMPERATURE PROFILES - 0.228 INCH ID TUBE

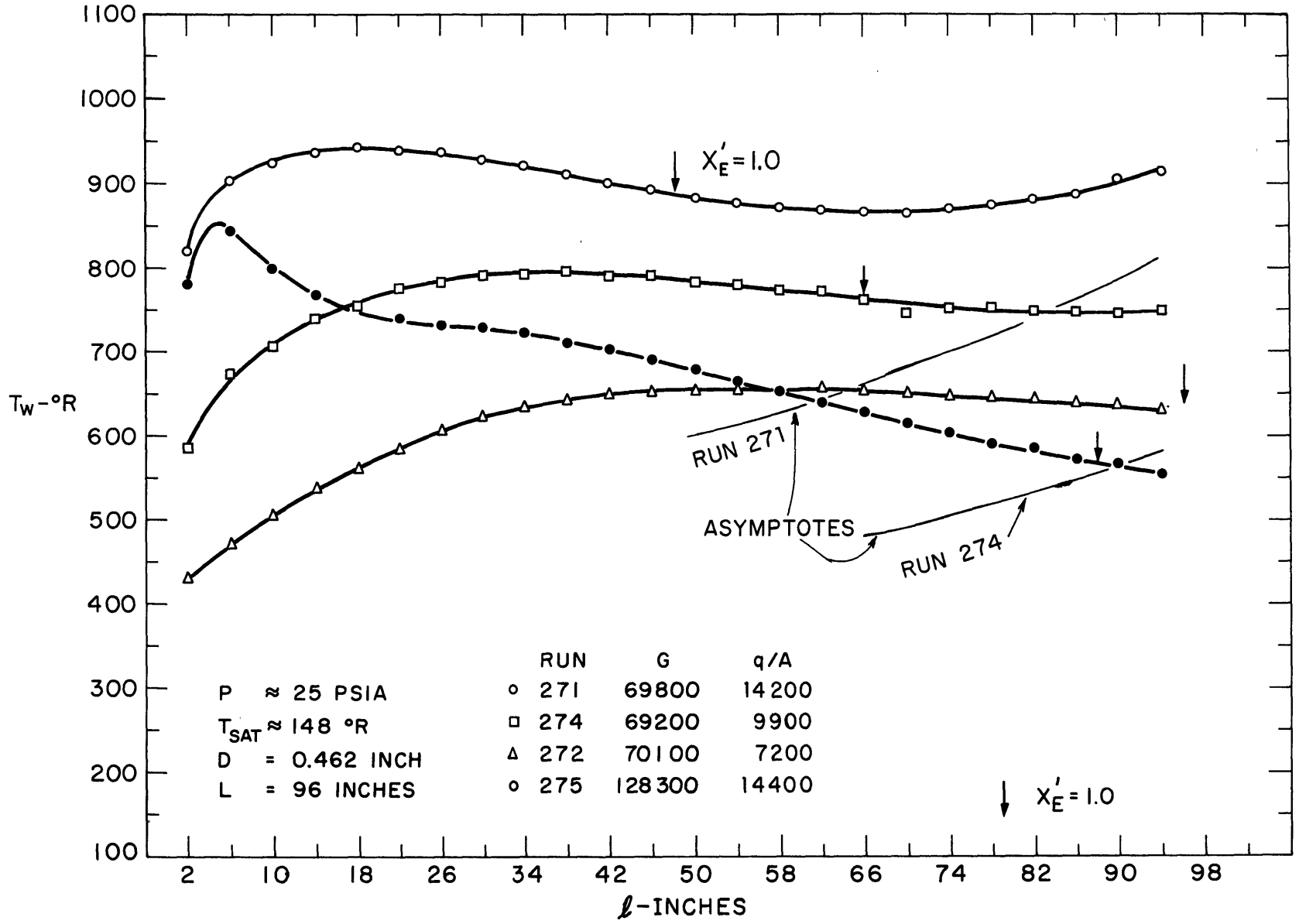

FIG. 12 TUBE WALL TEMPERATURE PROFILES - 0.462 INCH ID TUBE

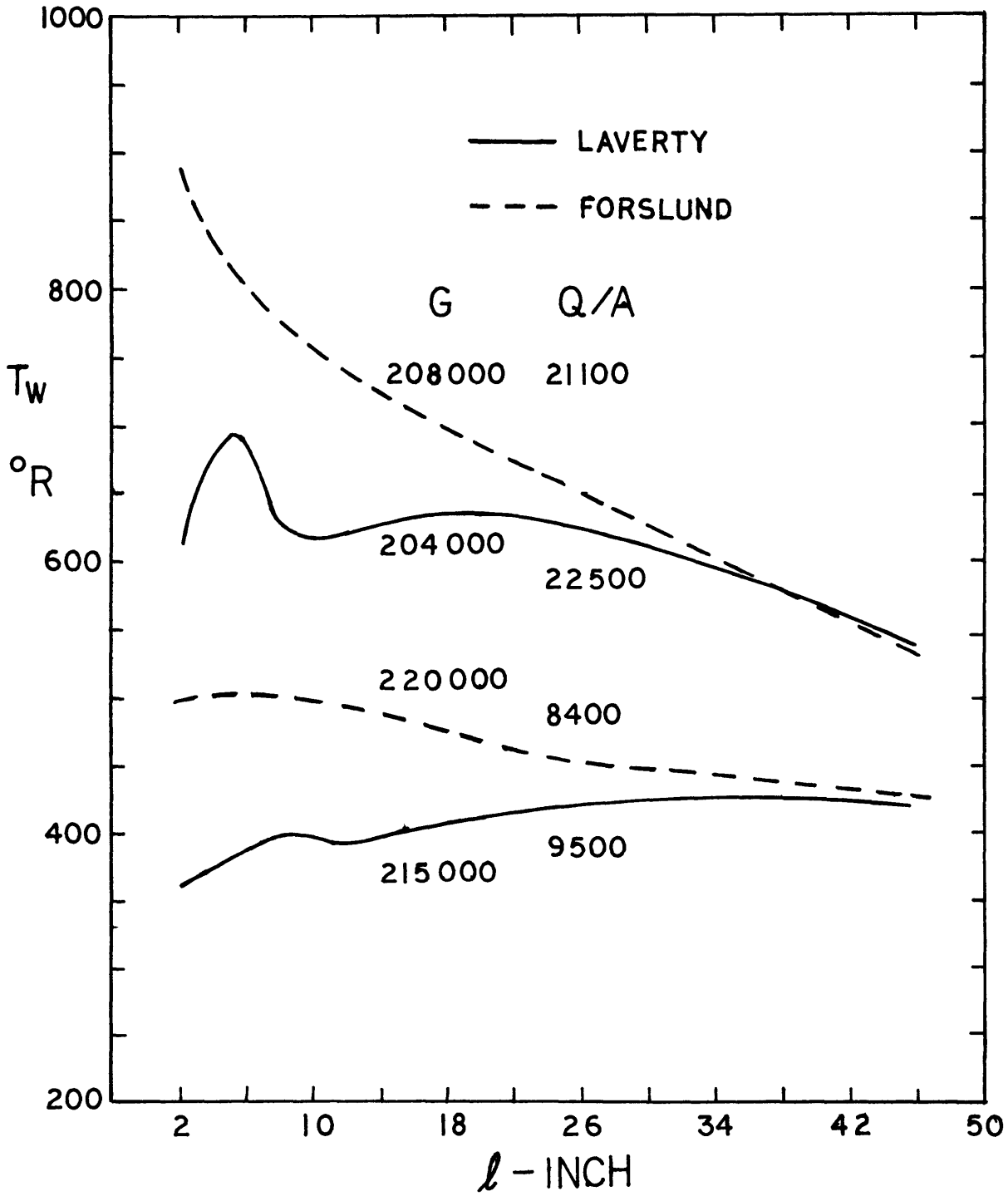

FIG. 13 COMPARISON OF LAVERTY'S TEMPERATURE PROFILE FOR HIGH MASS FLUXES WITH THOSE OF THIS STUDY

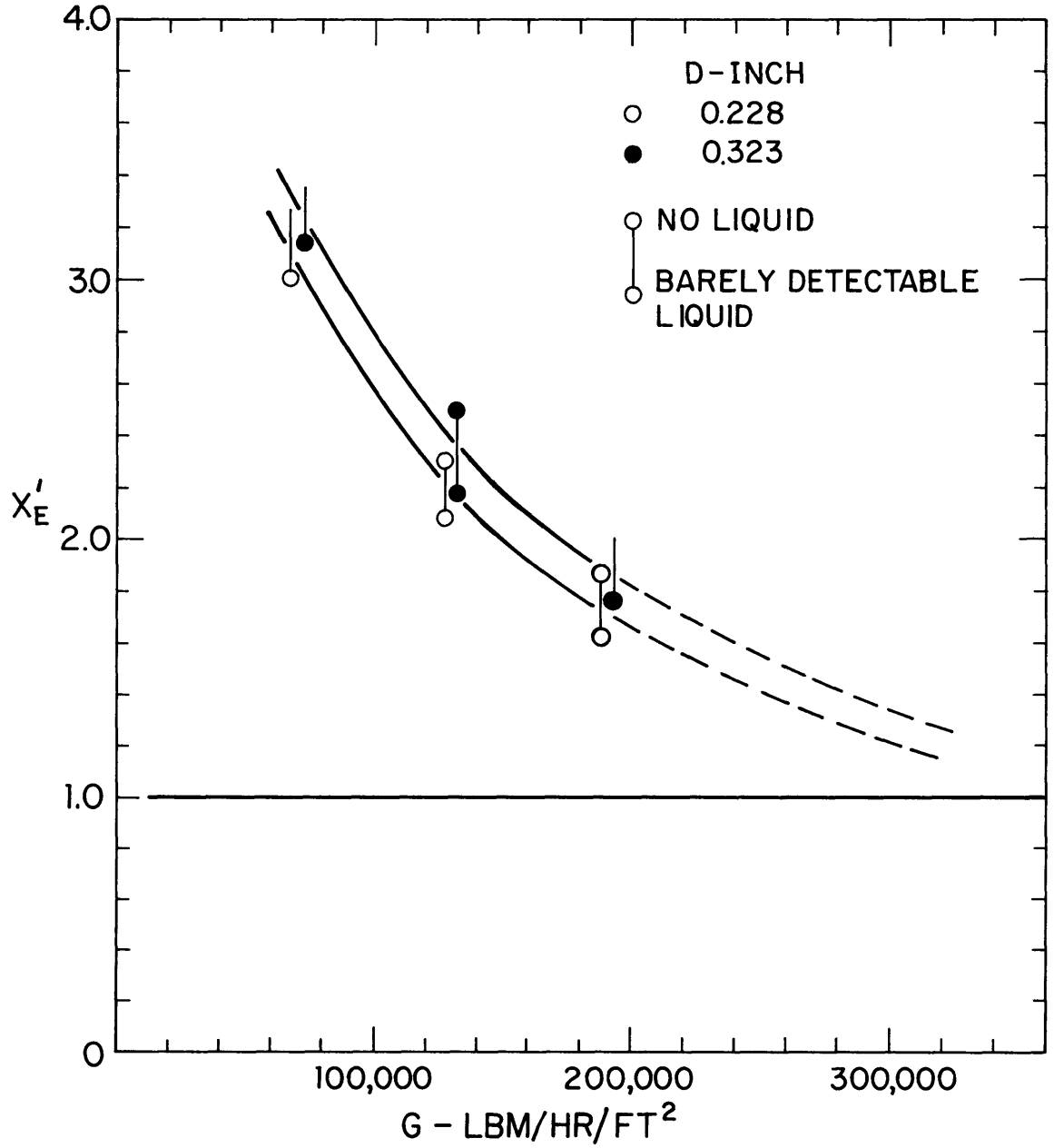

FIG. 14 LOCATION OF COMPLETE EVAPORATION

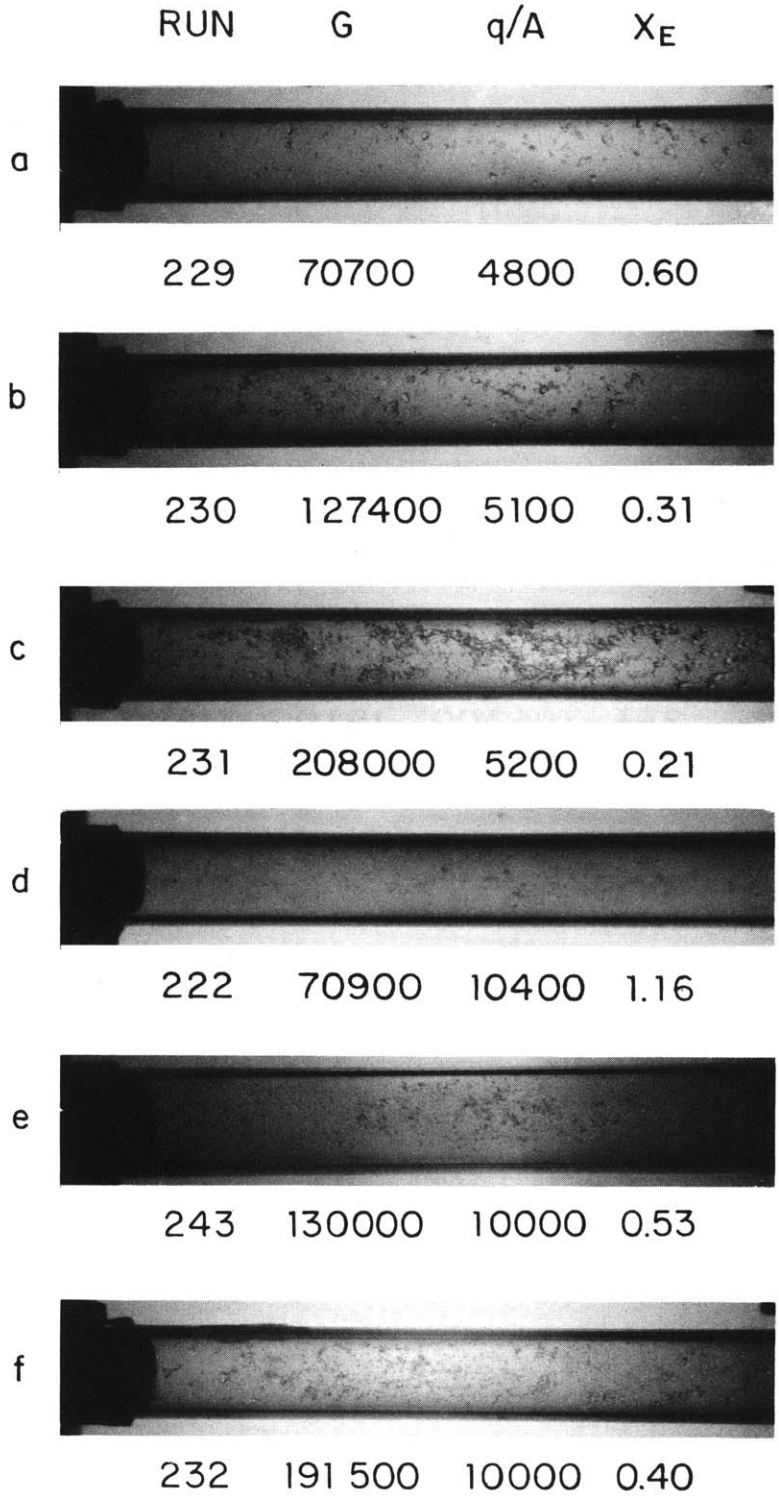

FIG. 15 PHOGOGRAPHS OF EXIT FLOW CONDITIONS FOR 4 FOOT TEST SECTION

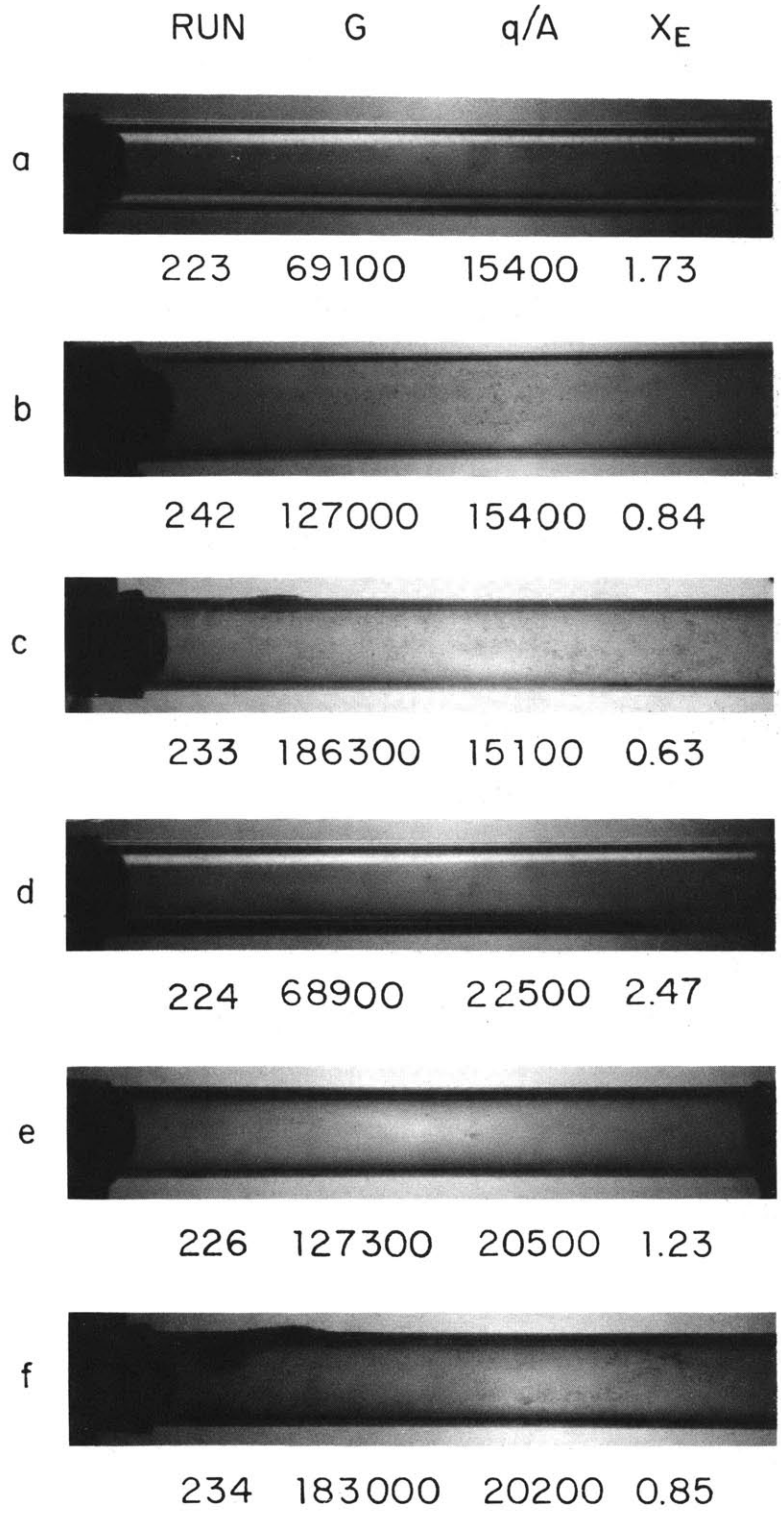

FIG. 16 PHOTOGRAPHS OF EXIT FLOW CONDITIONS FOR 4 FOOT TEST SECTION

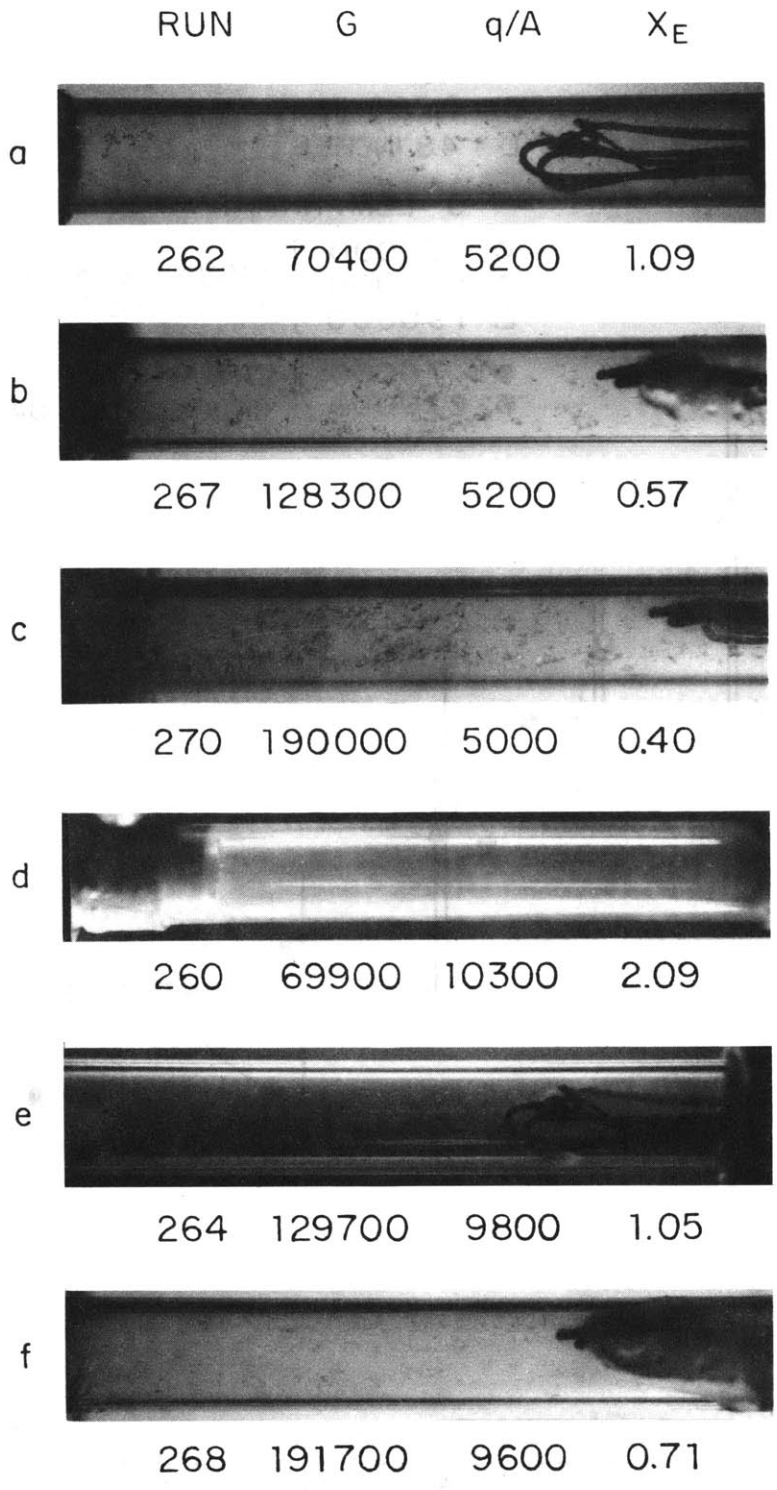

FIG. 17 PHOTOGRAPHS OF EXIT FLOW CONDITIONS FOR 3 FOOT TEST SECTION

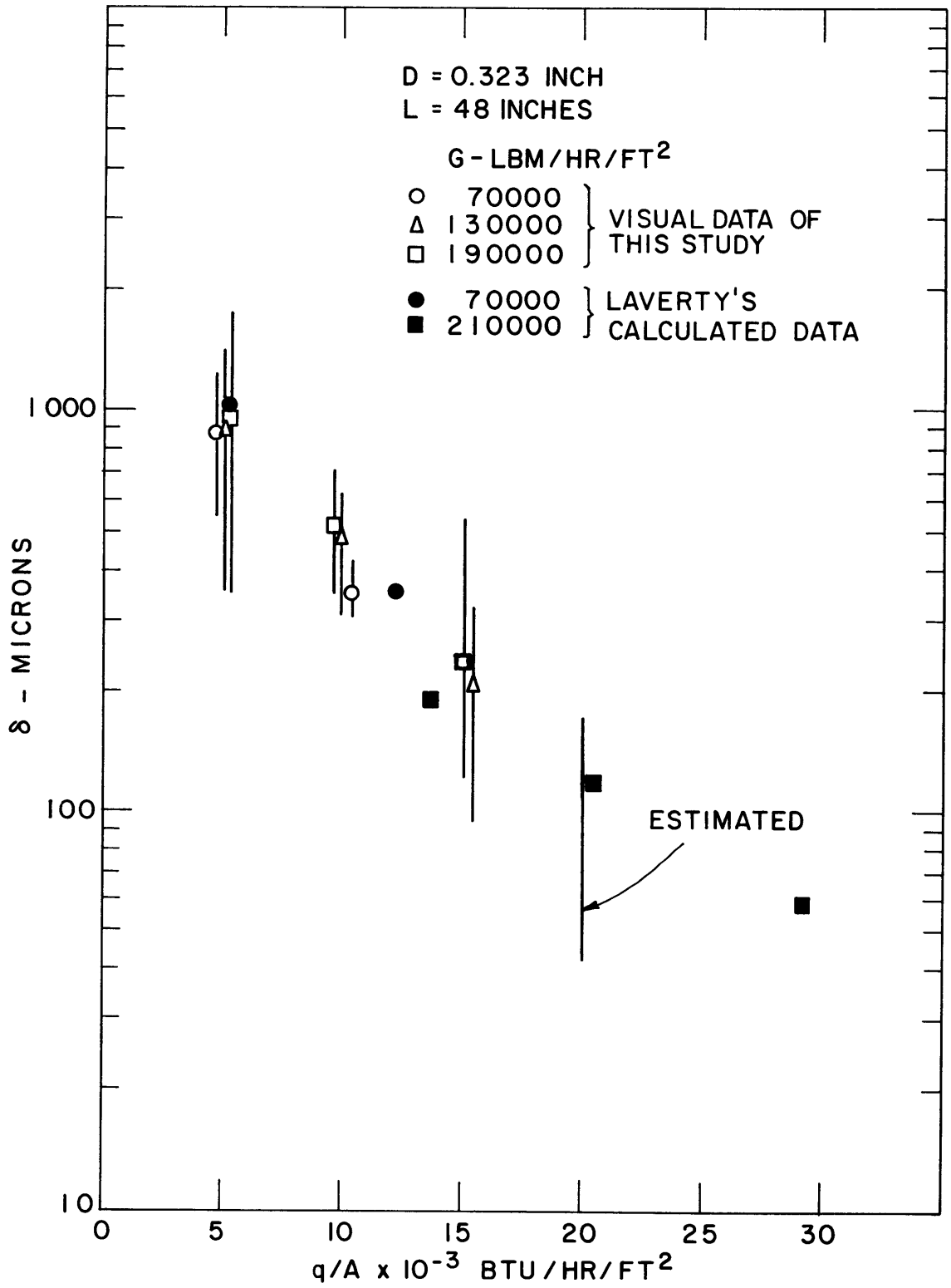

FIG. 18 OBSERVED DROPLET SIZES

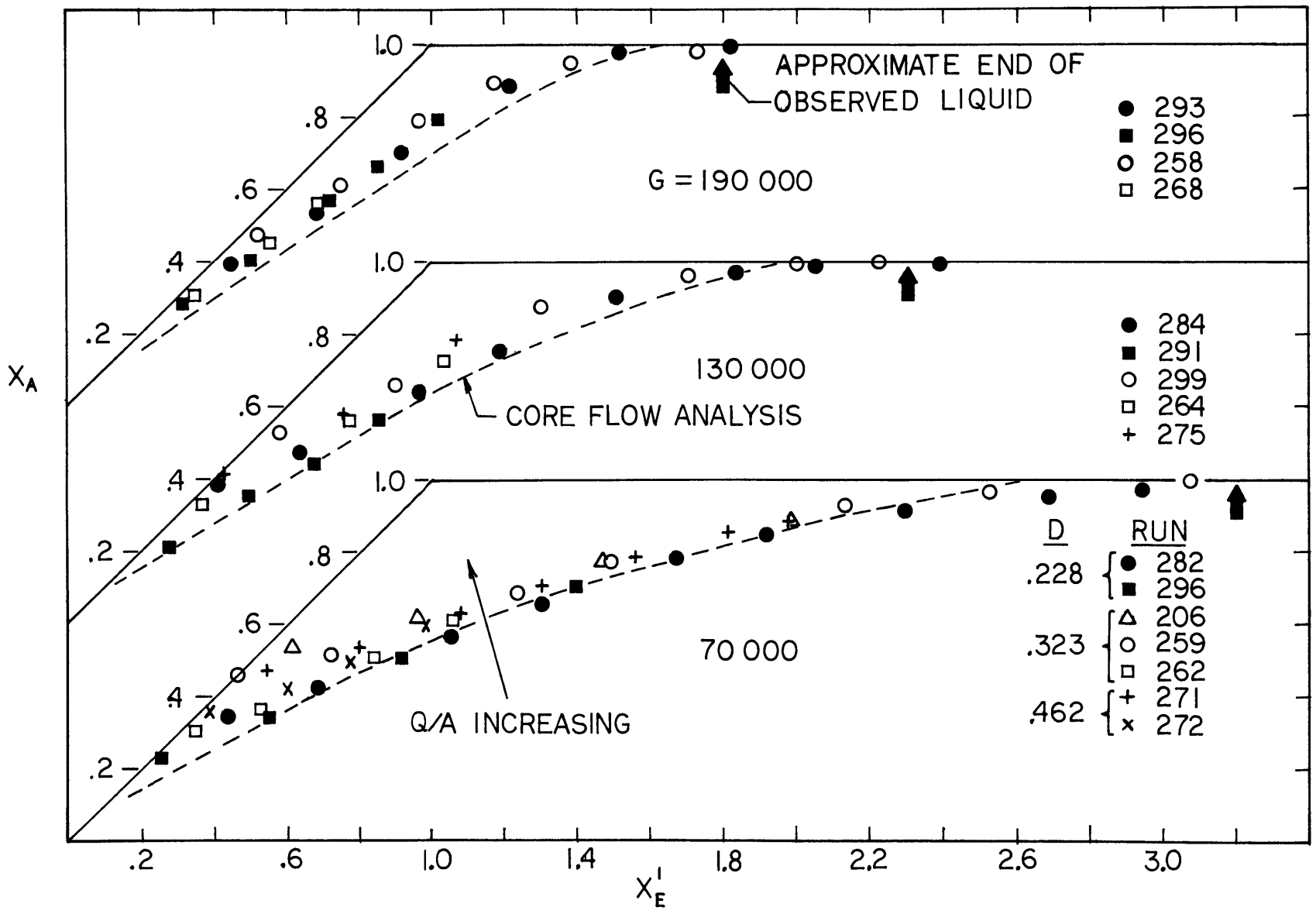

FIG. 19 CALCULATED NON-EQUILIBRIUM QUALITY

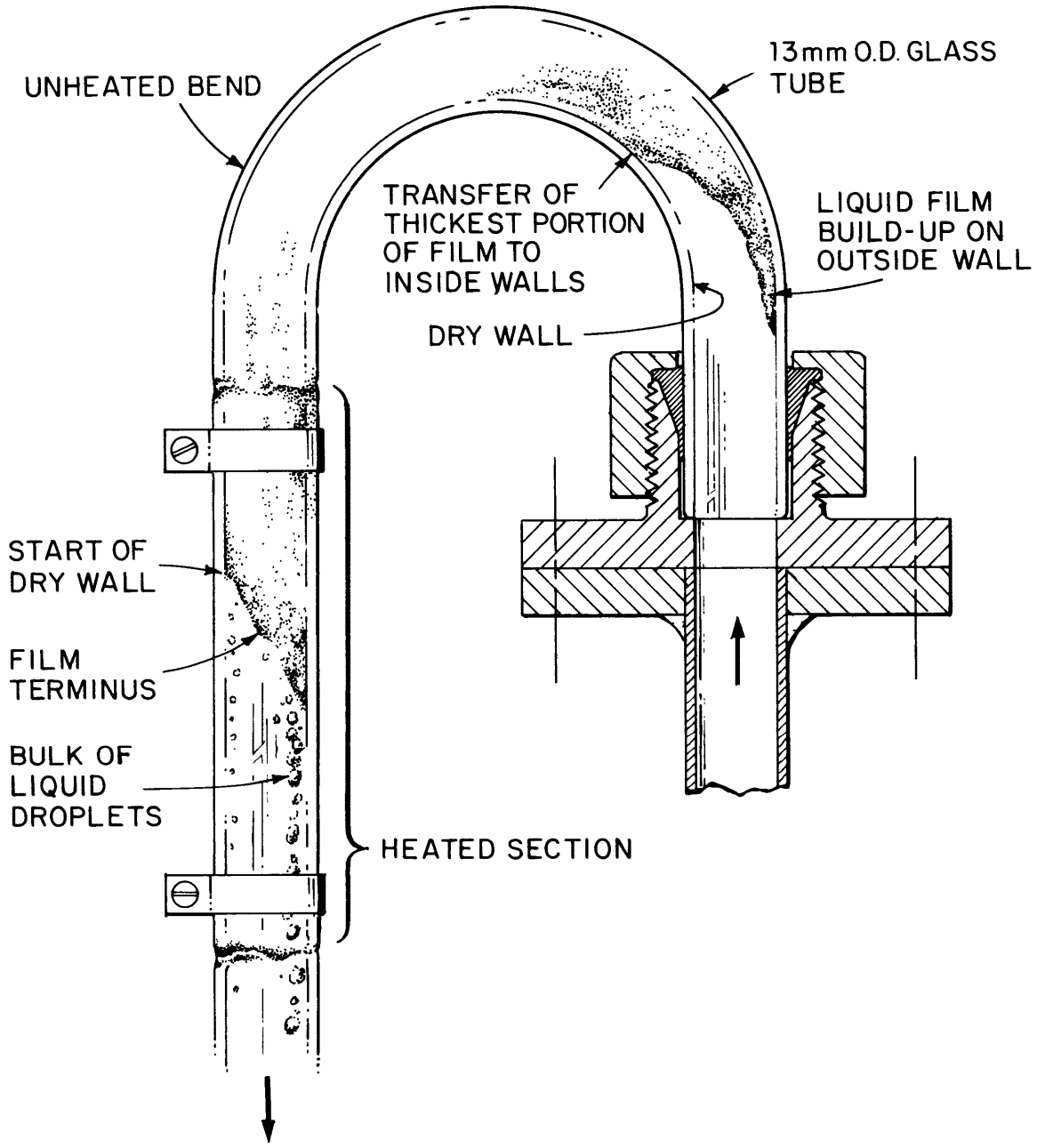

FIG. 20 U-TUBE LIQUID SEPARATOR

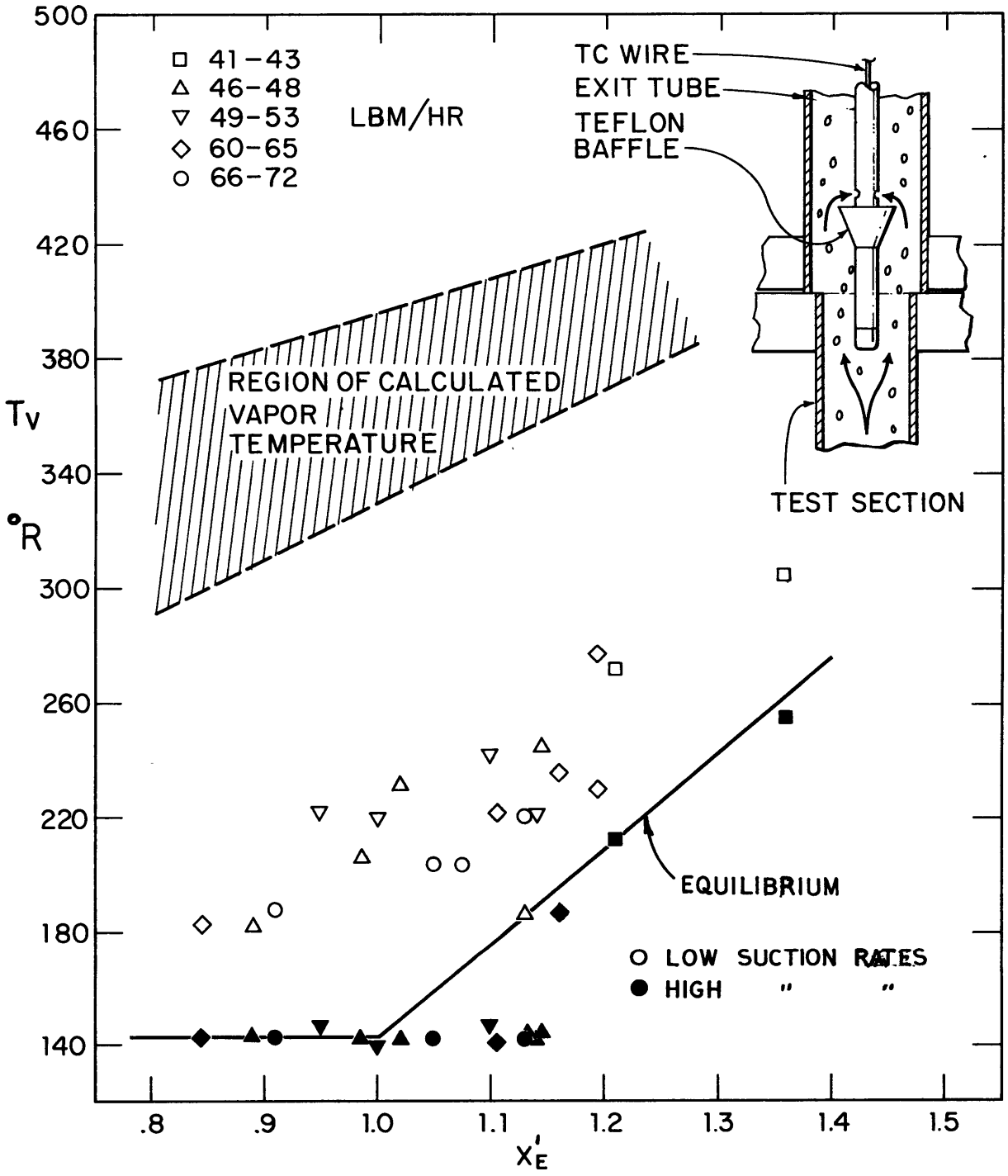

FIG. 21 RESULTS OF THERMOCOUPLE SUCTION PROBE

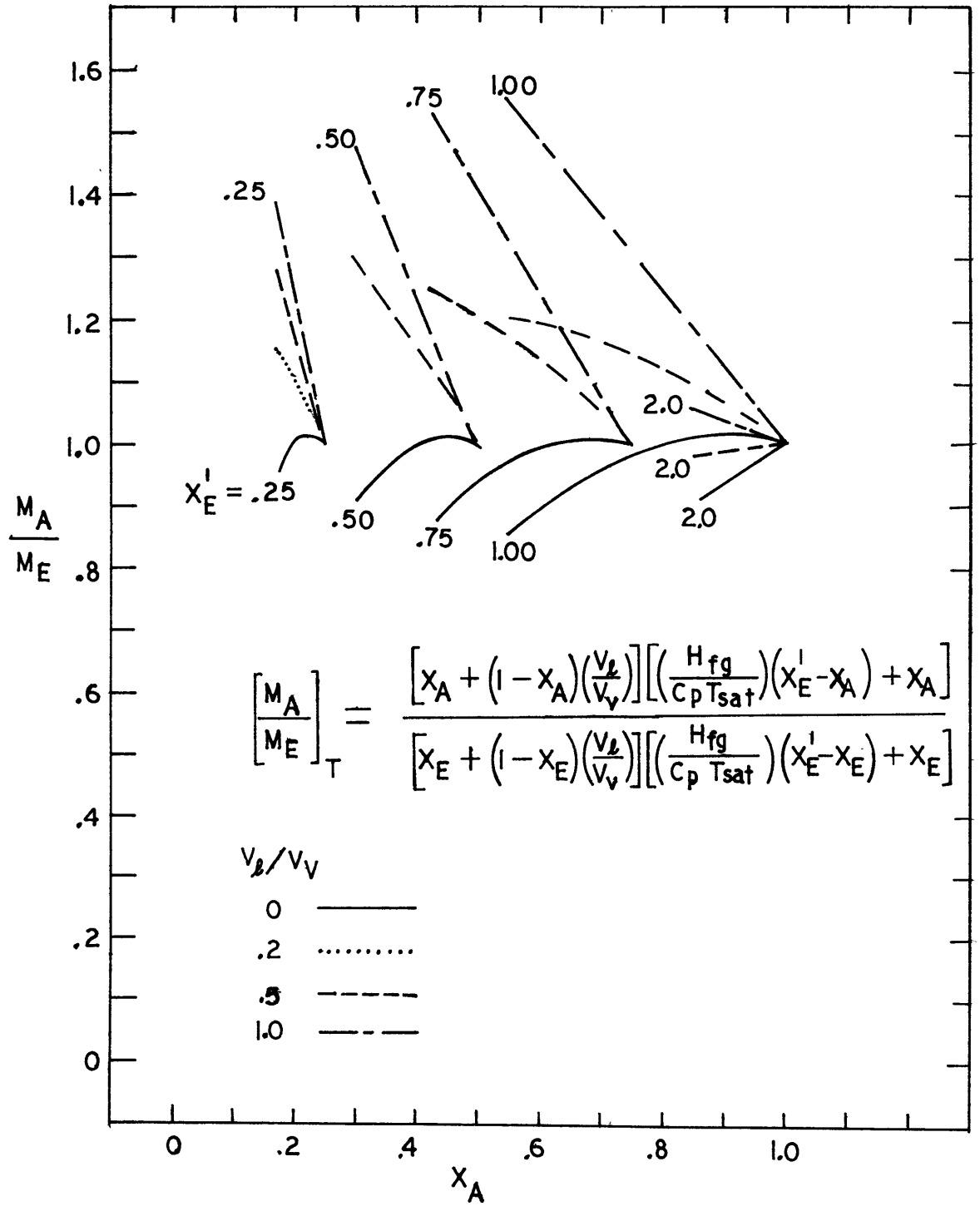

FIG. 22 NORMALIZED VARIATION IN MOMENTUM FLUX WITH DEPARTURE FROM EQUILIBRIUM FOR VARIOUS VELOCITY RATIOS

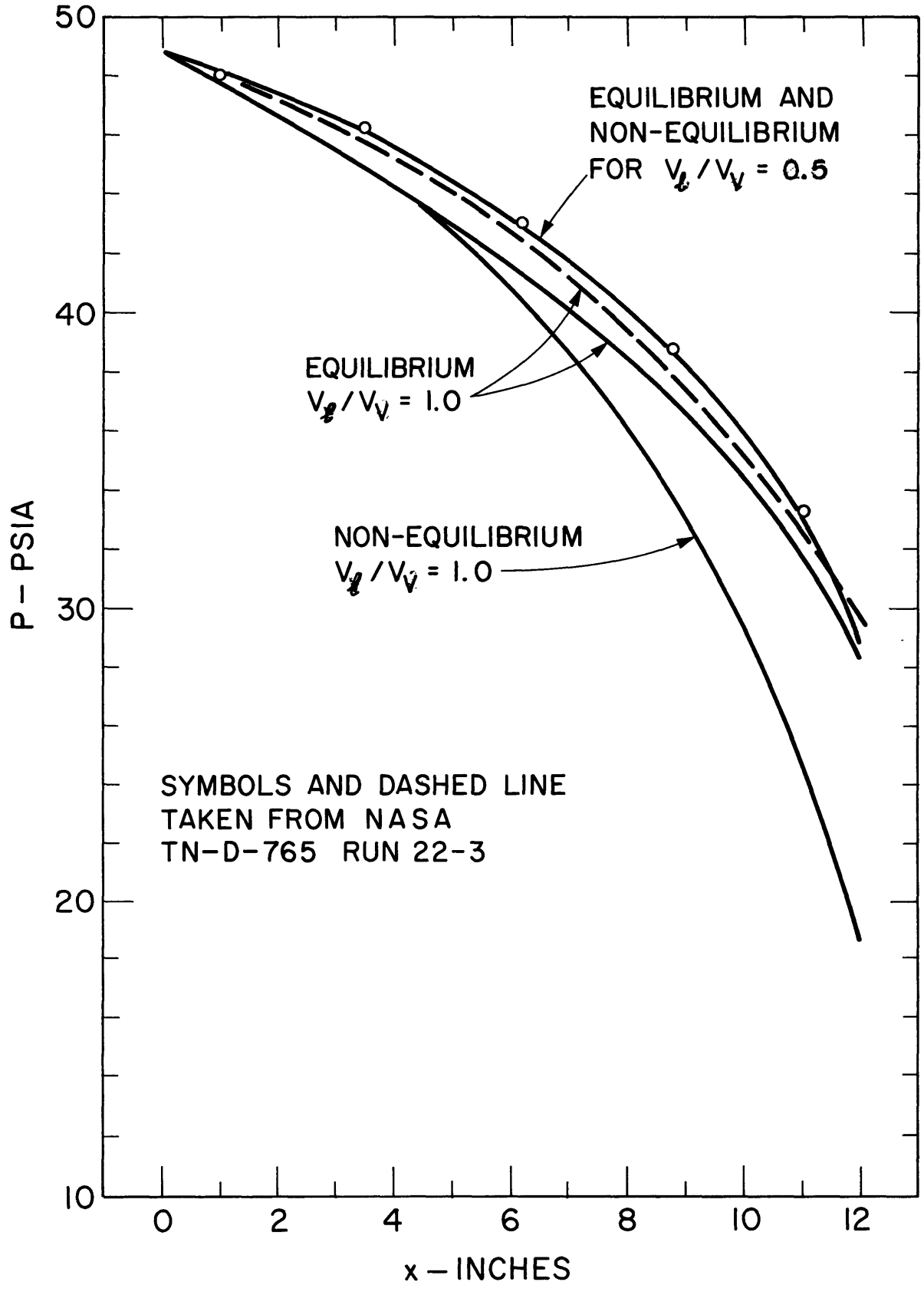

FIG. 23 VARIATION IN CALCULATED PRESSURE DROP WITH DEPARTURE FROM EQUILIBRIUM

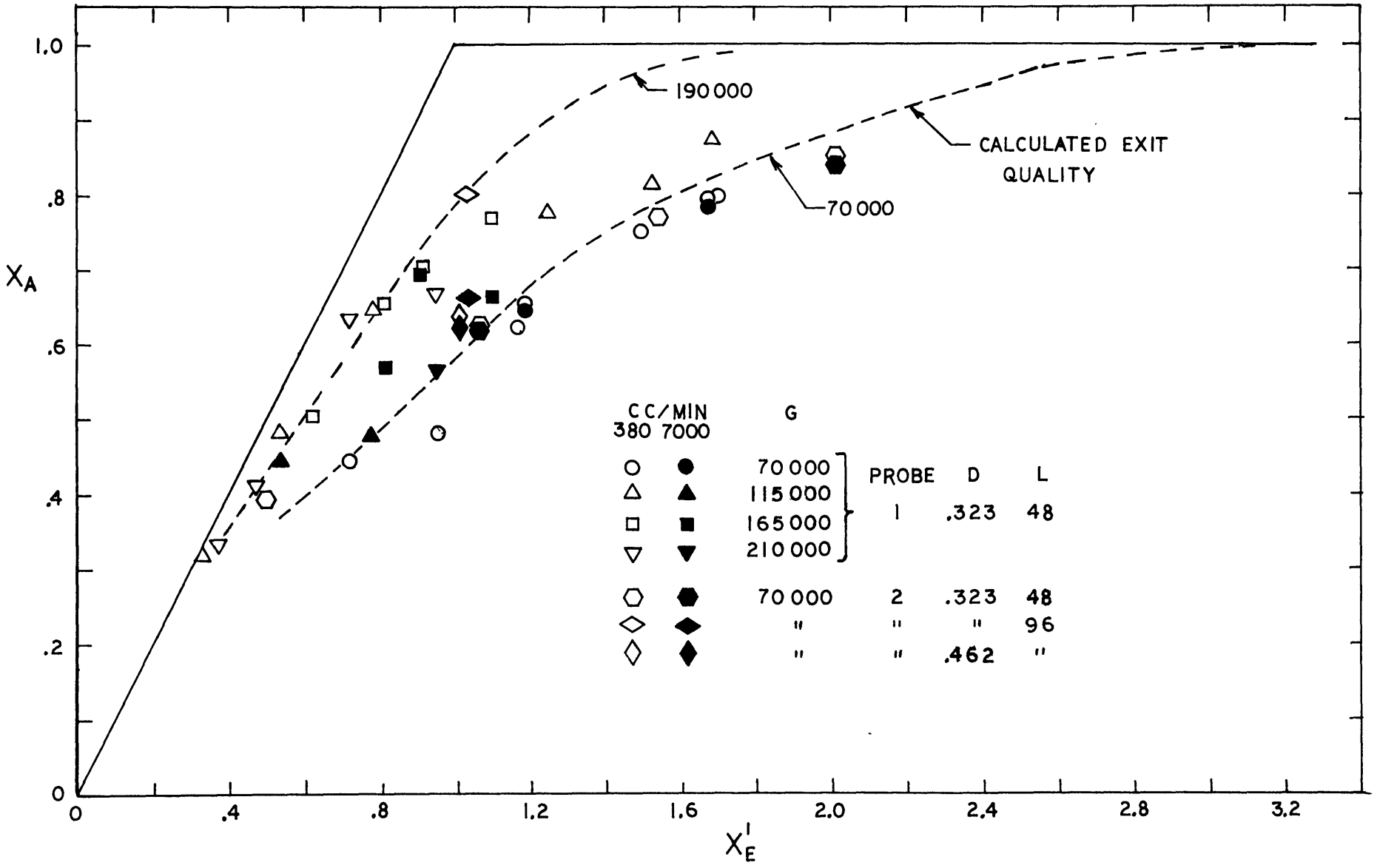

FIG. 24 ACTUAL QUALITY MEASURED BY HELIUM TRACER GAS TECHNIQUE

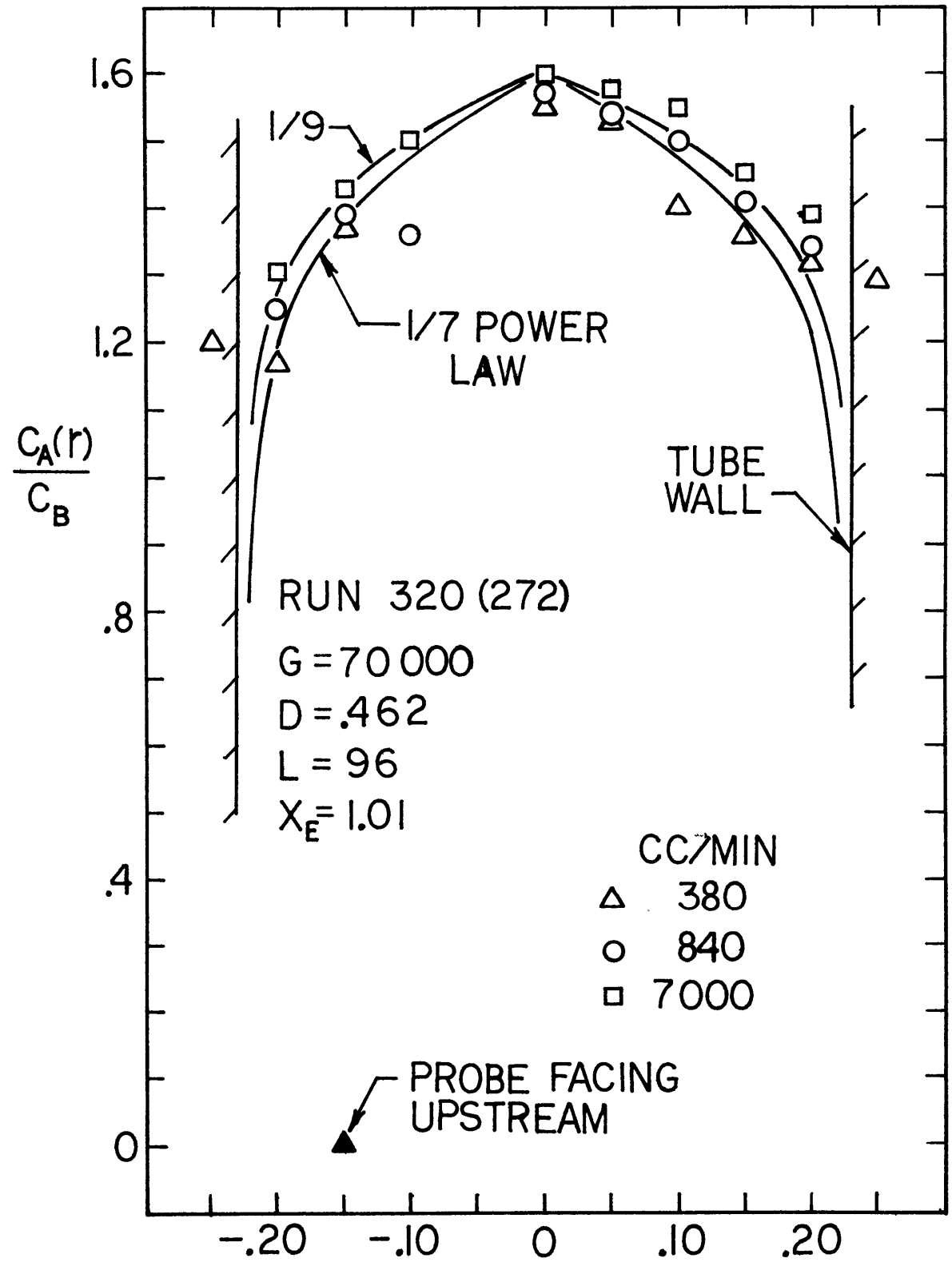

FIG. 25 RADIAL HELIUM CONCENTRATION PROFILES

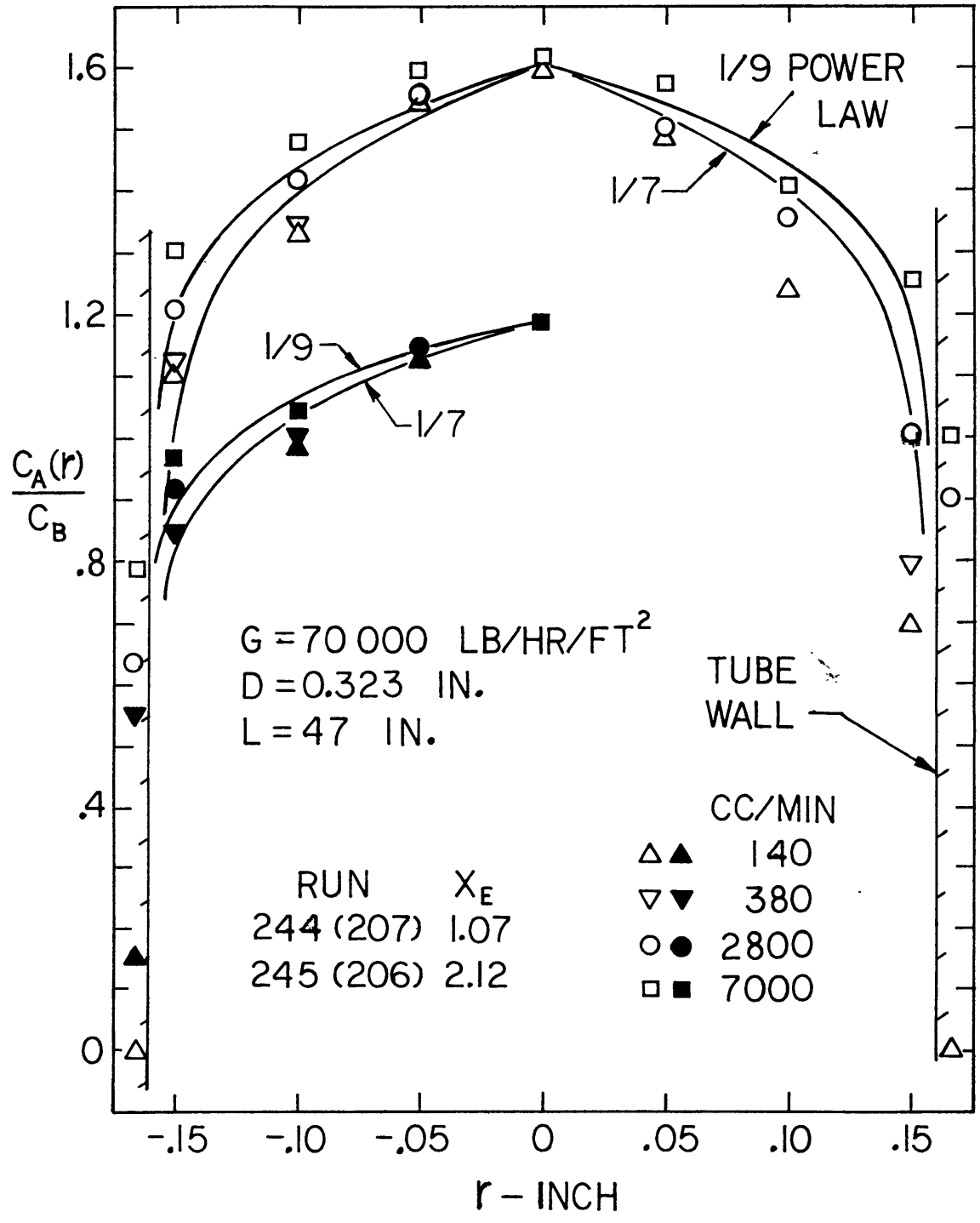

FIG. 26 RADIAL HELIUM CONCENTRATION PROFILES

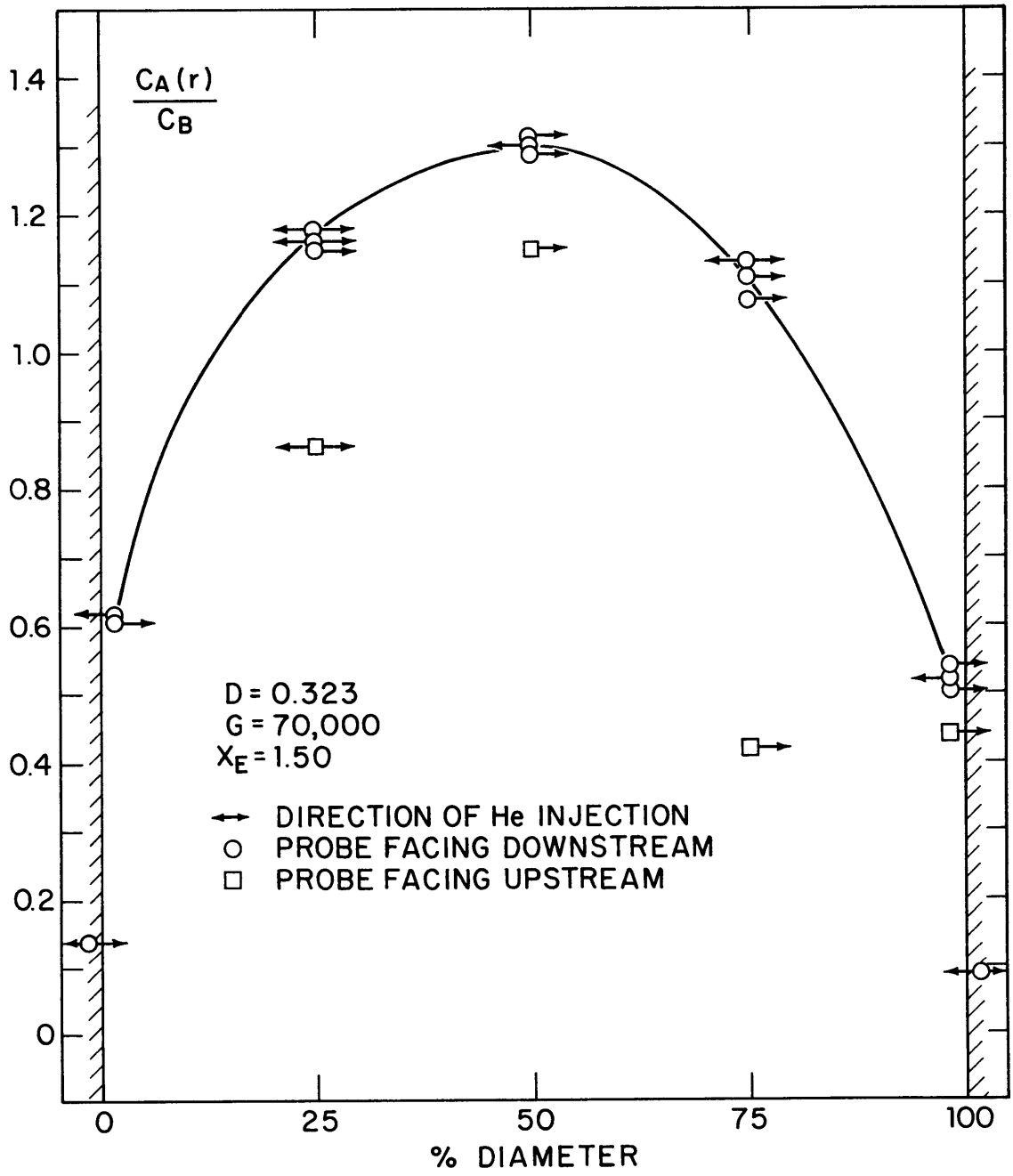

FIG. 27 RADIAL HELIUM CONCENTRATION PROFILES

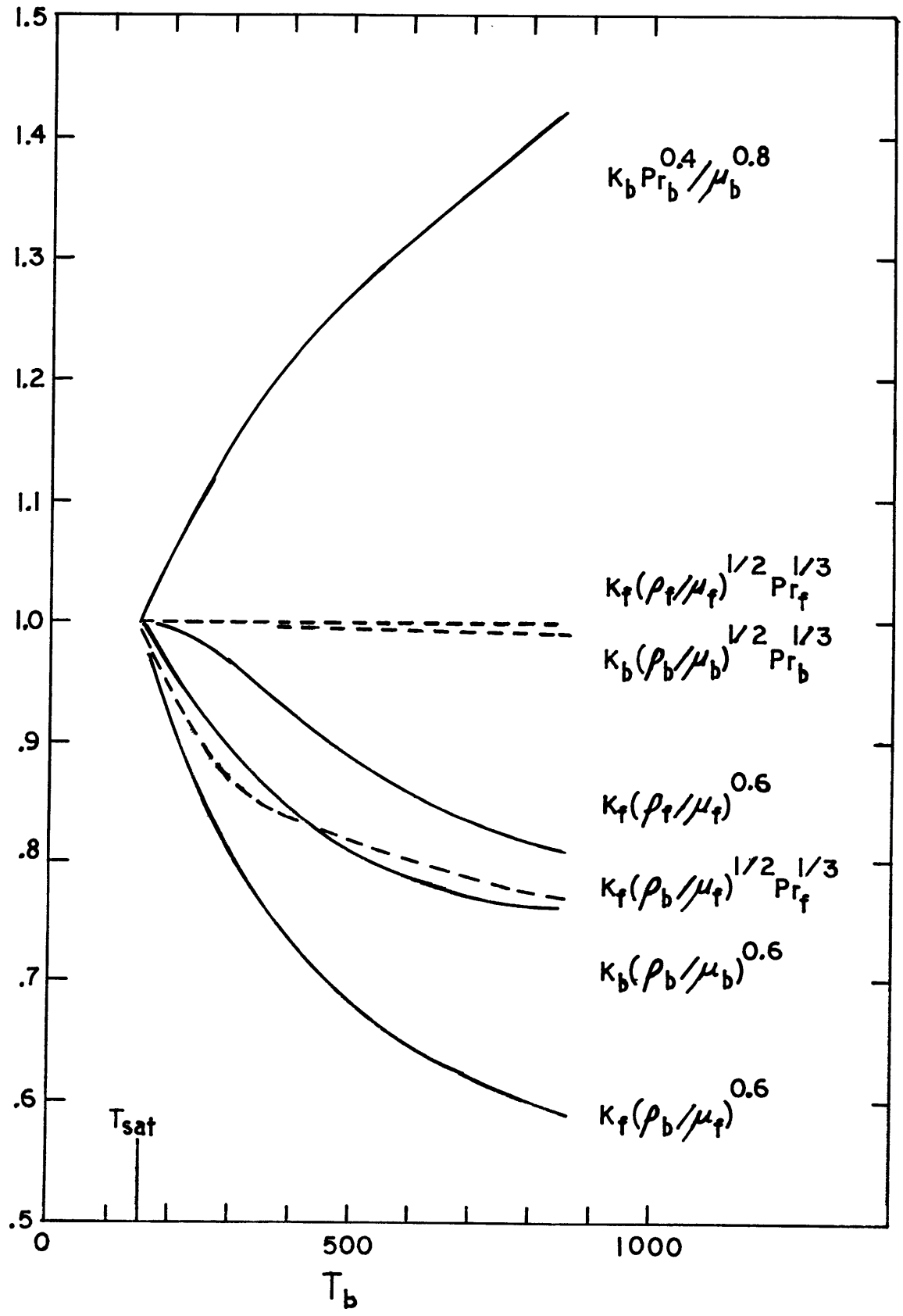

FIG. 28 VARIATION IN NORMALIZED HEAT TRANSFER PROPERTY GROUPS WITH TEMPERATURE

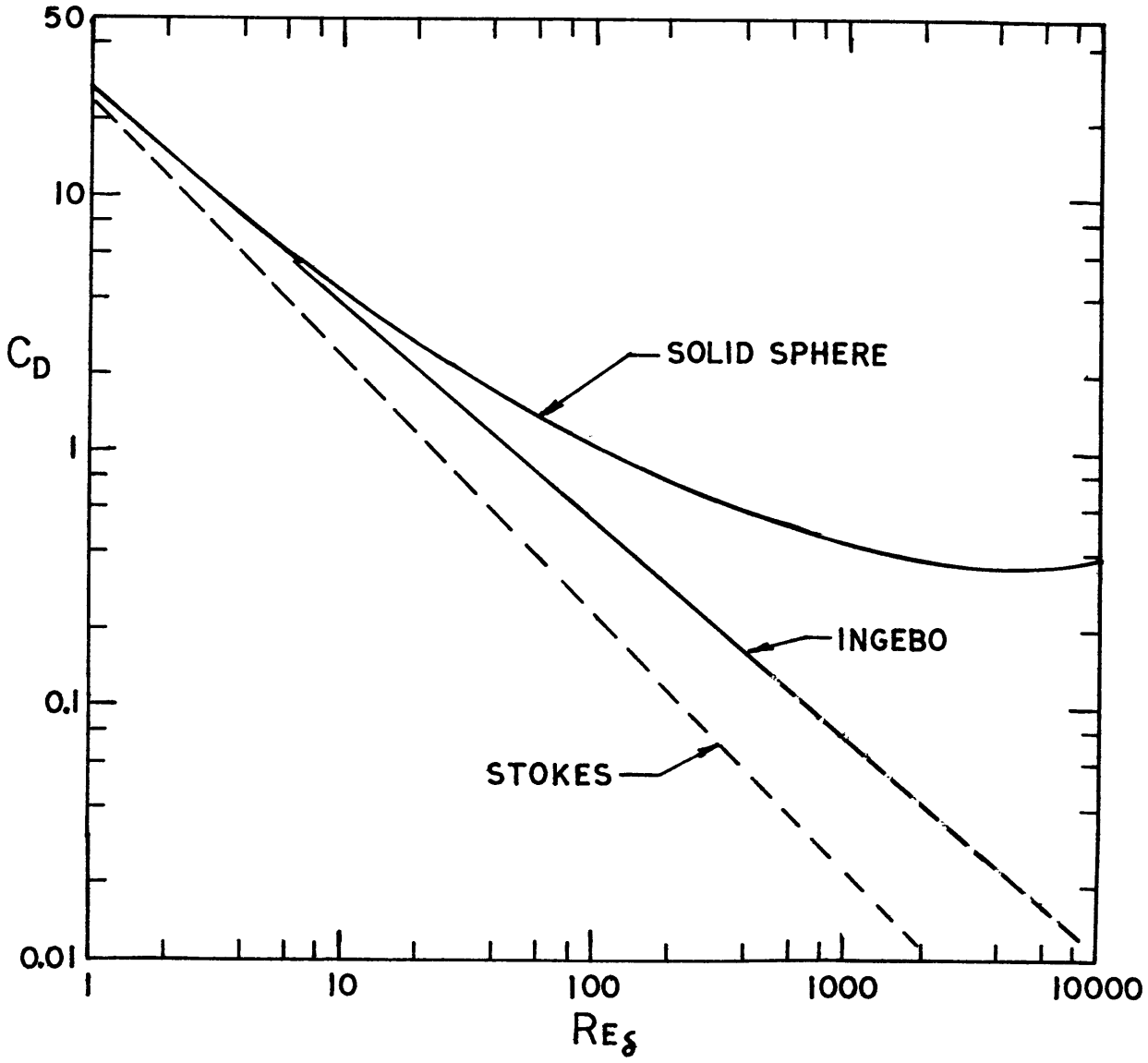

FIG. 29 DRAG COEFFICIENTS

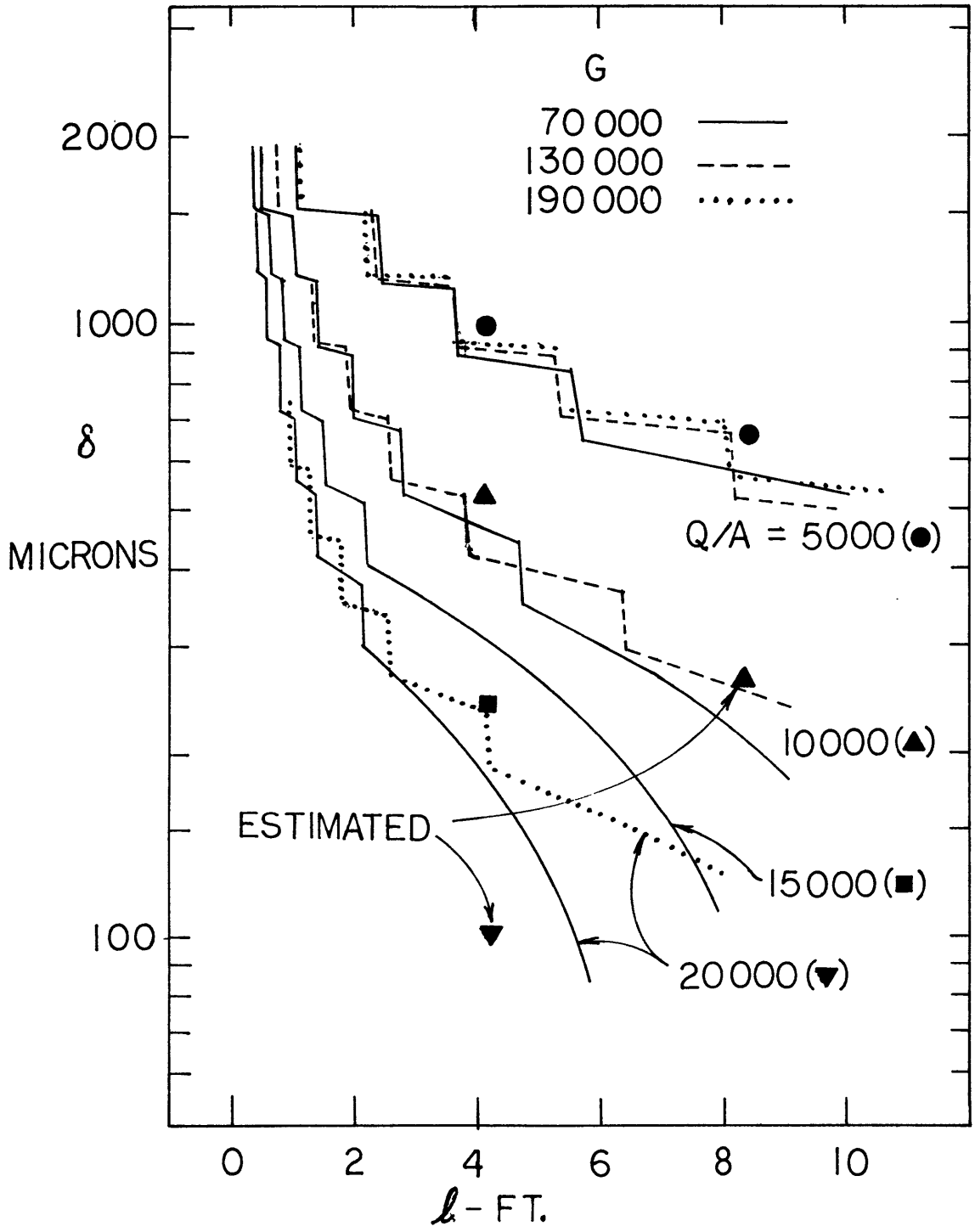

FIG. 30 DROPLET BREAKUP PROCESS FOR NOMINAL TEST CONDITIONS COMPARED WITH MEASURED DROPLET SIZES

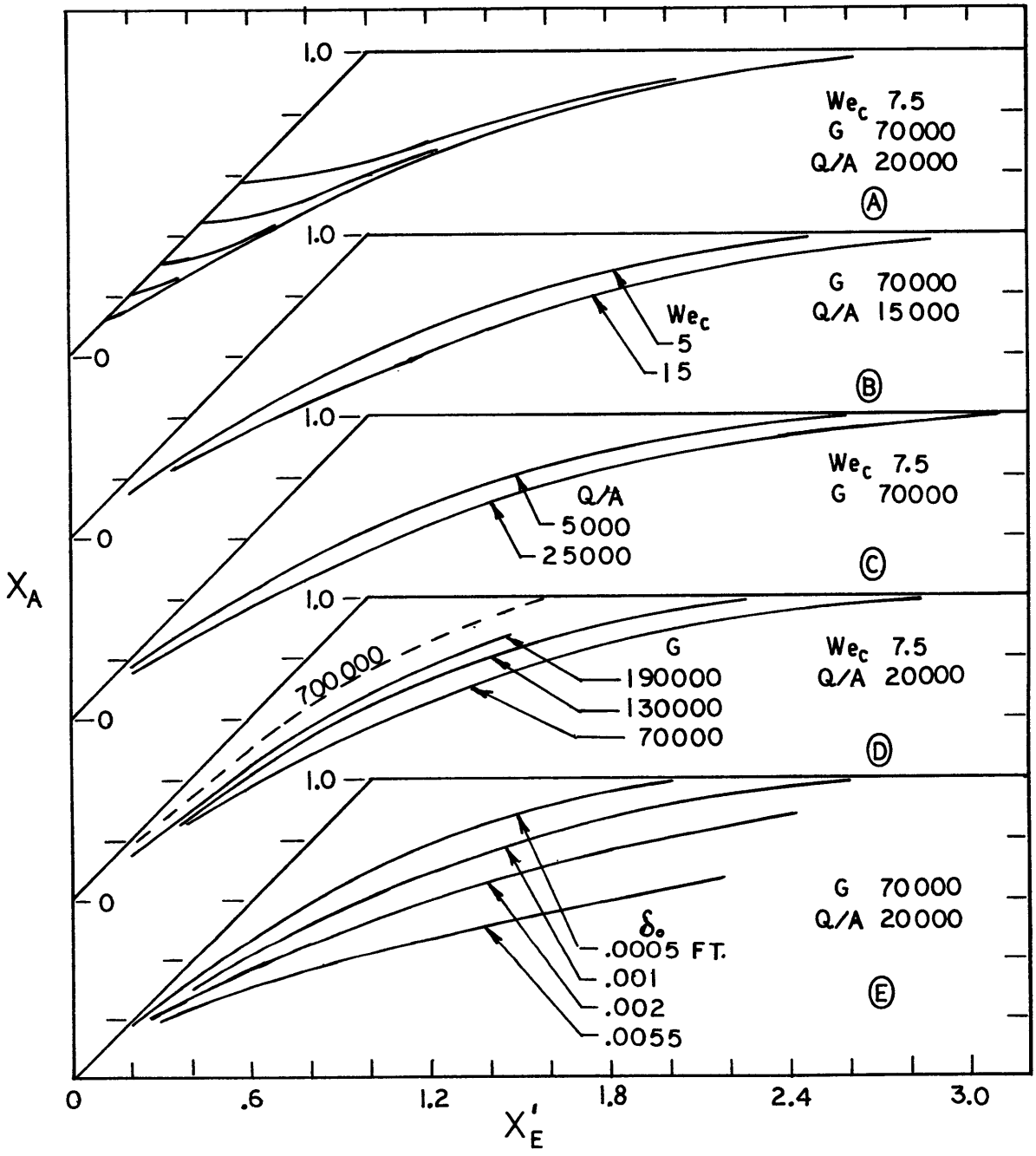

FIG. 31 DEPARTURE FROM EQUILIBRIUM PREDICTED BY CORE FLOW ANALYSIS

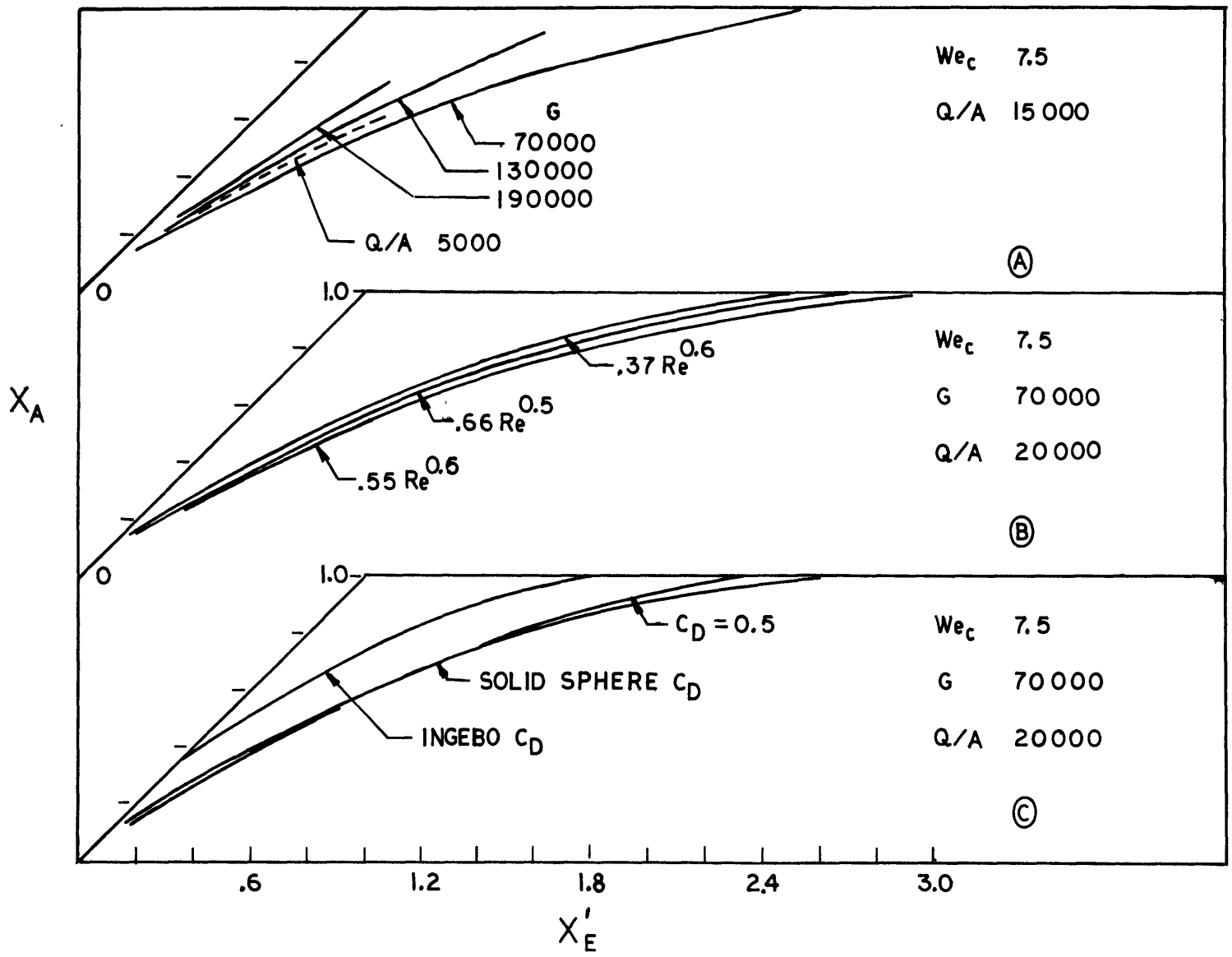

FIG. 32 DEPARTURE FROM EQUILIBRIUM PREDICTED BY CORE FLOW ANALYSIS

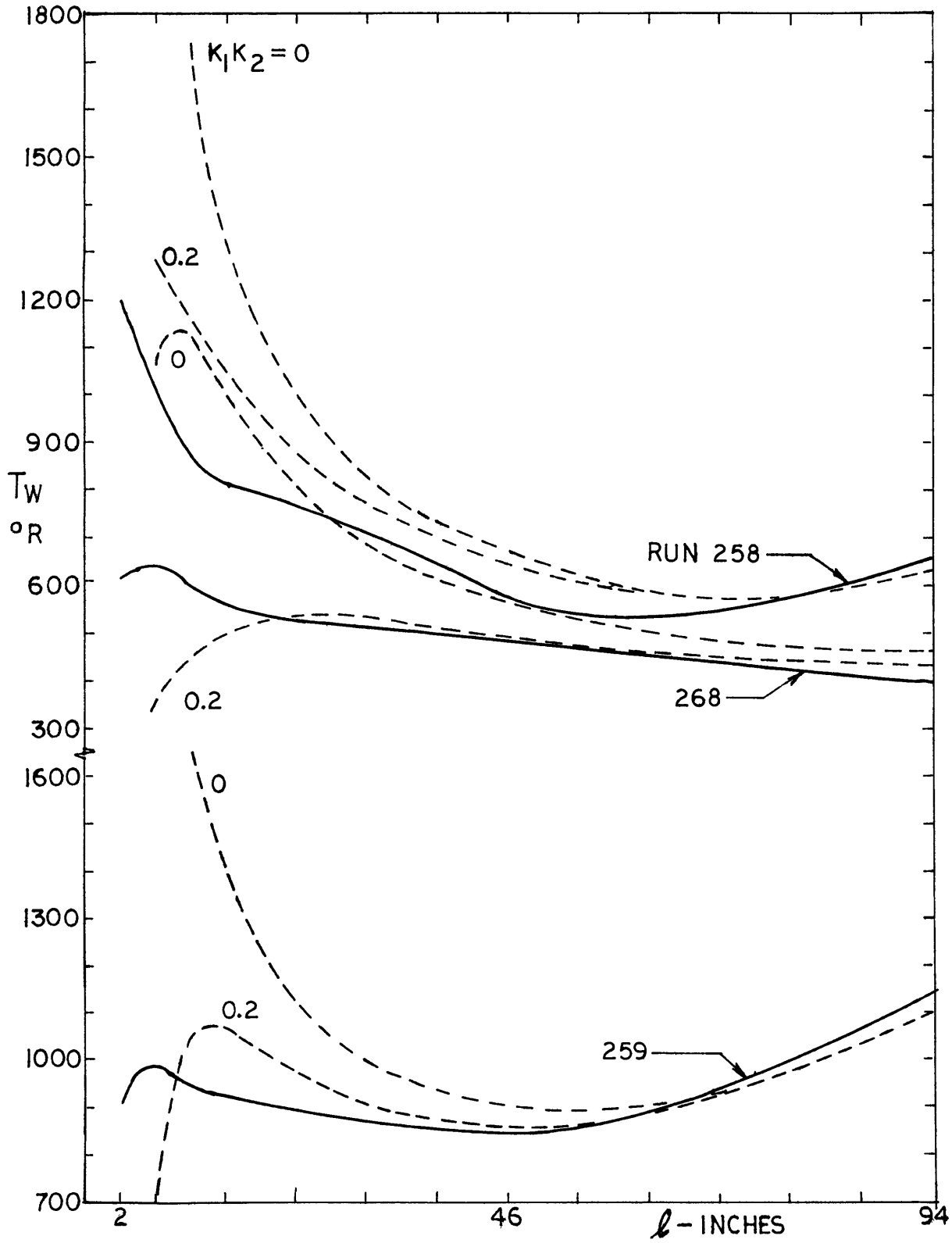

FIG. 33 COMPARISON OF THE PREDICTED TEMPERATURE PROFILES WITH THE MEASURED TEMPERATURES

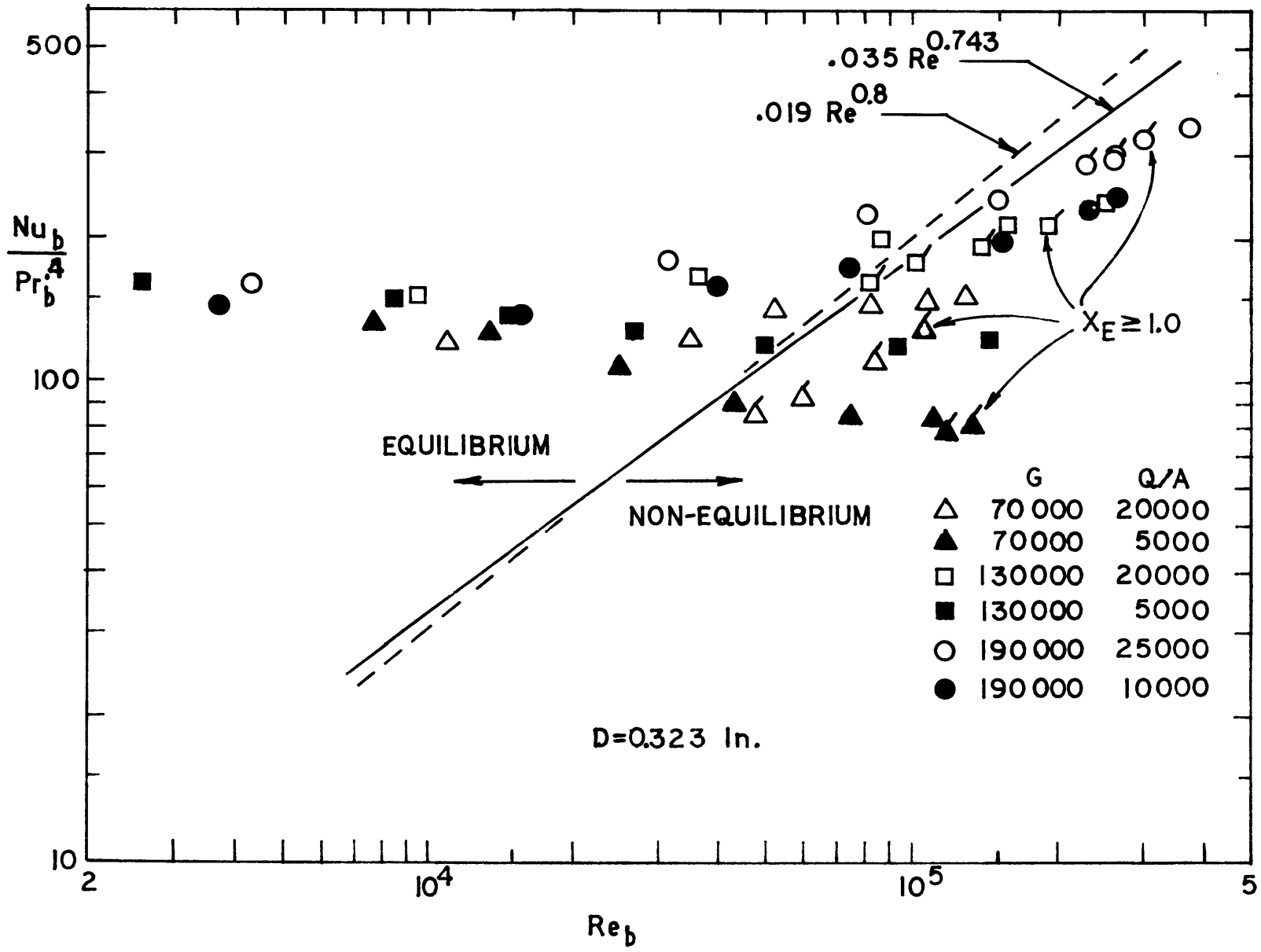

FIG. 34 REDUCED FILM BOILING DATA BASED ON EQUILIBRIUM CONDITIONS

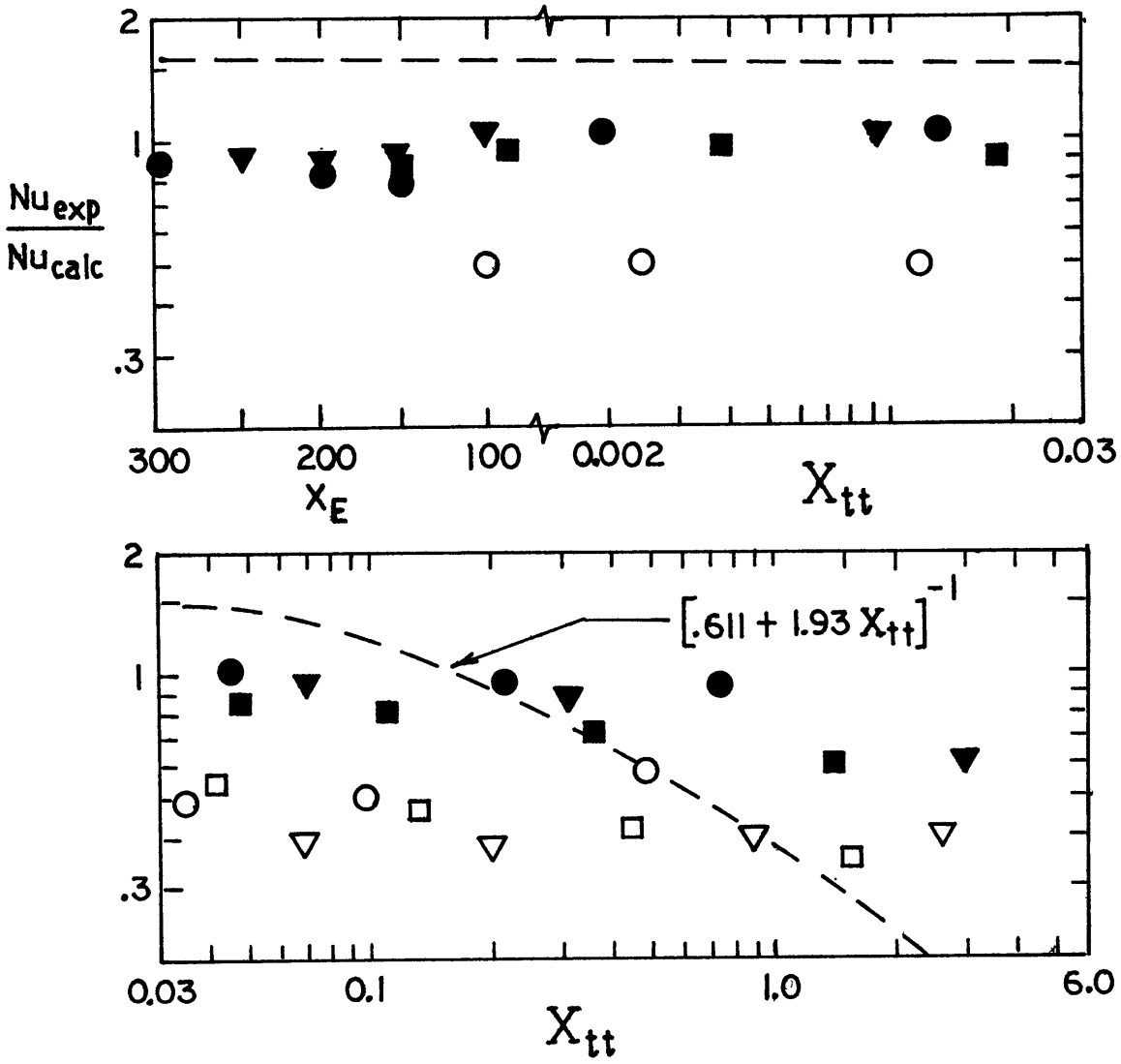

FIG. 35 CORRELATING TECHNIQUE OF REFERENCE 11

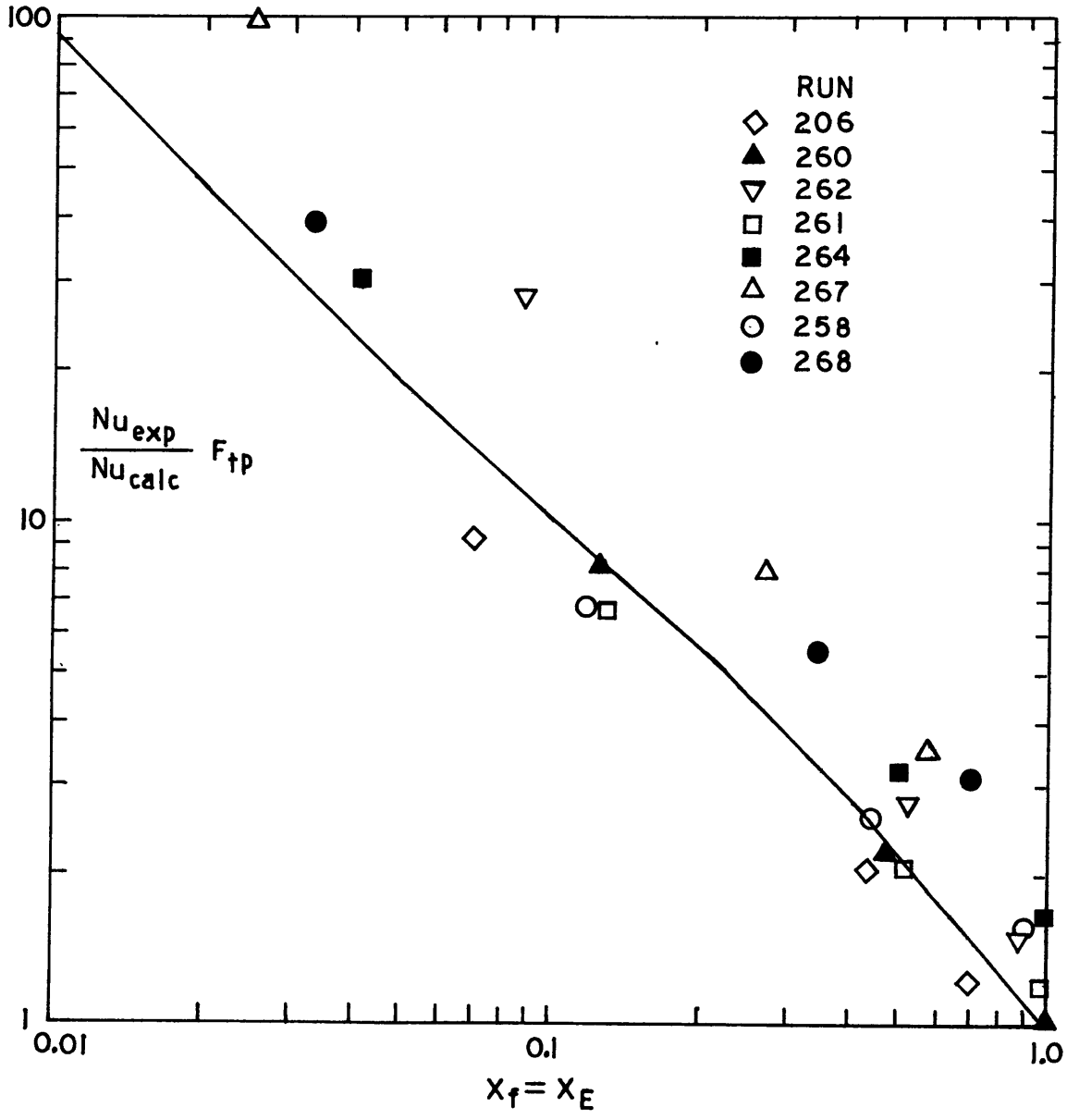

FIG. 36 CORRELATING TECHNIQUE OF REFERENCE 36

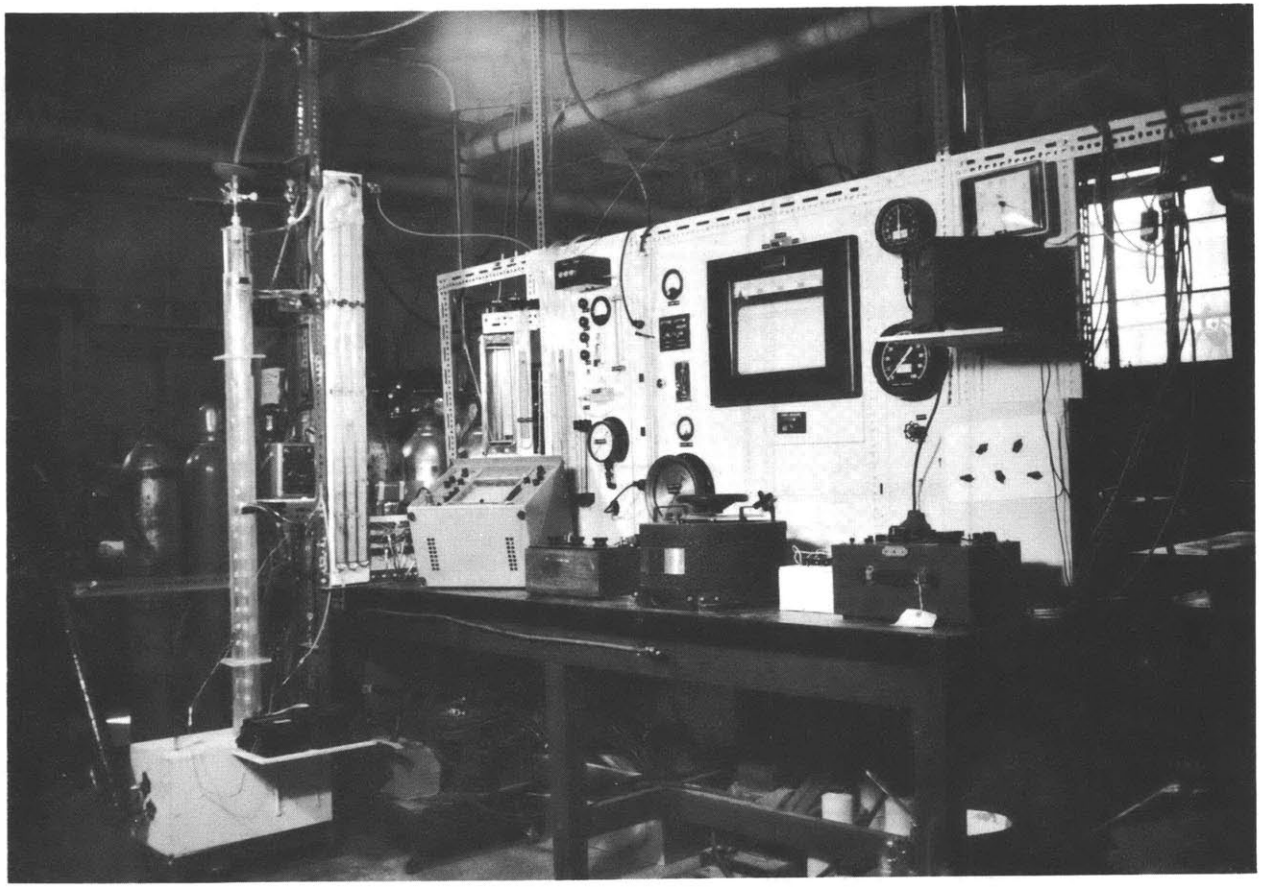

FIG. 37 FILM BOILING TEST APPARATUS

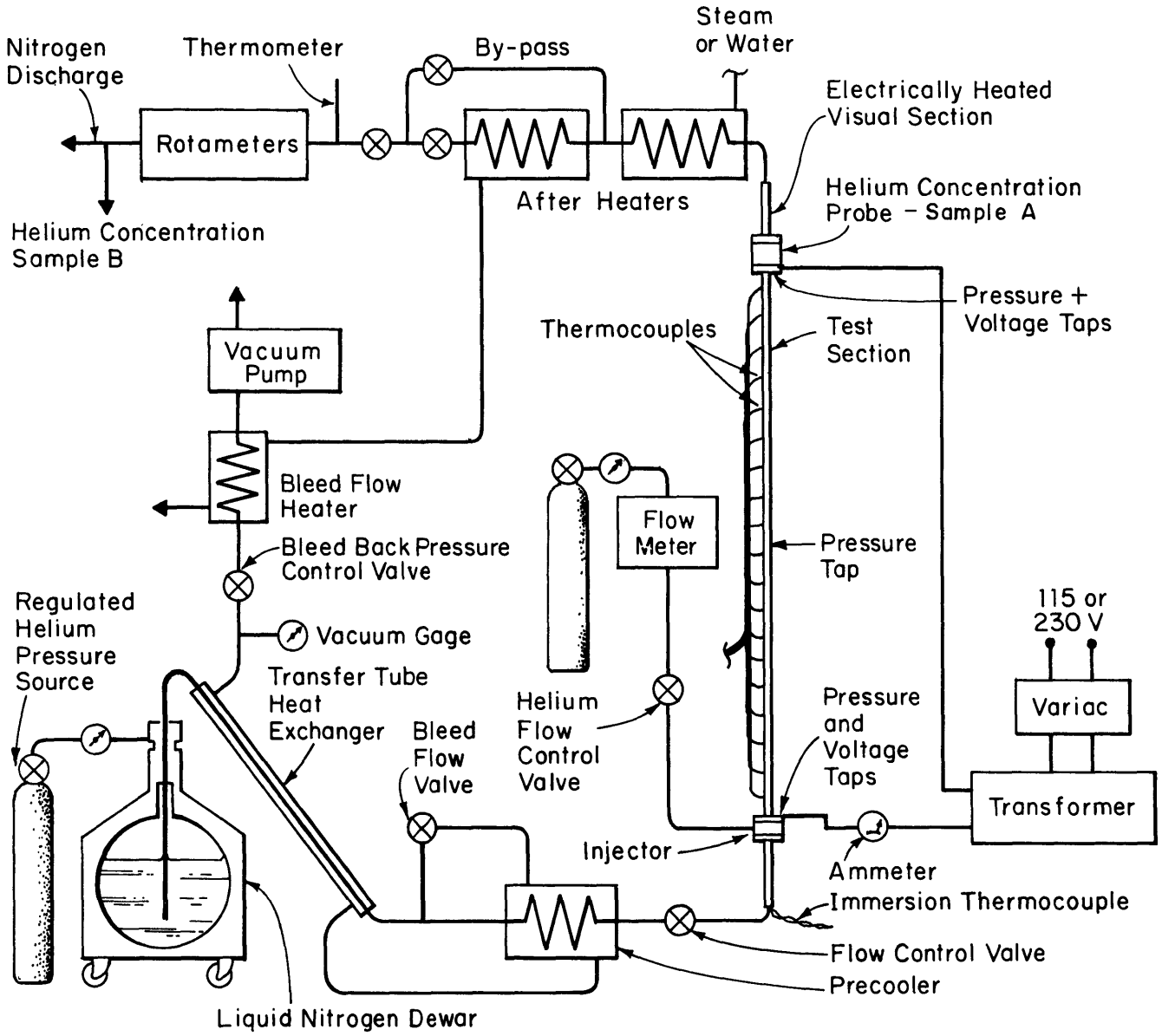

FIG. 38 SCHEMATIC DIAGRAM OF TEST APPARATUS

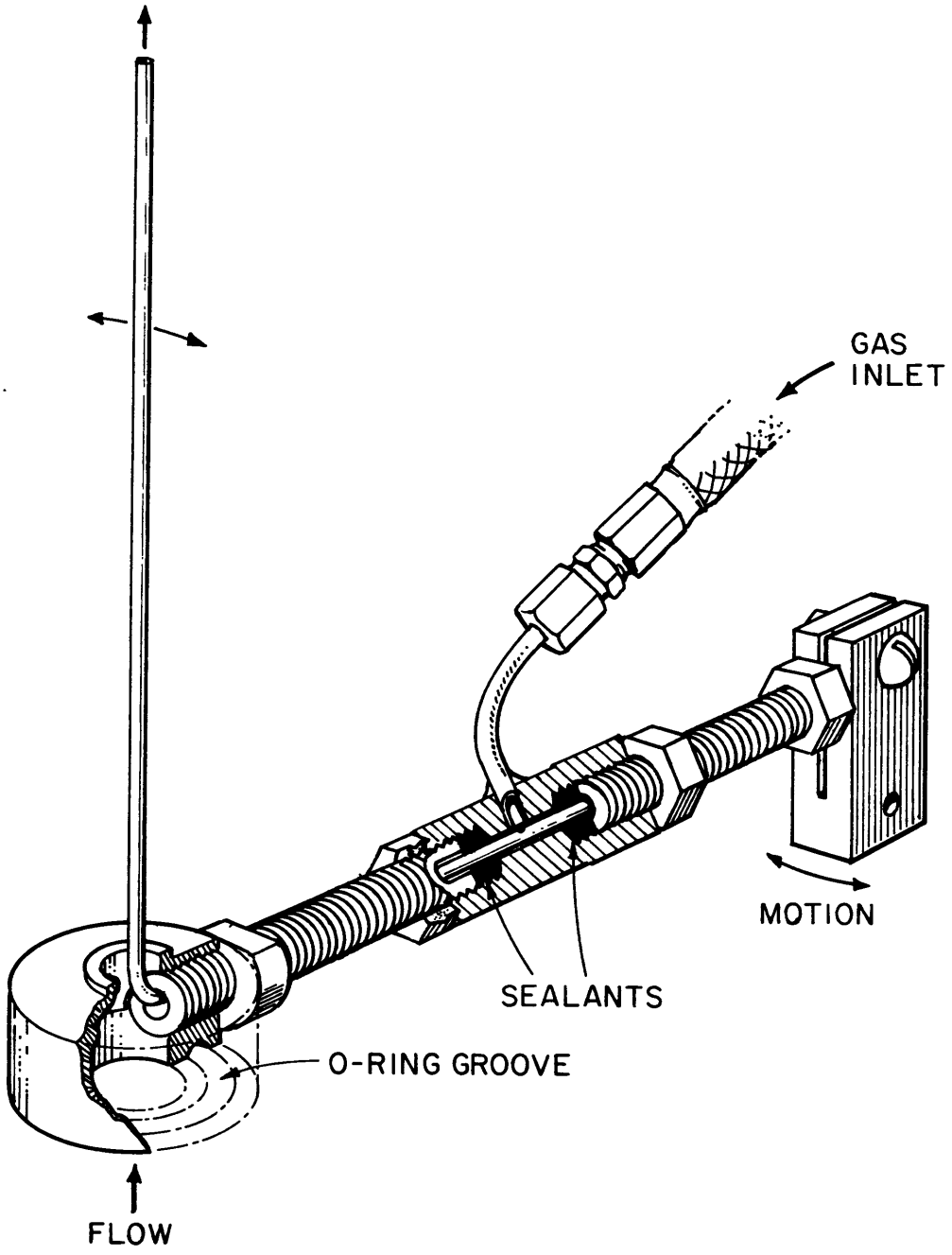

FIG. 39 HELIUM INJECTOR

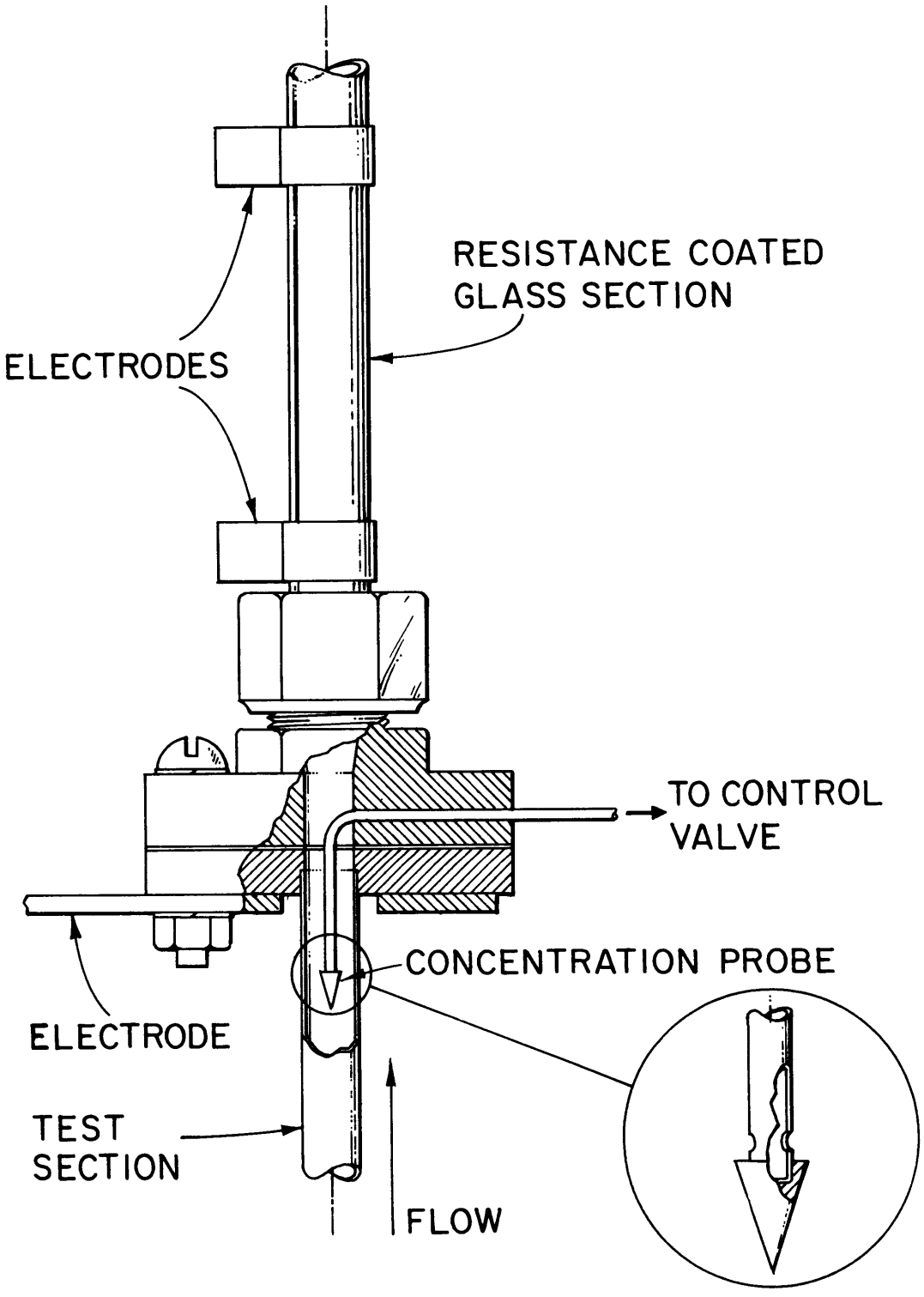

FIG. 40 STATIONARY HELIUM CONCENTRATION PROBE

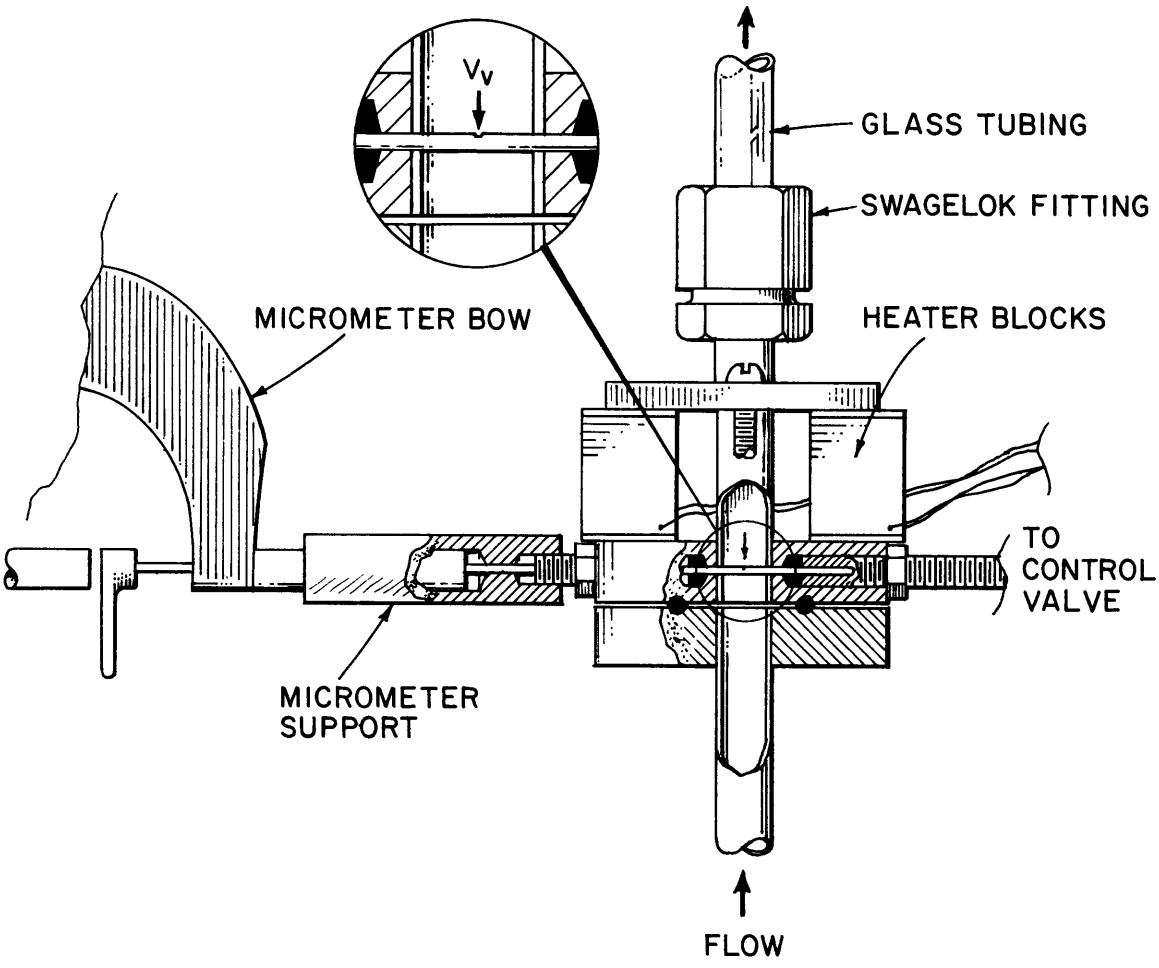

FIG. 41 TRAVERSING HELIUM CONCENTRATION PROBE

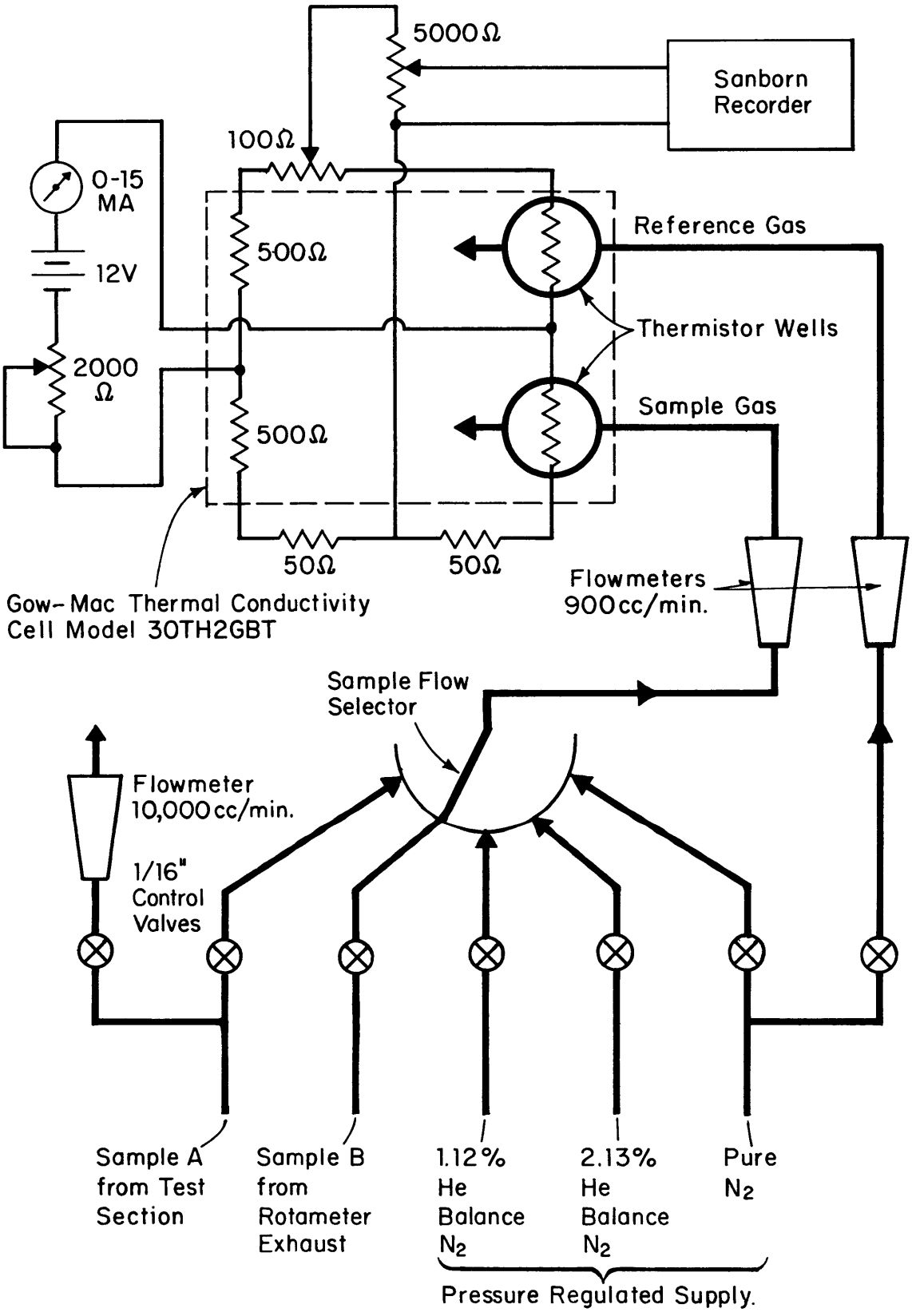

FIG. 42 FLOW DIAGRAM FOR HELIUM CONCENTRATION APPARATUS

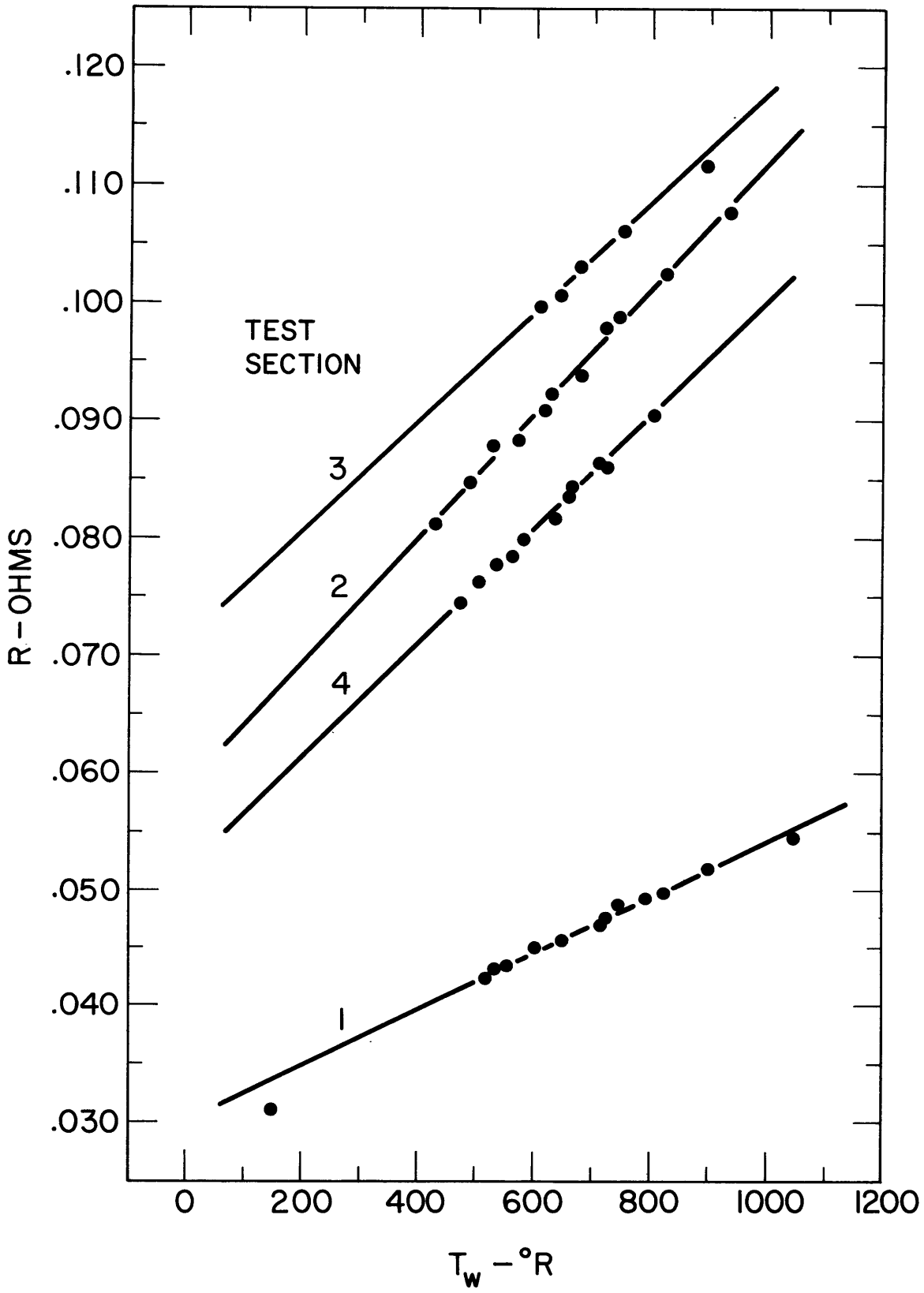

FIG. 43 RESISTANCE OF TEST SECTIONS VS AVERAGE TUBE TEMPERATURE

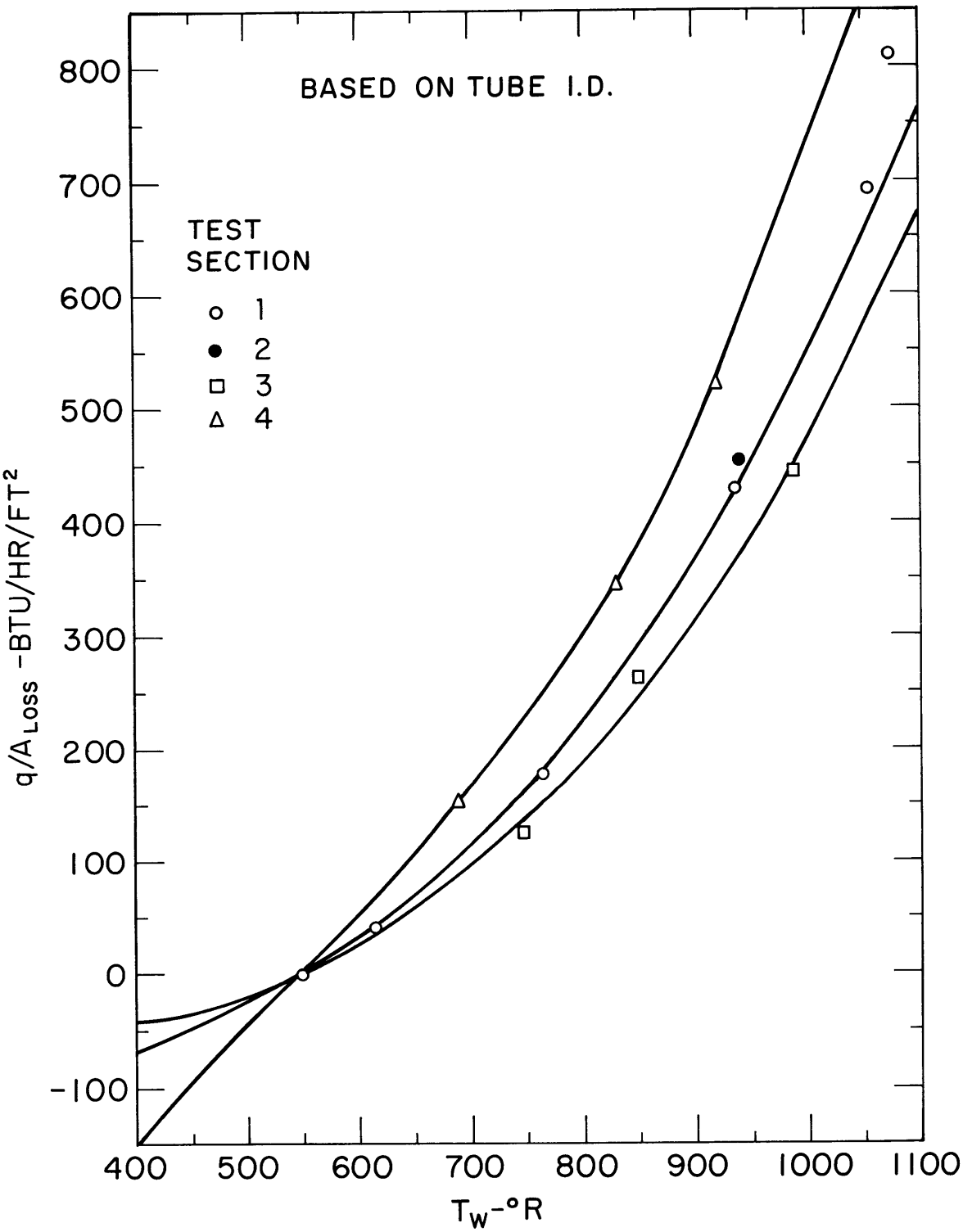

FIG. 44 RADIAL TEST SECTION HEAT LOSS VS LOCAL TUBE WALL TEMPERATURE

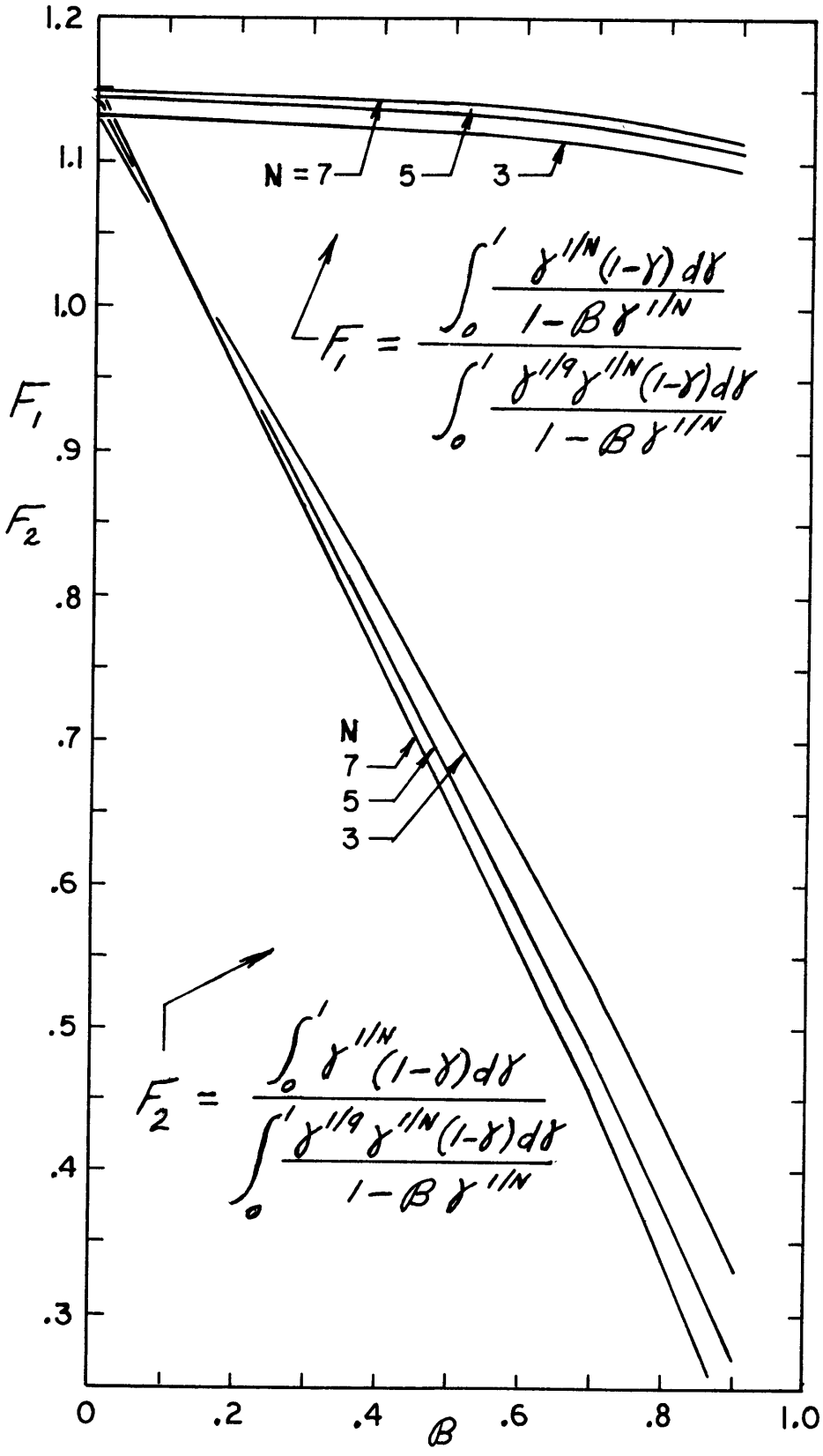

FIG. 45 FUNCTIONS OF AND (1/n) USED IN APPENDIX C

BIBLIOGRAPHY

1. Dougall, R.S., and W.M. Rohsenow., "Film Boiling on the Inside of Vertical Tubes with Upward Flow of the Fluid at Low Qualities", MIT, Dept. of Mech. Eng., EPL Report No. 9079-26, Sept., 1963.

2. Laverty, W.F., and W.M. Rohsenow, "Film Boiling of Saturated Liquid Flowing Upward Through a Heated Tube: High Vapor Quality Range", MIT, Dept. of Mech. Eng., EPL Report No. 9857-32, Sept., 1964.

3. Laverty, W.F., and W.M. Rohsenow, "Film Boiling of Saturated Nitrogen Flowing in a Vertical Tube", ASME Paper 65-WA/HT-26, 1965.

4. Parker, J.D., and R.J. Grosh, "Heat Transfer to a Mist Flow", ANL 6291, Jan., 1961.

5. Miroposki, Z.L, "Heat Release During the Film Boiling of a Steam-Water Mixture in Steam Generating Tubes", Teploenergetika, Vol 10, 1963.

6. Schmidt, K.R., "The Inside Heat Transfer Characteristics of a Forced Circulation Once Through Boiler (Film Boiling)", AEC-tr-4033.

7. Polomik, E.E., S. Levy, and S.G. Sawochka, "Film Boiling of Steam-Water Mixture in Annular Flow at 800, 1100, and 1400 psi", ASME Paper No 62-WA-136, Dec., 1962.

8. Swenson, H.S., et al., "The Effects of Nucleate Boiling vs Film Boiling on Heat Transfer in Power Boiler Tubes", Trans. ASME, Jour. of Eng. Power, Vol 84, 1962, pp 365-371.

9. Bishop, A.A., R.O. Sandberg, and L.S. Tong, "Forced Convection Heat Transfer to Water after the Critical Heat Flux at High Subcritical Pressures", WCAP-2056, Part 5, Dec., 1964.

10. Bennett, A.W., H.A. Kearsey, and R.K.F. Keeys, "Heat Transfer to Mixtures of High Pressure Steam and Water in An Annulus - Part VI", AERE - R4352, 1964.

11. Hendricks, R.C., R.W. Graham,Y.Y. Hsu, and R. Friedman, "Experimental Heat Transfer and Pressure Drop of Liquid Hydrogen Flowing Through a Heated Tube", NASA TN D-765, May, 1961.

12. Dengler, C.E., "Heat Transfer and Pressure Drop for Evaporation of Water in a Vertical Tube", Ph.D. Thesis, MIT, 1952.

13. Lewis, J.P., J.H. Goodykoontz, and J.F. Kline, "Boiling Heat Transfer to Liquid Hydrogen and Nitrogen in Forced Flow", NASA, TN D-1314.

14. Burke, J.C., and A.H. Rawdon, "An Experimental Study of Heat Transfer to Two Phase Film-Boiling Nitrogen" ASME Paper 65-HT-37, 1965.

15. Chi, J.W.H., and A.M. Vetere, "Two Phase Flow during Transient Boiling of Hydrogen and Determination of Non-Equilibrium Vapor Fractions", Advancements in Cryogenic Engineering, Vol. 9, pp 243-253.

16. Quinn, E.P., "Physical Model of Heat Transfer beyond the Critical Heat Flux", GEAP-5093, Jan., 1966.

17. Gill, L.E., G.F. Hewitt, and P.M.C. Lacey, "Sampling Probe Studies of the Gas Core in Annular Two-Phase Flow. Part II. Studies of the Effect of Phase Flow Rates on Phase and Velocity Distributions", U.K. Report AERE-R3955.

18. C.I.S.E., "A Research Program in Two Phase Flow", Euratom Contract No. 002-59-11 RDI(CAN-1), (1963)

19. Rohsenow, W.M., and H. Choi, Heat, Mass, and Momentum Transfer, Prentice-Hall, 1963.

20. Simoneau, R.J. and R.C. Hendricks, "A Simple Equation for Correlating Turbulent Heat Transfer to a Gas", ASME 64-Ht-36, Sept, 1964.

21. Dussourd, J.L., "A Theoretical and Experimental Investigation of a Deceleration Probe for Measurement of Several Properties of a Droplet Laden Stream", Research Report, MIT, Sc.D. Thesis, Oct. 1954.

22. Humble, L.V., W.H. Lowdermilk, and L.G. Desmon, NACA Report 1020, 1951.

23. Baroczy, C.J., and V.D. Sanders., "Pressure Drop for Flowing Vapors Condensing in a Straight Horizontal Tube", NAA-SR-6333, June, 1961.

24. Kearsey, H.A., personal communication

25. McAdams, W.H., Heat Transmission, McGraw-Hill Book Co., Inc., New York, 1954.

26. Tsubouchi and Sato, "Heat Transfer between Single Particles and Fluids in Relative Forced Convection", Chem. Eng. Prog. Symp. Series, Vol. 55, 1960.

27. Froessling, N., Gerlands Beitr. Geophys., 32, 170, (1938).

28. Elizinger, E.R. and J. T. Banchero, "Film Coefficients for Heat Transfer to Liquid Drops", Chem. Eng. Prog. Symp. Series No. 29, Vol. 55, 1960, P 149.

29. Kramers, H., Physica 12, 61 (1946).

30. Ranz,W.E., and W. R. Marshall, Jr., Chem. Eng. Progr. 48, No. 3 and 4,(1952)

31. Ryley, D.J. "The Evaporation of Small Liquid Drops with Special Reference to Water Drops in Steam", Journal of Liverpool Engineering Society 7, No. 1,1. (1961/62).

32. Ingebo, R.D., "Drag Coefficients for Droplets and Solid Spheres in Clouds Accelerating in Airstreams", NACA TN 3762, Sept. 1956.

33. Streeter, V.L., Fluid Mechanics, McGraw-Hill Book Co., Inc., New York, 1958.

34. Wicks, M., and A.E. Dukler, "In Situ Measurements of Drop Size Distribution in Two-Phase Flow-A New Method for Electrically Conducting Liquids", University of Houston, Texas, presented at the Int. Heat. Trans. Conference, 1966.

35. Isshiki, N., "Theoretical and Experimental Study on Atomization of Liquid Drop in High Speed Gas Stream", Report No. 35, Transportation Technical Research Institute, Tokyo, Japan.

36. von Glahn, U.H., "A Correlation of Film Boiling Heat Transfer Coefficients Obtained with Hydrogen, Nitrogen, and Freon 113 in Forced Flow", NACA TN D-2294, May 1964.

37. Strobridge, T.R., "The Thermodynamic Properties of Nitrogen from 114 to 540° between 1.0 and 3000 psia, Supplement A (British Units)", NBS Tech. Note 129A., Feb. 1963.

38. Scott, R.B., Cryogenic Engineering, D. Van Nostrand Co., Inc., Princeton, N.J. 1959.

39. N.B.S. Circular 564.

ERRATA

Page		
-x-	line 14	should read "o outer or zero"
-viii-	after line 16	add "K constant"
48	eq 41	"K" should be "k"
49	line 14	should read $(T_s - T_{sat})/(T_v - T_s)$
49	eq 42	term in brackets should be $2.0 + C(\rho \Delta v \delta / \mu)^{\alpha}$
61b	line 3	F_1 should be K_1
61c	eq 52	term in brackets should be $G_T (1 - X_A)/\pi \ell \; V_e \; V$
61c	line 3	F_2 should be K_2
61e	line 23 and 25	F_1F_2 should be K_1K_2
61f	line 2	F_1F_2 should be K_1K_2